FCTUC DEPARTAMENTO DE ENGENHARIA CIVIL
FACULDADE DE CIÊNCIAS E TECNOLOGIA
UNIVERSIDADE DE COIMBRA

André Filipe Ferreira Escudeiro

Experimental and numerical analysis of compressed cold-formed steel elements with sigma-plus cross-sections subjected to fire

Análise experimental e numérica de elementos comprimidos de aço enformado a frio com secção sigma-plus em situação de incêndio

Coimbra, Dezembro, 2016

AKNOWLEDGEMENTS

First of all, I would like to express my sincere gratitude to Professor João Paulo Correia Rodrigues, for the opportunity granted, as well for all the guidance, encouragement and support provided through every stage of this investigation providing me with the best possible conditions to develop this dissertation.

To Professor Leroy Gardner, for the warm welcome in Imperial College of London and from who I had pleasure to learn, having always a constructive suggestion, strongly contributing for my development, both professional and personal.

To Professor Luís Miguel Santos Laím, for all the knowledge showed and for being always present, helping me to overcome every obstacle with is expertise guidance, leading me through every stage of this process.

To the Laboratory staff members, Rafael Campos, Luís Gaspar, and Agostinho Roque, I thank you for all your assistance in helping me preparing the experimental tests.

To my friend and colleague Alexandre Mota, for all the help and assistance through this dissertation, which would not be possible to perform otherwise.

To my friends and colleagues Duarte Oliveira and Diogo Bazenga, for being available from the first to the very last day providing me all the help requested.

To my Mother and to my Father, for all the strength, the love, and sacrifice showed, both responsible for man I grew up to be.

To my grandmother, from who I have always received unconditional love, constantly remembering me that I will never be able to live up to her.

To Adriana Frutuoso, for all the patience and unbreakable will showed through this journey, tireless giving me the encouragement needed.

To all my friends, for sharing this experience with me and supporting me along the way.

To every and each one of you, I am grateful!

RESUMO

O aço enformado a frio tem vindo a assumir cada vez mais importância no mundo da construção civil, fato esse devido às inúmeras vantagens que pode oferecer, garantindo um bom desempenho estrutural. A crescente popularidade conseguida nas últimas décadas é devida às propriedades únicas características do aço enformado a frio como, a sua leveza, a sua alta resistência e rigidez, a sua não combustibilidade, assim como a redução tanto no tempo da sua montagem como nos custos associados.

A falta de estudos e investigações em relação a elementos de aço enformado a frio é avassaladora, especialmente em colunas em situação de incêndio, e o conhecimento adquirido até à data é ainda escasso sendo necessário mais investigações nesta matéria. A ausência de estudos torna-se, mais evidente se os efeitos da restrição axial e rotacional forem considerados na investigação, fator que simula uma situação real em que a coluna é parte integrante de uma estrutura.

A presente dissertação, foi elaborada como parte de um projeto de pesquisa nacional denominado *FireColdSteel – Análise experimental e numérica de elementos estruturais de aço enformado a frio sujeito a incêndio* – PTDC/EMC/116859/2010 (FCT) e realça a necessidade do desenvolvimento de metodologias especificas para este tipo de elementos. A norma atualmente disponível está presente na EN1993-1-2:2005 (2005) e foi especificamente desenvolvida para aços laminados a quente, e também é aplicável a elementos de aço enformado a frio com secção transversal de classe 4.

Os resultados obtidos experimentalmente foram posteriormente usados na validação dum modelo de elementos finitos desenvolvido, usando o software *Abaqus* (2014), para reproduzir o comportamento das colunas observado nos ensaios experimentais. O modelo numérico foi validado de encontro com os dados recolhidos na análise experimental, com o objetivo de expandir as simulações a um maior número de casos para lá dos limites impostos nesta dissertação.

Os testes realizados mostraram que as colunas apresentaram baixa resistência ao fogo. Durante os ensaios experimentais foi observado que para colunas compostas o colapso foi controlado pela restrição axial imposta, já para as simples o colapso parece ter sido controlado pelo aumento das temperaturas levando a uma deterioração das propriedades mecânicas do material.

Palavras Chave: fogo, aço enformado a frio, sigma-plus, colunas, restrição, dilatação térmica, análise experimental, análise numérica.

Experimental and numerical analysis of compressed cold-formed steel
elements with sigma plus cross-section subjected to fire

ABSTRACT

ABSTRACT

The cold-formed steel has become more popular over the years in construction industry, mostly due to its innumerous advantages that this type of steel can offer, ensuring both structural behaviour. The increase popularity achieved over the last decades it is due to a number of unique properties characteristic of this steel such as, its lightness in weight, high strength and stiffness, non-combustibility, and a reduction in both erection time and construction costs.

The lack of studies and researches regarding cold-formed steel members is overwhelming, specially in terms of columns in fire situation, and the knowledge achieved up to date is still scarce requiring a better understanding on this type of columns. The absence of studies regarding cold-formed steel columns is even clearer if the effects of axial and rotational restraint are considered within the research, which simulates a real-life situation when the column is an integral part of the structure.

The present dissertation was conducted as part of a National Research Project entitled *FireColdSteel – Experimental and Numerical Analyses of Cold-Formed Steel Members Under Fire Conditions* – PTDC/EMC/116859/2010 (FCT) and enhances the need to develop specific guidelines for cold-formed steel members. The current available design standards are present in EN 1993-1-2:2005 (2005) specifically designed for hot-rolled steel members that are also applicable to cold-formed steel members with class 4 cross-section.

The experimental results obtained were posteriorly used as input in order to validate the finite element models developed, using the finite element analysis *Abaqus* (2014), to reproduce the behaviour of the cold-formed steel specimens observed in the experimental fire tests. The finite element model was validated against the retrieved experimental data, and it is intended to expand the simulations into a larger number of elements outside of the bounds of this dissertation.

The tests conducted showed that cold-formed steel columns present low fire resistance. During the experimental tests, it was observed that for built-up columns the restraint to thermal elongation seemed to control the failure, whereas for single columns the failure was due to the temperature increase leading to the degradation of the mechanical properties.

Keywords: fire, cold-formed steel, sigma-plus, columns, restraining, thermal elongation, experimental analysis, numerical analysis.

Experimental and numerical analysis of compressed cold-formed steel
elements with sigma plus cross-section subjected to fire

TABLE OF CONTENTS

TABLE OF CONTENTS

Experimental and numerical analysis of compressed cold-formed steel
elements with sigma plus cross-section subjected to fire

TABLE OF CONTENTS

Experimental and numerical analysis of compressed cold-formed steel
elements with sigma plus cross-section subjected to fire

LIST OF FIGURES

LIST OF FIGURES

Experimental and numerical analysis of compressed cold-formed steel
elements with sigma plus cross-section subjected to fire

1 INTRODUCTION

LIST OF TABLES

NOTATION

Roman upper case letters

A cross-sectional area

A_c gross area of the compression element

$A_{c,eff}$ Effective area of a flat compression element

A_{eff} effective cross-sectional area

A_s effective cross-sectional area of the edge stiffener

E, E_{20} modulus of elasticity at ambient temperature

E_θ modulus of elasticity at temperature T or θ

H height of the column

I second moment about the strong axis of a cross-section

I_s second moment of effective area of the edge stiffener

K spring stiffness of the edge stiffener per unit length

K_{Ra} axial stiffness of the surrounding structure

K_{Rr} rotational stiffness of the surrounding structure

L length of the column

$N_{b,Rd}$ design buckling resistance of a compression member

N_{cr} elastic critical force for the relevant buckling mode

P axial restraining force generated in the column

P_0 initial applied load on the cold-formed steel column

P_{Num} maximum numerical load-carrying capacity of the column

P_{max} maximum axial force generated in the column

T_i thermocouple i

Roman lower case letters

b width of the flange
or

	width of the plate
b_{eff}	effective flange width
b_p	width of the flange taking into account the influence of rounded corners
$b_{p,c}$	width of the edge stiffener
$\bar{b}$	appropriate width
c	width of the edge stiffener
c_a	specific heat of steel according to EN 1993-1-2:2005
c_{eff}	effective width of the edge stiffener
c_p	width of the edge stiffener taken into account the influence of rounded corners
d_1	maximum local imperfection in a stiffed element
d_2	maximum deviation from straightness for a lip stiffened or unstiffened flange
d_a	axial displacement of the cold-formed steel columns
f_y , $f_{y,20}$	yield strength at ambient temperature
f_{yb}	nominal yield strength
$f_{y,T}$	yield strength at temperature T
h	height of the cross-section
i	minimum radius of gyration
$k_{E,\theta}$	reduction factor for the modulus of elasticity at the steel temperature θ
k_σ	plate local buckling factor
t	thickness
t_{cr}	critical time of the column
t_{peak}	time when the maximum restraining forces in the column are reached

Greek lower case letters

α	Imperfection factor, corresponding to the appropriate buckling curve, according to the type of cross-section, axis of buckling and yield strength
α_c	heat transfer coefficient
γ_{M0}	partial factor for resistance of cross-sections

γ_{M1}	partial factor for resistance of members
$\gamma_{M,fi}$	partial factor for the relevant material property for the fire situation
$\bar{\theta}_c$	mean temperature of the column
θ_{cr}	critical temperature of the column
θ_{peak}	temperature registered when the column achieved the maximum load-bearing capacity
$\bar{\theta}_s$	mean temperature of the cross-section
$\theta_{cr,Num}$	critical numerical temperature of the column
$\bar{\lambda}$	non-dimensional slenderness
$\bar{\lambda}_p$	plate slenderness
$\bar{\lambda}_{p,red}$	reduced plate slenderness
$\bar{\lambda}_\theta$	non-dimensional slenderness for temperature θ
ν	poisson ratio
ρ	reduction factor for plate buckling
$\sigma_{com,Ed}$	maximum design compressive stress in the plate
σ_{cr}	critical elastic buckling stress
$\sigma_{cr,s}$	elastic critical buckling stress of the edge stiffener
σ_e	design stress
ϕ	resistance factor
χ	reduction factor for relevant buckling mode
χ_{fi}	reduction factor for flexural buckling in fire design situation
ψ	stress ratio in the plate

1 INTRODUCTION

1.1   General

Cold-Formed Steel (CFS) is the common term used to refer to products that are manufactured by pressing or rolling the steel at ambient temperature, taking advantage of its ductility. The first appearances of cold-formed steel elements in building construction industry started in the 1850's in the United States and Great Britain, but since there was no adequate design standard, and the information as a structural element in building codes were limited, its acceptance was still limited. The most recent normative published for Europe was the European Standard Eurocode 3: *Design of Steel Structures. Part 1-3: General Rules. Supplementary rules for cold-formed thin gauges members and sheeting* (EN 1993-1-3, 2006). There are no specific guidelines for the fire design of cold-formed steel structural elements, and the only guidelines available are present in EN 1993-1-2 (2005) specifically design for hot-rolled steel members that are also applicable to cold-form steel members with class 4 cross-section.

The use of CFS members in building construction industry has been increasing in the past few years and that can be acknowledge considering its numerous advantages when comparing it with other structural materials. CFS prove to be a better choice due to many factors such as, its lightness in weight, its high strength and stiffness, its ease of prefabrication and fast installation, as well as its economy in transportation and handling, its ability to be not shrink and not to creep at ambient temperatures, its capability to be recyclable, and its non-combustibility.

CFS members can be manufactured by roll forming, which consists in a continuous bending operation of a long strip coiled steel metal, at ambient temperature into the required cross-section. CFS members can also be obtained by press-braking, this technique is more appropriate for smaller quantities of a specific product, given the fact that the maximum length of the member to be manufactured cannot be larger than the length of the press-brake.

As previously mentioned, the use of CFS members in building construction industry has suffered an increase over the last years, and with that, comes the need to ensure its safety in any possible situations likely to happen during a building's lifetime.

When compared to a high used structural steel member, hot-rolled steel for instance, the CFS members prove to be a strong solution due to its accurate detailing, in which provides a considerable number of different types of cross-section that gives flexibility in design. In the other hand, its high slenderness and torsional stiffness brings a more complex analysis, due to the non-coincidence of the centre of gravity and the shear centre that the major part of these

Experimental and numerical analysis of compressed cold-formed steel
elements with sigma plus cross-section subjected to fire

1 INTRODUCTION

sections presents. In addition to the buckling modes present in hot-rolled steel members, the CFS members are usually subjected to other buckling modes such as, local, distortional, flexural and flexural-torsional.

Regarding the fire design, as previously mentioned, there are no specific guidelines, and so it becomes urgent the necessity to conduct a profound research about the behaviour of CFS structural members when subjected to high temperatures. And it is based in the limitations mentioned before that this work, contributing for the knowledge development in Civil Engineering as well in future studies for the possibility to achieve simple design methods, takes a major importance in the experimentation and analysis of the behaviour of CFS columns when subjected to fire.

The research presented in this dissertation was conducted as part of a National Research Project entitled *FireColdSteel – Experimental and Numerical Analyses of Cold-Formed Steel Members Under Fire Conditions* funded by the *National Foundation for Science and Technology –* PTDC/EMC/116859/2010 (FCT).

1.2   Motivation and Objectives

With the Cold-formed steel market increasing significantly over the last years due to its numerous advantages when compared with other construction building materials, and its ease of manufacturing and erection, added some extra value to this type of solution. Due to its low thickness, and therefore the several buckling modes that may occur at stress levels lower than the yield stress levels of the material, the necessity to study and understand the behaviour not only at ambient temperatures but at fire conditions as well of cold-formed steel members becomes urgent after a great number of studies showed the existing limitations for the current standards.

The overall purpose of this dissertation was to investigate the structural behaviour of cold-formed steel columns with sigma plus cross section when subjected to fire. To achieve this objective, two approaches had been made, the first stage developed was the experimental part which has taken part in the Laboratory of Testing Materials and Structures (LEME) of University of Coimbra (UC), followed by a numerical research developed in Imperial College London, as part of the UE funded program ERASMUS+. Based on both experimental and numerical investigation carried out along the present dissertation and on future parametric studies to be conducted it is intended to present accurate design methodologies for fire situations, similar to those that already exist for hot-rolled steel.

Regarding the experimental part, a great number of tests was made in the Laboratory of Testing Materials and Structures (LEME) of UC as part of the research project *FireColdSteel* as previously mentioned. Two different CFS columns were studied, namely $\Sigma+$ single cross-section, and open built-up $\Sigma+$ double cross section back-to back. The specimens were tested

with an initial applied load of 50% of the load-bearing capacity at ambient temperature, in order to study the fire behaviour of CFS columns with restrained thermal elongation.

Within the numerical part, the objective was to develop a finite element numerical models using the finite element program *Abaqus* (2014), capable to reproduce the behaviour of CFS columns previously achieved in the experimental part, accurately under fire conditions. The numerical model developed and presented within this dissertation will be calibrated and validated converging with the results obtained before in the experimental analysis, in order to expand the numerical simulations to a larger number of elements not tested experimental, and to enable the development of parametric studies of CFS columns, with different parameters to the ones initially tested.

1.3 Contents of the dissertation

The following thesis is divided in five chapters, in which are presented and discussed all the research developed and all the conclusions obtained as well.

The first chapter presents a general introduction about cold-formed steel members and a briefly preview about the work developed, mentioning the objectives and the motivation of this dissertation.

In the second chapter, it is presented the most relevant literature review findings on the subject as a support to the work developed further on, in which are included experimental analysis on CFS columns at both ambient and elevated temperatures, numerical investigations conducted by other researchers.

The third chapter leans on the experimental study carried out to access the behaviour of CFS sigma-plus columns at elevated temperatures. The results of the experimental study are presented and analysed through the comparison with the results available in the literature. All the test set-up is thoroughly described.

In chapter four it's presented the finite element modelling of cold-formed steel compression members at elevated temperatures and the validation and calibration of those models as well as the explanation of all parameters adopted.

The fifth chapter presents the relevant finding of this research based on the results obtained mentioned in the previous chapters as well as all the conclusions achieved while developing this dissertation. A critical analysis of these conclusions is made, with the clear objective to understand the importance that these could have in the development of future studies.

2   LITERATURE REVIEW

2.1   General

There are three major groups in the metallic building construction industry, and they are the hot-rolled steel members, welded members, and cold-formed steel members. The most popular are the hot-rolled members (Figure 2.1 b)), being the cold-formed members are mostly used as secondary members, or for smaller structures. The cold-formed steel members (Figure 2.1 a)) are manufactured from thin steel plates with a uniform thickness, which allows a great number of different types of cross-section that comes with a very good mechanical performance behaviour and an economic use of the material (Simões, 2007). Bear in mind that the cold-formed steel members are pre-galvanised steel sections usual covered with a zinc coating to protect against corrosion which brings a major durability and reduced maintenance requirements.
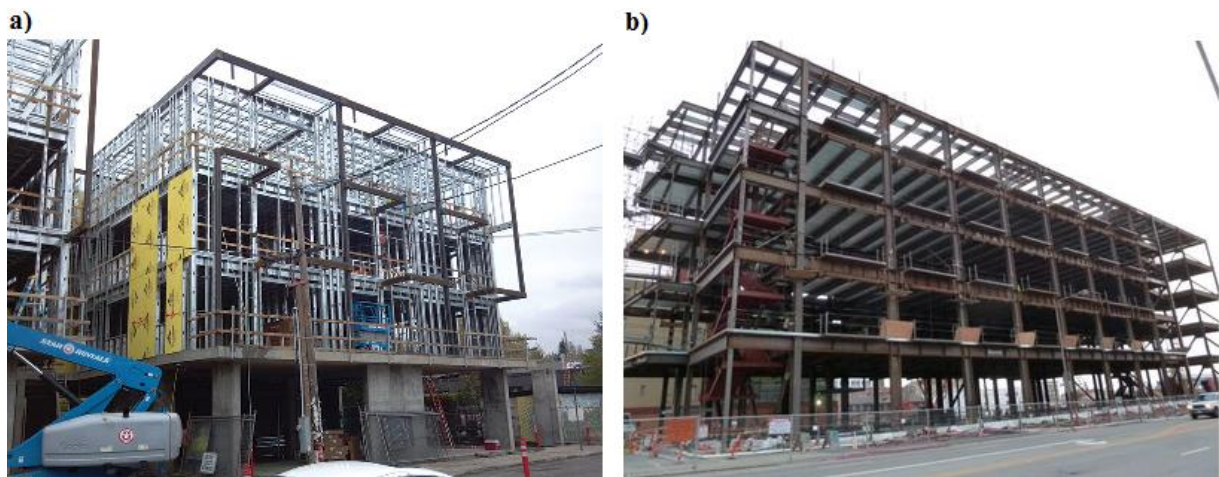
Figure 2.1 - Steel Structures a) Composed by cold-formed steel members (Structure Magazine@, 2014) b) Composed by hot-rolled steel members (GEM Nexus@, 2013).

There's been a major increasing in the past over the last decade of the XIX century. United States and Great Britain were the first pioneers. The real use of cold-formed steel members in building construction industry only started in 1946, after the American Iron and Steel Institute (AISI) publication, one of the first design normative regarding leaning on the behaviour CFS members. This was based on the research work developed by Professor George Winter. Since that there was a considerable increasing of the use of CFS members in building construction, what led to an increasing number of studies and investigations about the mechanical behaviour of CFS members. The normative AISI S100 – North American Cold-Formed Steel

Specification, published in 2007 by AISI (AISI, 2001) is the current standard in the United States, Canada and Mexico. In 1987 the British Standards Institute published, in the United Kingdom, the BS 5950 – Structural Use of Steelwork in Building, Part 5: Code Practice for design of Cold-formed Steel Sections (BS 5950, 1987). Australia and New Zeeland are both still using the standard published in 1996, AS/NZS 4600 – Cold-Formed Steel Structures (AS/NZS 4600, 1996). The design standard used in Europe is the Eurocode 3: Design of steel structures, Part 1-3: General rules, Supplementary rules for cold-formed steel members and sheeting, published in 2004 by the European Committee for Standardisation (EN 1993-1-3, 2006).

The main advantages regarding the application of cold-formed steel in building construction are:

- Huge flexibility in the manufactured process, since it is possible to do an economic production with a numerous variability of cross-sections with different geometry, adding to the fact that CFS members are light weighted brings a relation between weight and load-bearing not available in other structural materials.

- Ease manufacturing process, and the ability to produce the desire cross-sections with a specific thickness proving the ability to provide for long spans.

- Fast and Simple erection and installation, due to its lightness in weight, economic transportation and limited length for storage.

- Its non-combustibility.

- Non-shrinking capacity and non-creeping at ambient temperatures.

- Uniform quality.

- Recyclable material.

In the opposite direction, the main disadvantages in using CFS member's usage are:

- Low Torsional stiffness, due to the low thickness of its sections, and the fact that the majority of single members have open sections and asymmetric sections resulting in a non-coincidence of the centroid and the shear centre.

- More complex calculation of the load-bearing capacity in CFS members, when compared to hot-rolled steel members.

- Several buckling modes, that aren't usually present in traditional structural steel design, due to CFS members section's low thickness (Dubina et al., 2012).

Experimental and numerical analysis of compressed cold-formed steel
elements with sigma plus cross-section subjected to fire

2 LITERATURE REVIEW

2.2   Structural elements

2.2.1 Element types

In steel construction, several commercial sections are available as individual structural framing members, namely C-sections, U-sections, Z-sections, Σ-sections, etc. (Figure 2.2). All the available single sections can be combined in order to make an open built-up and closed built-up cross-sections.

The ability of this material to grant a very large number of sections with different geometry, presents an easy and simple solution for design of cold-formed steel structures.
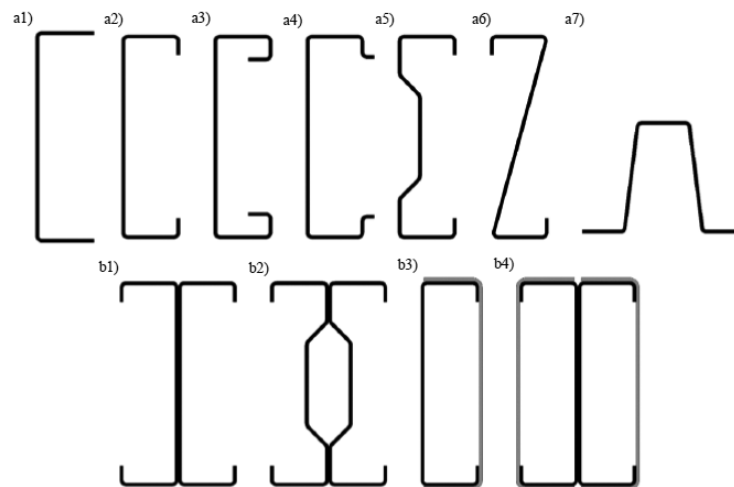
Figure 2.2 - Typical CFS cross-section shapes used in building construction industry. a1) Plain channel (U). a2) Lipped channel (C). a3) Double lipped channel (C). a4) Double lipped U. a5) Σ section. a6) Z section. a7) Ω section. b1) and b2) Open built up cross-section (Craveiro, 2015)

2.2.2 Manufacturing process

As previously mentioned cold-formed steel products can be manufactured by press-braking or roll forming. A roll forming machine has a specific number of consecutive rolls, in which they are in a continuous bending operation until the desire cross-section is obtained (Figure 2.3). This process is made at ambient temperature, and in order to obtain a more complex cross-section shape a large number of rolls will be needed.
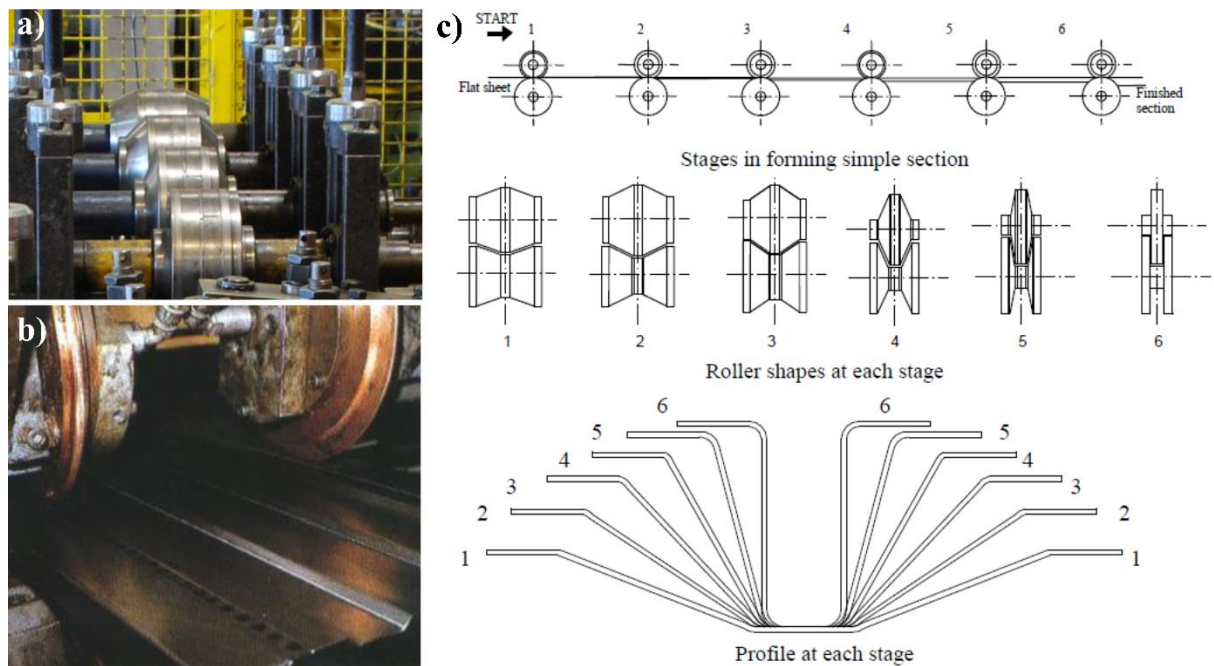
Figure 2.3 – a) and b) roll forming lines (Dubina, 2005) c) stages in
roll forming a simple sections (Rhodes, 1991)

Press-braking is a limited process when compared to roll forming, and its major use leans on small members with simpler cross-sections. The press-brake is responsible for molding the shape of the steel plate (Figure 2.4), and as previously mentioned, the maximum length of the desired member is fully dependent on the length of the press-brake.
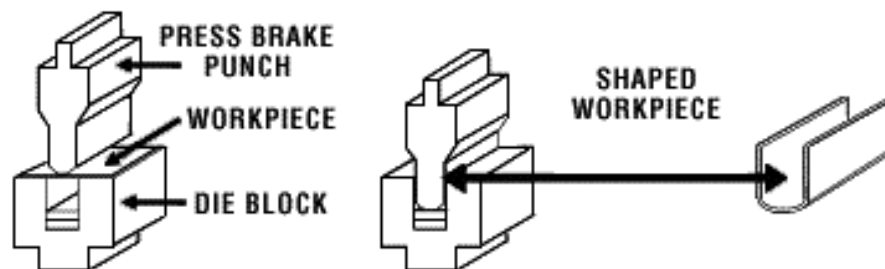
Figure 2.4 - Press-braking process (Advantage Fabricated Metal@, 2009)

2.3   Mechanical and thermal properties

2.3.1 Mechanical properties at ambient temperatures

The mechanical properties of cold-formed steels, unlike hot-rolled steels who have available design standards with accurate mechanical properties in both ambient and high temperatures, can be significantly different of the initial steel sheet before forming due to the cold-forming process. This process changes the mechanical properties of the initial sheet, as yield strength and ultimate tensile strength increases while the ductility of the steel is reduced (Yu and LaBoube, 2010).

Essentially there is three major phenomena responsible by the change of the mechanical properties, namely strain hardening (increased strength of the steel due to plastic deformation), strain aging (when after the steel has been deformed through plastic deformation, and aged after, the ductility of the steel decreases as the strength increases), and lastly, the Bauschinger effect that refers to the fact that the longitudinal compression yield strength of the stretched steels is smaller than the longitudinal tension yield strength (Yu and LaBoube, 2010). The Figure 2.5 represents the influence of forming at ambient temperature in the mechanical properties of the steel, in which strain hardening and strain aging are the most influents.
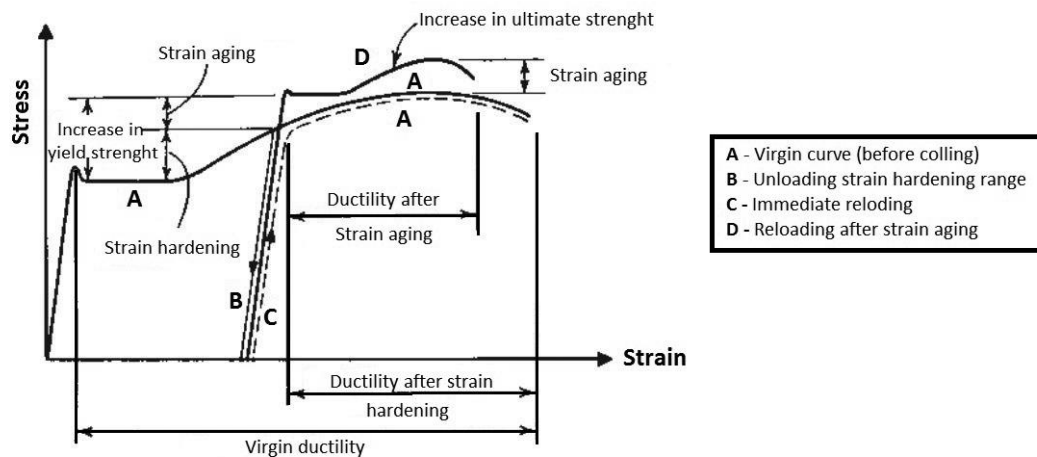
Figure 2.5 - Effects of strain hardening and aging on stress-strain characteristics
of structural steels (Yu and LaBoube, 2010)

The stress-strain curves for hot-rolled and cold-formed steels are different, and the reason lies in the manufacturing process. For hot-rolled steels, the yielding point is well defined by the time as the stress-strain curve becomes horizontal, in the case of cold-formed steels the yielding point is not so clear, as the stress-strain curve is gradually growing reaching the yielding stage without a visible peak (Figure 2.6).
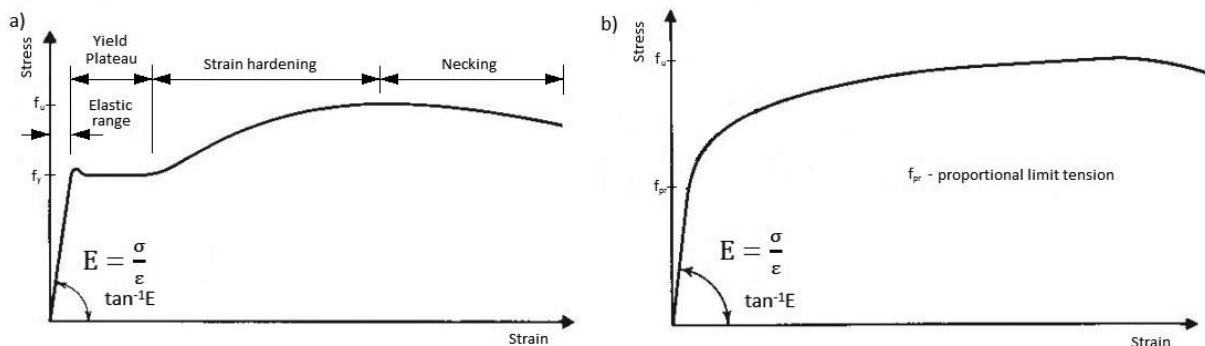
Figure 2.6 - Stress-strain curves of a) Hot-rolled steels and b) Cold-worked steels (Yu and
LaBoube, 2010)

2.3.2 Mechanical properties at high temperatures

Regarding the performance of cold-formed steel structural elements in fire conditions, deterioration of the mechanical properties is the key issue, namely the elasticity modulus, and the yield strength. The loss of the mechanical properties due to elevated temperature is responsible for a significant loss of buckling load of CFS structural elements (Craveiro, 2015). To prevent this loss, the EN 1993-1-2:2005 (2005), provide reduction factors for the mechanical properties of cold-formed steels at high temperatures which are the same used for class 4 hot-rolled steel sections (Table 2.1).

Steel Temperature θ_a	Reduction factor (relative to f_y) for effective yield strength of hot-rolled and welded class 4 sections $k_{0.2,p,\theta} = f_{0.2,p,\theta}/f_y$	Reduction factor (relative to f_{yb}) for effective yield strength of cold-formed and welded class 4 sections $k_{0.2,p,\theta} = f_{0.2,p,\theta}/f_{yb}$
20°C	1.00	
100°C	1.00	
200°C	0.89	
300°C	0.78	
400°C	0.65	
500°C	0.53	
600°C	0.30	
700°C	0.13	
800°C	0.07	
900°C	0.05	
1000°C	0.03	
1100°C	0.02	
1200°C	0.00	

NOTE 1: For intermediate values of the steel temperature, linear interpolation may be used.
NOTE 2: The definition for f_{yb} should be taken from EN 1993-1-3

Table 2.1- Reduction factors for carbon steel for the design of class 4 sections at elevated temperatures (EN 1993-1-2, 2005)

An exhaustive experimental research for the investigation of the mechanical properties of different types of structural steels at elevated temperatures using transient and steady state test method, was conducted by (Outinen et al., 2000). Outinen (2000) stated that transient state method provides more realistic results as it simulates a structural member under static loading subjected to fire conditions since creep effects are also taken into account. The transient tests consist in a constant load applied in the specimen under a constant rate of temperature increase, whereas for the steady-state the specimen is firstly heated up to the desired temperature and then applied the respectively load. The tested piece specimens were cut form the initial steel plate with a nominal thickness of 2 mm. It was found that the reduction factors for the elastic modulus for the transient state and steady state method are convergent with exception at 400 and 500ºC (Fig. 2.7). Neither elastic modulus nor yield strength reduction factors agree with EN 1993-1-2:2005 (2005) design for hot-rolled steels (Figure 2.7 and Figure 2.8). The reviewed version of EN 1993-1-2:2005 (2005) presents new yield strength reduction factors for hot-rolled

steel class 4 cross-section, but it is still limited since they still not converge with the proposed values by (Outinen et al., 2000).
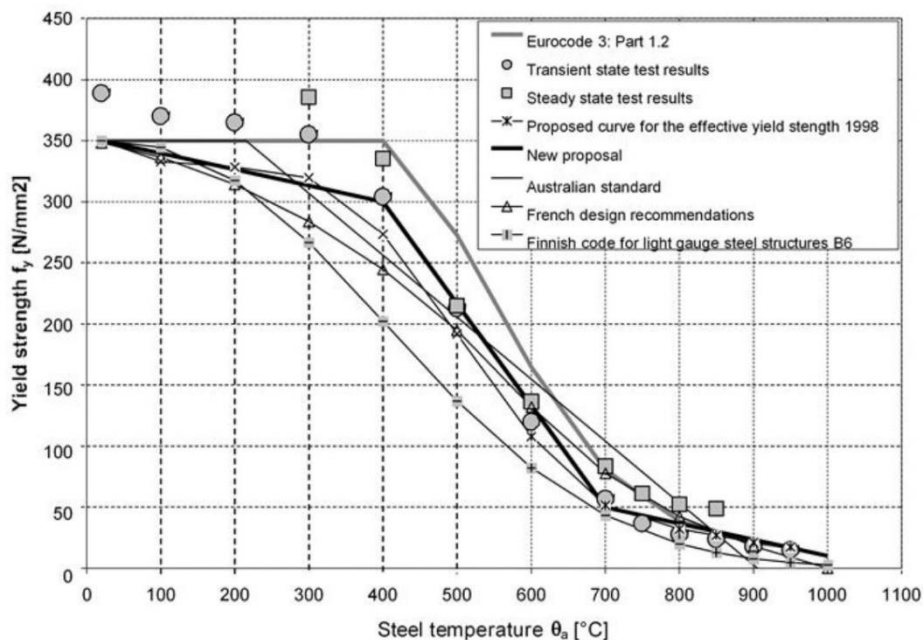
Figure 2.7 - Yield strength of structural steel S350GD+Z determined form test results compared with yield strength given in different design codes (Outinen et al., 2000)
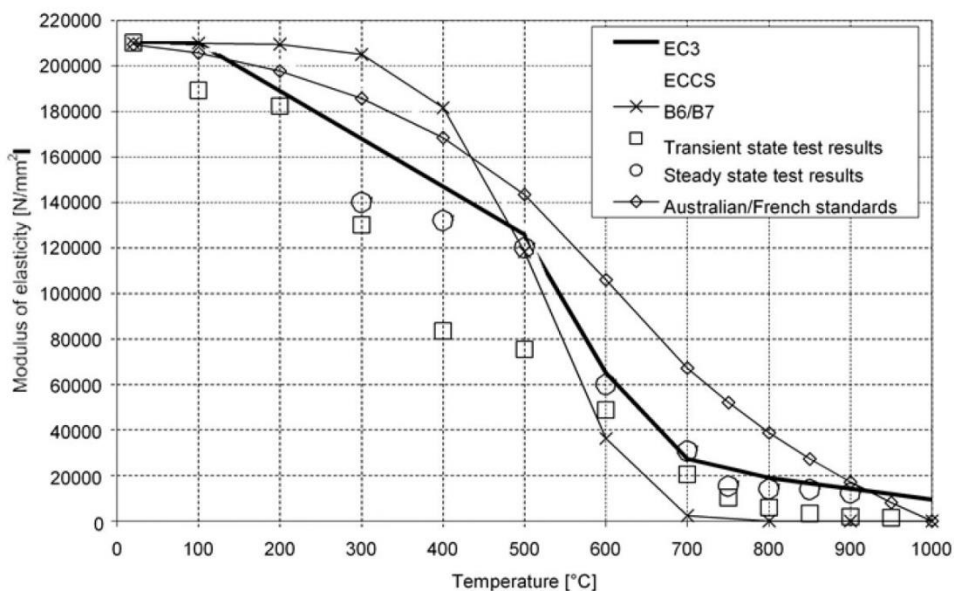
Figure 2.8 - Modulus of elasticity of structural steel S350GD+Z determined form test results compared with yield strength given in different design codes (Outinen et al., 2000)

Later on, Outinen and Makelainen (2002), conducted an experimental research on the mechanical properties of structural steel at elevated temperatures and after cooling down, in

which the steel S350GD+Z was tested. The authors established a comparison between the tensile tests taken before and after high temperature (heated up to 950ºC) compression tests, and it was observer that after cooling down the mechanical properties seemed to be near the nominal values of the material (Figure 2.9). Bear in mind for the importance of this observation regarding the buckling load of a steel structure after fire, which may still be useful if the distortions are within the shape and straightness tolerances of the structure (Craveiro, 2015).
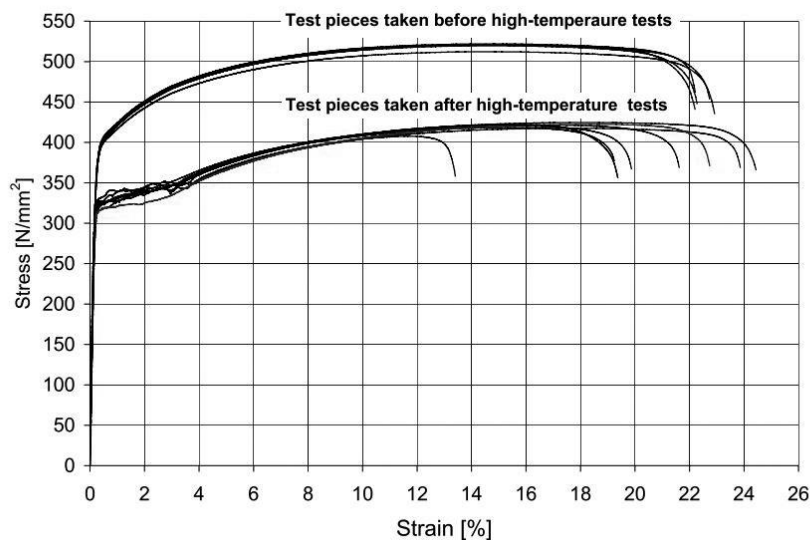
Figure 2.9 - Tensile tests for specimens taken before and after high temperature compression
tests (Outinen and Mäkeläinen, 2002)

Another experimental study on cold-formed steel at elevated temperatures (Chen and Young, 2007b) was presented. This research leans on the deterioration of the mechanical properties of cold-formed steel grades G550 and G450 at elevated temperatures (up to 1000ºC). The reduction factor of 0.2% yield strength was compared with both Australian and British standards, and with the European standard as well EN 1993-1-2:2005. It was observed that the Australian standard provides conservative predictions between 220ºC and 400ºC, and unconservative between 450ºC and 850ºC. Still regarding the yield strength, it was also observed that the reduction factors of 2% predicted in the EN 1993-1-2:2005 were conservative for G450 for temperatures roaming from 20ºC to 550ºC and G550 for temperatures roaming from 20ºC to 400ºC. The predictions presented in the EN 1993-1-2:2005 were very different from the results observed for the G450 and G550, for temperatures above 660ºC and temperatures between 450 and 800ªC.

Ranawaka and Mahendran (2009) and Kankanamge and Mahendran (2011) conducted a study on the mechanical properties of CFS at elevated temperatures leaning on the influence of the strength and thickness of steel plates. Steady state was the test method chosen by the authors to access the mechanical properties of CFS specimens. A great number of tensile tests were performed with temperatures ranging from 20ºC to 800ºC using G550 and G250 with

thicknesses of 0.60, 0.80 and 0.95mm (Ranawaka and Mahendran, 2009). In the second case the temperatures roamed from 20ºC to 700ºC for G250 with the thicknesses of 1.55 and 1.95mm, and for G450 with the thicknesses of 1.50 and 1.90mm (Kankanamge and Mahendran, 2011). It was observed that the reduction factors changed with the strength of the steel, but the thickness of the plate had no influence at all. Regarding the influence of the strength of the steel in the yield strength, it was also observed that for lower temperatures, low class steels lose their resistance quickly than the high class, but on the other hand, after 400ºC the opposite occurs, being the high class steel losing the resistance faster than the low class steel. The authors hold the process of manufacturing responsible by these differences in the deterioration of the resistance of these two types of steel, enhancing that when submitted to high temperatures, CFS tend to lose the resistance gained along the process. The authors established a comparison between the results obtained, the British standard, the EN 1993-1-1:2005 and some previous research (Figure 2.9), and it was observed that neither the normative or the proposals form previous studies were capable to predict with rigour the behaviour of CFS considered within their study subjected to fire. The authors proposed and presented new expressions for the reduction of the yield strength for low class and high class steels, and for the reduction of the elasticity modulus according to the temperature.
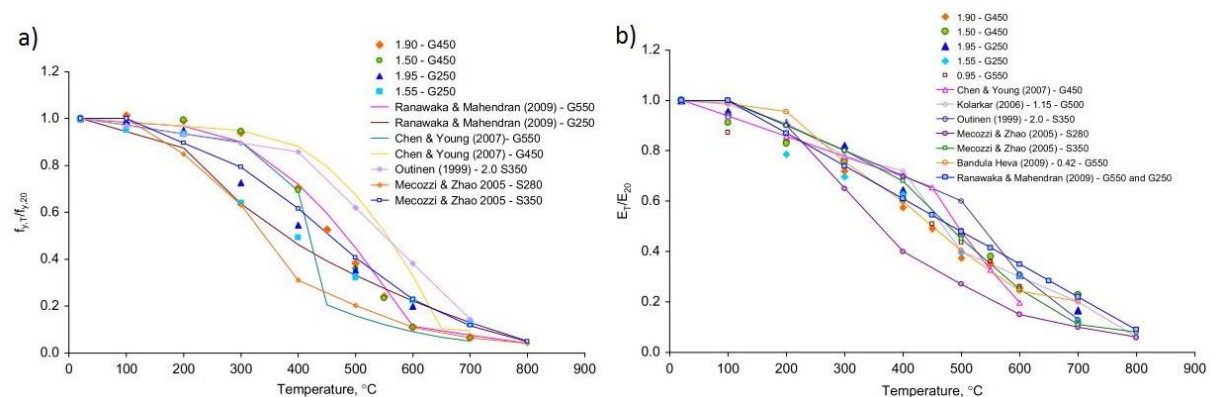
Figure 2.10- Comparison of the reduction factors obtained by Kankanamge and Mahendran with those obtained by other researchers: a) yield strength and b) elastic modulus (Kankanamge and Mahendran, 2011)

2.4 Residual stresses

Residual stresses are commonly present in steel structural elements due to manufacturing processes. In hot-rolled steels residual stresses result from uneven air cooling after hot-rolling or welding (assuming a uniform thickness of the member), as for cold-formed steels the residual stresses are generally of flexural or through thickness variation and result from the cold-forming process and coiling and uncoiling process (Yu and LaBoube, 2010). Usually it is difficult to accurately know the values to adopt for residual stress in numerical models, this leads to an overlook of the residual stresses, or alternately, modifying the stress-strain curve in order to obtain the desired effect.

In cold-formed steel members, opposing to what happens in hot-rolled steels, the values of residual stresses change through the thickness variation of the cross-section. This variation of residual stresses leads to a prematurely yielding on the faces of cold-formed steel plates (Schafer and Peköz, 1998a).

There are two different types of residual stress, namely membrane residual stress and flexural residual stress (Figure 2.11). Shafer and Peköz (1998) presented a study on characterizing geometric imperfections and residual stresses, from which they concluded that membrane residual stresses are averagely lower when compared to flexural residual stresses, and considering that, it can be ignored. For press-braked sections that takes even more relevance, since residual stress are still more common in rolled-formed members that in press-braked members (Table 2.2 and 2.3). It can also be observed in Table 2.2 that residual stresses in the corners are lower for rolled formed sections than for press-braked sections, the opposite happens in the flat portions of the sections.
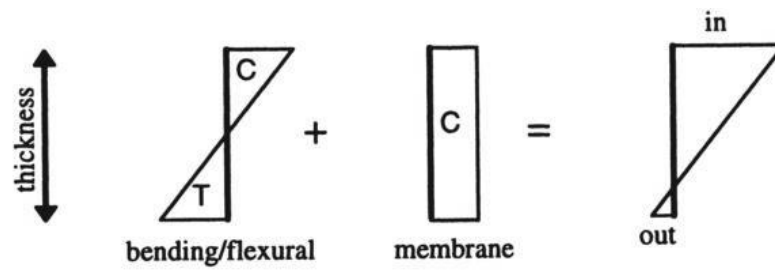
Figure 2.11- Definition of flexural and membrane residual stress

| | Roll-formed | | Press-braked | |
Element	Mean	Variance	Mean	Variance
Corners	6.8	1.1	5.2	0.4
Edge stiffened	3.9	1	0.9	1
Lip	7.9	1.5	0.2	0.3
Stiffened	-1.7	1.2	0.9	0.1

Table 2.2- Membrane residual stress as %f_y (Schafer and Peköz, 1998a)

| | Roll-formed | | Press-braked | |
Element	Mean	Variance	Mean	Variance
Corners	26.8	5.0	32.7	3.3
Edge stiffened	23.5	1.0	8.0	2.5
Lip	6.7	6.4	56.0*	11.6
Stiffened	38.9	6.2	16.9	4.5

* Some flips are flame-cut, thus distorting this value

Table 2.3- Flexural residual stress as %f_y (Schafer and Peköz, 1998a)

2.5   Geometric imperfections

Geometric imperfections take a major importance in CFS members due to fabrication process, in these imperfections are mostly presented under the form of, bowing, warping, twisting and local deviations (Schafer and Peköz, 1998a). There are two types of geometric imperfections, local imperfection and global imperfection, the first influences the distortional buckling capacity, and second the buckling load of the member. One of the main problems regarding to CFS's modelling is the definition of the initial state of the element in terms of geometric imperfections (Craveiro, 2015).

To consider the effect of global imperfections usually it is considered a sinusoidal curve along the member (Kaitila, 2002). Kaitila (2002), conducted an imperfection sensitivity analysis, using the finite element analysis software *Abaqus* (2014), of lipped channel columns in order to perform an analysis. In this research was observed a relation between the magnitude of initial imperfections and the ultimate load. The author suggests the values for initial imperfections used to determine the ultimate loads, *h/200* for local imperfection and values ranging from *L/1000* to *L/400* for global imperfections.

Schafer and Peköz (1998), developed a probabilistic study on geometric imperfections in cold-formed steel members as mentioned before. In this research the authors established two types of local imperfections: maximum local imperfection in a stiffed element (local buckling), and deviation from straightness for a lip stiffened or unstiffened flange (distortional buckling). The first type is represented by d_1, and the second type is represented by d_2 in Figure 2.12. The authors concluded that the maximum value of the initial deformation depends on the thickness of the plate, being approximatly equal to $6te^{-2t}$ being t the thickness of the plate in mm or to 0.006b with b being the with of the section also in mm (Figure 2.12 a)). The maximum value for the initail buckling of the flanges is approximatly equal to the thickness of the plate (Figure 2.12 b)). For local imperfections is the authors assumed a sinusoidal curve along the web, followed by a smoothly buckle in the flanges.
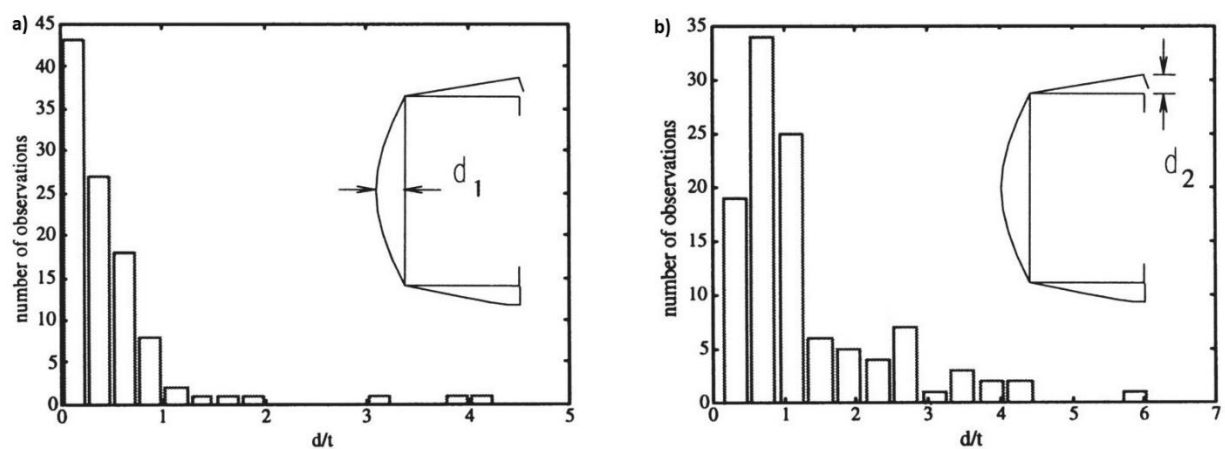
Figure 2.12- Histogram of local imperfections: a) type 1 and b) type 2 (Schafer and Peköz, 1998a)

2.6   Cold-Formed Steel Columns at Ambient Temperature

As previously mentioned cold-formed steel columns are usually associated to instability modes, due to high slenderness and low torsional rigidity. Normally steel sections may be subjected to one of four types of buckling. There are three different major types of general buckling modes, namely local buckling, global buckling and distortional buckling.

Local buckling is particularly prevalent in cold-formed steel sections and is characterised by the relatively short wavelength buckling of individual plate element (Dubina, 2005). Global buckling embraces Euler (flexural) and flexural-torsional buckling of columns and lateral-torsional buckling of beams (Dubina, 2005). Sometimes referred to as "rigid-body" buckling because any given cross-section moves as a rigid body without any distortion of the cross-section (Dubina, 2005). Distortional buckling, is the buckling that occurs as a consequence of distortion of the cross-section. In cold-formed sections, it is characterised by relative movement of the fold-lines (Dubina, 2005). The wavelength of distortional buckling is generally intermediate between that of local buckling and global buckling (Dubina, 2005). These instability modes can interact with one another as well with global buckling, in Figure 2.13 both single and interactive (coupled) modes of instability can be observed for a lipped channel section in compression.
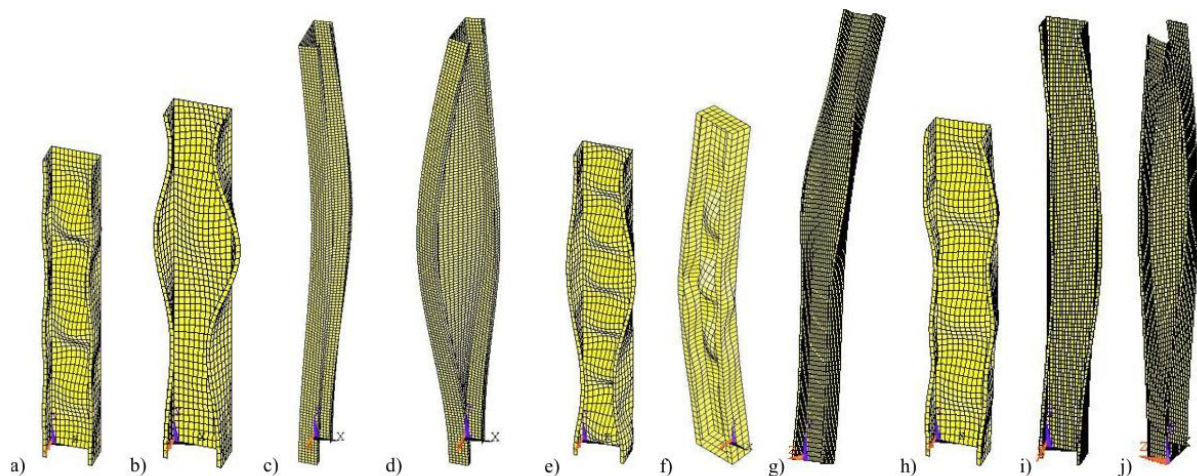
Figure 2.13 - Buckling modes for a lipped channel in compression Single modes: a) local; b) distortional; c) flexural; d) flexural-torsional; e) local and distortional; f) flexural and local; g) flexural and distortional; h) flexural-torsional and local; i) flexural-torsional and distortional; j) flexural and flexural-torsional (Dubina et al., 2012)

2.7   Research on cold-formed steel columns

Over the past few decades there is been major improvement in cold-formed steel members, and it's due to many factors, namely corrosion protection and improved technology of manufacture. As consequence to a better structural solution, its demand in the market of building construction

increased leading on to the development of a great number of studies on this subject. The researchers have been focused on the behaviour of cold-formed steel members over the last few decades, testing different cross-sections, different support conditions as well as different lengths. Following the experimental research numerical models have also been developed using the Finite Element Method (FEM) in order to validate additional parametric studies. Some of them are briefly described within this section.

2.7.1 Behaviour at ambient temperatures

An experimental study testing compressed plain channels with two different cross-sections and lengths ranging from 280 mm to 3500 mm was performed by Young and Rasmussen (1998) with pinned and fixed end support conditions. The specimens tested were manufactured by a press-braking machine. Regarding the failure modes, the authors concluded that the local buckling does not induce overall bending in fixed-ended singly symmetric columns as it does in pin-ended singly symmetric columns. Later, and based on Young and Rasmussen (1998) experiment, a finite element model was developed and validated (Yan and Young, 2002). After the development of parametric studies using the finite element model developed, the objective was to understand the influence of the cross-section geometry. To accomplish that objective, different geometrical parameters were tested namely, the width of the web (ranging from 100 to 200 mm) and the thickness (with 1.5, 3.0 and 6 mm) while the flanges were kept constant (with 80 mm). Both experimental and numerical studies were compared with the American, Australian and European standards, and it was observed that the design methodologies were conservative.

Later, parametric studies were developed by Yan and Young (2004), based on the experimental research developed by Yan and Young (2002). An advanced non-linear finite element model incorporating geometric imperfections and material non-linearity was developed and verified against experimental results.

Based on a series of compression testes on lipped channel columns with web and flange stiffeners, once again braked-pressed, Yang and Hancock (2004) studied the local and distortional buckling as well as the interaction between both. The specimens were fabricated with structural steel G550 with lengths ranging from 360 to 2000 mm and 0.42 mm thickness, and were tested with fixed-ended support conditions. It was observed that the columns showed a very high post local buckling strength, and for columns with intermediate length, the ultimate strength was reduced due to local and distortional buckling interaction (Yang and Hancock, 2004). Three kinds of failure modes were observed during the experimental tests, namely with the flanges going inwards, the flanges going outwards, and with one flange moving inwards as the other one moving outward. The experimental results were compared with the Australian standard (AS/NZS 4600, 1996) and it was observed an unconservative prediction at intermediate lengths because it ignores interaction of local and distortional buckling, and

Experimental and numerical analysis of compressed cold-formed steel
elements with sigma plus cross-section subjected to fire

2 LITERATURE REVIEW

American standard (AISI, 2001) which also gave unconservative predictions since it ignores distortional buckling (Yang and Hancock, 2004).

Yan and Young (2002) developed an experimental investigation on cold-formed steel channels with complex stiffeners subjected to pure axial compression for fixed-ended columns. The specimens tested were braked pressed from high strength zinc-coated G450 structural steel sheets with 1.5 and 1.9 mm thickness, lengths ranging from 500 to 3500 mm, while the complex stiffeners were simple lips with return lips (Figure 2.14). Generally, the failure modes observed in the tests were combined, local and distortional buckling for short and intermediate columns, and an interaction between local and flexural-torsional buckling for longer columns. The authors then compared the experimental results with the design methodologies presented by the American standard (AISI, 2001), and the Australian standard (AS/NZS 4600, 1996). The predictions presented by AISI (1996) was found to be unconservative while the predictions given by AS/NZS 4600 (1996) were found to be conservative due to the fact that the standard had a separate check for distortional buckling of singly symmetric sections.
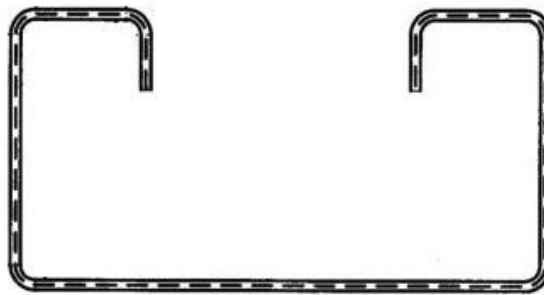
Figure 2.14 - Configuration of the tested cross-section (Yan and Young, 2002)

A numerical study on the post-buckling behaviour of pinned channel columns undergoing local/distortional, distortional/global, local/distortional/global buckling mode interaction was developed by Camotim and Dinis (2011). The results were obtained using the finite element analysis software *Abaqus* (2014). For the initial geometric imperfections magnitudes of *0.1t* for local and distortional imperfection and *L/1000* for global imperfection were adopted. The authors found that the columns were affected by interaction between local, symmetric distortional and anti-symmetric flexural-torsional-distortional, and distortional-flexural-torsional modes. It was also observed that the imperfections responsible for lower column strength are pure distortional for columns with local and distortional buckling interaction, and pure global for columns with interaction between distortional and global buckling or the interaction between the three failure modes local, distortional and global (Camotim and Dinis, 2011).

Testing sigma single cross-sections, Young and Chen (2008) presented an experimental research on compressed fixed-ended cold-formed steels built-up closed sections with intermediate stiffeners. The two single sections (Figure 2.15 a)) were fastened in the flanges

with self-tapping screws 100 mm spaced (Figure 2.15 b)). Two types of steel were tested, namely G450 and G550, with lengths ranging from 300 to 3000 mm, and with 1.5, 1.9, and 1.0 mm thickness. For shorter columns, the predominant failure mode observed was the interaction between local and distortional buckling while for longer columns was the interaction between flexural and distortional buckling.
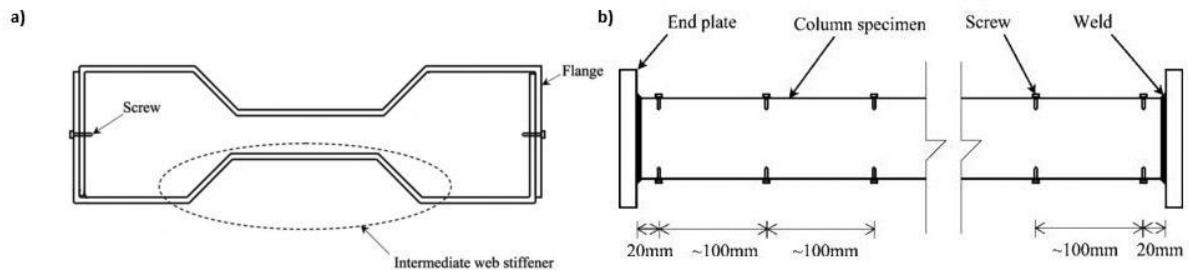
Figure 2.15 – a) Cross section of cold-formed steel member and b) arrangement of screw spacing (Young and Chen, 2008)

Zhang and Young (2012) developed and presented a series of columns tests on cold-formed steel built-up I-shaped open sections with edge and web stiffeners (Figure 2.16). Different geometric parameters were tested, namely thickness and length. The failure modes observed by the authors were distortional buckling for shorter and intermediate columns, and interaction between distortional and flexural buckling for longer columns. For thinner columns (0.48 mm) it was observed local buckling, as for longer columns (ranging from 1400 to 3200 mm) the interaction between local, distortional and flexural buckling was observed. Thicker columns (1.2 mm) with a superior length of 2000 mm showed pure flexural buckling.
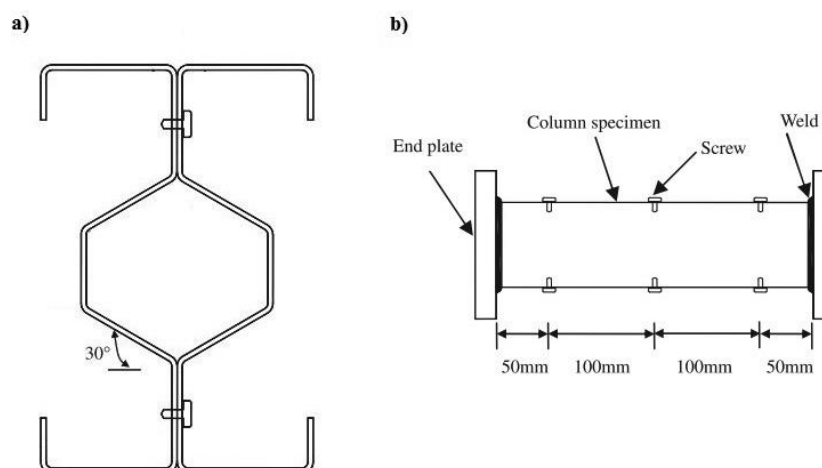
Figure 2.16 – a) Cross section of cold-formed steel member I-shaped and b) arrangement of screw spacing (Zhang and Young, 2012)

A series of axially-compressed tests on built-up box section members composed of two C-section by self-screws at flanges were conducted by Li *et al* (2014). The screws were spaced

from 300 or 600 mm, with 1 mm of thickness, and fabricated with structural steel G550. A finite element model was developed and posteriorly validated against the results obtained experimentally, from which the authors found that for screws spaced with 600 mm there was no decrease on the buckling load. The position of fasteners could improve the distortional buckling capacity of built-up sections, due to the fact of the flanges of the single sections are restrained (Li et al., 2014).

To fully understand the instability problems mentioned before, von Kàrmàn *et al* (1932) developed a research on the analysis of the behaviour of thin plates subjected to compression, and as result the author observed that when the buckling occurred, the stress diagram becomes non-uniform with a major concentration near the edges while the loading continuously increases. Von Kàrmàn (1932) introduced the concept of *"effective width"*, which consisted on the analysis of the elastic post-buckling behaviour of the plate assuming a uniform stress distribution over the effective width instead of non-uniform stress distribution over the entire plate.

Based on the design stress (σ_e) and critical elastic buckling stress (σ_{cr}), the Equation 2.1 was proposed by von Kàrmàn (1932) in order to determine the effective width of the plate.

$$\frac{b_{eff}}{b} = \sqrt{\frac{\sigma_{cr}}{\sigma_e}} \qquad (2.1)$$

With the elastic buckling stress being determined using the following equation (Equation 2.2).

$$\sigma_{cr} = \frac{k_\sigma \pi^2 E}{12(1-v^2)(b/t)^2} \qquad (2.2)$$

Later on, some modifications to this formula were proposed by George Winter in order to determine effective width of stiffened and unstiffened elements (Craveiro, 2015). It was observed that this method presented some limitations, since it required a huge amount of time for solving the equations regarding the effective width, becoming even more time consuming with complex shapes and additional stiffeners (Craveiro, 2015).

Later, Schafer and Peköz (1998b) developed a new design method called Direct Strength Method (DSM) based on the member elastic stability, this method considers the gross section instead of the effective width considered in the previous method. Applying this new method, the interaction between local buckling with flexural or flexural-torsional buckling is allowed (Schafer and Peköz, 1998b).

In order to determine the elastic buckling loads there are a great number of tools that can be used. The finite element analysis software *Abaqus* (2014) is one example, but other software based on Finite Strip Method (FSM) and the constrained finite strip method (cFSM) (Ádány

and Schafer, 2006a, 2006b) are currently the most used methods for elastic buckling prediction (Craveiro, 2015).

The Finite Strip Method is more commonly used to members with simply supported ends under longitudinal stress. In this method the member is divided in longitudinal strips, and an elastic stiffness matrix is formulated for each strip based on the plane stress assumption and Kirchhoff thin plate theory (Li and Schafer, 2010). The constrained finite strip method (cFSM) was propose by (Ádány and Schafer, 2006a, 2006b) in order to access the pure buckling modes which couldn't be individually identified by FSM. It is worth mentioning that the solutions presented by the cFSM are slightly different from the ones given by FSM and cannot be used for cross-section with corners (Craveiro, 2015). This brings a whole new problem regarding the application of the cFSM, considering that the current DSM available is calibrated to the conventional FSM. After several parametric studies Li and Schafer (2010) found out that the critical half-wavelengths could be used to automatically identify local and distortional buckling in FSM models. Given the fact that the critical half-wavelengths in cFSM can be used in FSM with rounded corners, it was suggested that the analysis of FSM and cFSM are run, and only the critical half-wavelengths values correspondent to the cFSM model are considered.

Another approach to determine the elastic buckling loads was also presented, the Generalised Beam Theory (GBT) (Silvestre and Camotim, 2002a, 2002b) which is able to perform an elastic buckling analysis with no restriction regarding the type of end-support. This approach can also characterize the buckling modes automatically. Later the cFSM was developed considering the conditions assumed in the GBT method allowing the identification and calculation of pure buckling modes (Ádány and Schafer, 2006b).

2.7.1.1 Design according to EN 1993-1-3:2006

In designing process, in order to determine the resistance of the structural member it is mandatory to find its cross-section behaviour. The EN 1993-1-1:2005 (EN 1993-1-2, 2005) established that the cross-section resistance as well as the rotation capacity are both limited by the effects of local buckling. The normative defined four different types of cross-sections types depending on material yielding strength, width-to-thickness ratios of individual compression parts, and loading arrangement. Usually cold-formed steel cross-sections are considered Class 4, which means that the local buckling will occur in the elastic range, before the yield stress is achieved in at least one part of the cross-section. Design guidelines for the verification of local, distortional, global flexural and global flexural-torsional are present in EN 1993-1-1 (EN 1993-1-1, 2005), EN 1993-1-2 (EN 1993-1-2, 2005), and in the EN 1993-1-5 (EN 1993-1-5, 2006). The guidelines presented in EN 1993-1-3 (EN 1993-1-3, 2006) allow the determination of the effective areas for Class 4 cross-section used for cold-formed steels.

According to the current normative the effective area of a flat compression element is determined using Equation 2.3:

$$A_{c,eff} = \rho A_c \tag{2.3}$$

Where ρ is the reduction factor used to determine the effective width (b_{eff}) based on the compressive stress in the element $\sigma_{com,Ed}$, and A_c is the gross area of the compression element.

If $\sigma_{com,Ed} = f_{yb}/\gamma_{M0}$ the reduction is determined by the following equations (Equations 2.4 and 2.5) (EN 1993-1-5, 2006):

- For internal compression elements:

$$\rho = 1 \qquad\qquad \text{for } \bar{\lambda}_p \leq 0.5 + \sqrt{0.085 - 0.55\psi} \tag{2.4}$$

$$\rho = \frac{\bar{\lambda}_p - 0.055(3 + \psi)}{\bar{\lambda}_p^2} < 1.0 \qquad \text{for } \bar{\lambda}_p > 0.5 + \sqrt{0.085 - 0.55\psi} \tag{2.5}$$

- For outstand compression elements (flange type):

$$\rho = 1 \qquad\qquad\qquad \bar{\lambda}_p \leq 0.748 \tag{2.6}$$

$$\rho = \frac{\bar{\lambda}_p - 0.188}{\bar{\lambda}_p^2} < 1.0 \qquad\qquad \text{for } \bar{\lambda}_p > 0.748 \tag{2.7}$$

With the ψ as the stress ratio, and the plate slenderness, $\bar{\lambda}_p$ can be determined by (Equation 2.8):

$$\bar{\lambda}_p = \frac{\bar{b}/t}{28.4\varepsilon\sqrt{k_\sigma}} \tag{2.8}$$

Being $\bar{b}$ the appropriate width, t the thickness of the plate and k_σ the buckling factor corresponding to the stress ratio ψ and boundary conditions. If the condition $\sigma_{com,Ed} < f_{yb}/\gamma_{M0}$ verifies, then the reduction factor ρ should be obtained using the reduction plate thickness $\bar{\lambda}_{p,red}$ (Equation 2.9):

$$\bar{\lambda}_{p,red} = \bar{\lambda}_p \sqrt{\frac{\sigma_{com,Ed}}{f_{yb}/\gamma_{M0}}} \tag{2.9}$$

The normative assumes that the stiffeners form plane elements with edge stiffeners behave as a compression member, and so it is represented by a linear spring depending on the boundary conditions and the flexural stiffness of the adjacent plate elements. The cross-section of an edge stiffener should be taken as comprising the effective portions of the stiffener, or stiffeners if that is the case, plus the adjacent effective portion of the plane element (Figure 2.17).

The first step of the procedure is to determine an initial effective cross-section for the stiffener using effective width for local buckling assuming that the stiffener gives full restraint and that

$\sigma_{com,Ed} = f_{yb}/\gamma_{M0}$. The initial values for the effective width c_{eff}, presented in Figure 2.13, are given by the following expression (Equation 2.10):

$$c_{eff} = \rho b_{p,c} \tag{2.10}$$

The buckling factor is obtained differently on this case:

$$k_\sigma = 0.5 \qquad\qquad \text{for } b_{p,c}/b_p \le 0.35 \tag{2.11}$$

$$k_\sigma = 0.5 + 0.83 \sqrt[3]{(b_{p,c}/b_p - 0.35)^2} \qquad \text{for } 0.35 < b_{p,c}/b_p \le 0.6 \tag{2.12}$$

where, $b_{p,c}$ and b_p are the width of the edge stiffener and the flange width for a lipped channel section respectively (Figure 2.17).
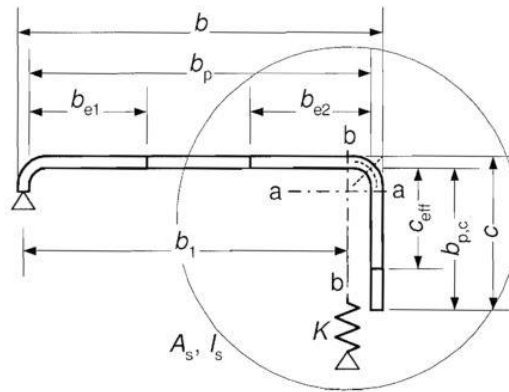
Figure 2.17 - Edge stiffener of a lipped channel section.

The elastic buckling stress $\sigma_{cr,s}$ for an edge stiffener should be obtained from (Equation 2.13):

$$\sigma_{cr,s} = \frac{2\sqrt{KEI_s}}{A_s} \tag{2.13}$$

where:

K is the spring stiffness per unit length;

I_s is the effective second moment of area of the stiffener, taken as that of its effective area A_s about the centroidal axis a-a of its effective cross-section (Figure 2.17);

Finally, the design buckling resistance of a compression member with a class 4 cross-section can be calculated using Equation 2.14 (EN 1993-1-1, 2005):

$$N_{b,Rd} = \frac{\chi A_{eff} f_y}{\gamma_{M1}} \tag{2.14}$$

For axial compression, the reduction factor χ should be determined using the following expression (Equation 2.15):

$$\chi = \frac{1}{\phi + \sqrt{\phi^2 - \bar{\lambda}^2}} \qquad \text{but } \chi \le 1.0 \qquad (2.15)$$

where,

$$\phi = 0.5[1 + \alpha(\bar{\lambda} - 0.2) + \bar{\lambda}^2] \text{ and } \bar{\lambda} = \sqrt{\frac{A_{eff}f_y}{N_{cr}}} \text{ for class 4 cross-sections.}$$

α is the imperfection factor, corresponding to the appropriate buckling curve, according to the type of cross-section, axis of buckling and yield strength used (EN 1993-1-1, 2005);

N_{cr} is the elastic critical force for the relevant buckling mode based on the gross cross sectional properties.

2.7.2 Behaviour under fire conditions

There is a well-known lack of research and studies on cold-formed steel structures under fire conditions when compared to hot-rolled structures. This results in a series of specific guidelines for hot-rolled steels under fire conditions, namely EN 1993-1-2:2005 (EN 1993-1-2, 2005), and the lack of the same specific guide lines for cold-formed steels. The methods presented in the EN1993-11-2:2005 (EN 1993-1-2, 2005) for hot-rolled steels are also applicable to cold-formed steel members with class 4 cross-sections, establishing the same reduction factors for the yield strength and limiting the critical temperature up to 350ºC.

A research was developed by Feng et al (2003b) on lipped and unlipped short channel columns, with and without perforations, at elevated temperatures with the objective to gain a better understanding of its physical behaviour and failure modes. The fire tests were conducted were performed with different temperatures, namely 250, 400, 550, and 700 ºC, in which the columns could freely expand. After the desire temperature was achieved the specimens were then applied an axial compression load until failure. From the experimental tests two main issues were observed, the first was the predominant failure mode observed was an interaction between local and distortional buckling, and second, that columns with same cross-section can have different failure modes depending on the initial imperfections. Later a finite element model was developed and calibrated against this experimental research (Feng et al., 2003a). The results obtained from the experimental analysis were then compared with some design methodologies at ambient temperature, and it was showed that the formulations available for ambient temperature could be extendable to elevated temperatures, using the reduced yield strength and the reduced elastic modulus.

An investigation on the behaviour of CFS lipped channel columns at elevated temperatures using the software *Abaqus* (2014) was performed by Chen and Young (2007a) based on the stress-strain curve equations previously developed for CFS members at elevated temperatures by Chen and Young (2007b). In this finite element model was validated against the

experimental results, testing different cross-sections and lengths within the parametric study. The results obtained were compared with some design methodologies, in which the author concluded that using properly reduced material properties the design provision give conservative results.

Craveiro et al. (2014) developed a research in order to gain access to the fire behaviour of CFS lipped channel C and built-up 2C (I) slender columns with restraint to thermal elongation. The parameters studied in this experimental investigation were, the stiffness of the surrounding structure, type of cross-section, end-support conditions and initial applied load level in the columns. The initial applied load corresponded to 30% and 50% of the design buckling load at ambient temperature, as for the axial stiffness of the surrounding structure the values tested were 3 kN/mm and 13 kN/mm. Two end-support conditions were tested, namely semi-rigid and pin-ended. All specimens studied were fabricated with structural steel S280GD+Z, galvanized with zinc on each side and with 2.5 mm thick. With the obtained results, the authors concluded that the end-support conditions and initial applied load level on CFS columns may affect significantly their fire performance. As for the level of axial restraint, it is stated that it may also affect significantly the critical temperature on CFS columns, especially on built-up columns. With higher values for the stiffness of surrounding structure, higher will be the maximum restraining forces, for both cross-sections. The authors also considered that for lipped channel columns with 30% load level the limit of 350ºC for the critical temperature may be conservative, whereas for built-up columns, that limit could be realistic.

2.7.2.1 Design rules according to the EN 1993-1-2:2005

The normative establishes specific design guideline steel compression elements divided in four classes. For class 4 cross-sections the area and the section modulus it is replaced by an effective area and an effective section modulus respectively. Additionally, the normative presents the same yield stress reduction factors for class 4 cross-section for both hot-rolled and cold-formed steels without distinguish one from the other.

The design buckling resistance, of a compression member can be obtained with the following equation (Equation 2.16):

$$N_{b,fi,t,Rd} = \chi_{fi} A k_{y,\theta} f_y / \gamma_{M,fi} \qquad (2.16)$$

where,

χ_{fi} is the reduction factor for flexural buckling in a fire design situation;

$k_{y,\theta}$ is the reduction facto for the yield strength of steel at the temperature θ_a;

$\gamma_{M,fi}$ partial safety factor for fire situation.

The values of χ_{fi} should be taken as the lesser of the values of $\chi_{y,fi}$ and $\chi_{z,fi}$ determined according to (Equation 2.17a):

$$\chi_{fi} = \frac{1}{\varphi_\theta + \sqrt{\varphi_\theta^2 - \bar{\lambda}_\theta^2}} \tag{2.17a}$$

with,

$$\phi_\theta = \frac{1}{2}[1 + \alpha\bar{\lambda}_\theta + \bar{\lambda}_\theta^2] \tag{2.17b}$$

and the imperfection factor, α (Equation 2.17c):

$$\alpha = 0.65\sqrt{235/f_y} \tag{2.17c}$$

The non-dimensional slenderness $\bar{\lambda}_\theta$ for temperature θ_a is determined with the following expression (Equation 2.17d):

$$\bar{\lambda}_\theta = \bar{\lambda}[k_{y,\theta}/k_{E,\theta}]^{0.5} \tag{2.17d}$$

with,

$k_{E,\theta}$ is the reduction factor for the modulus of elasticity at the steel temperature θ_a;

$\bar{\lambda}$ is the non-dimensional slenderness at ambient temperature.

where,

l_{fi} is the buckling length of the column in fire situation;

i is the minimum radius of gyration;

E is the elastic modulus at ambient temperature;

f_y is the yield strength at ambient temperature.

2.8　Final remarks

Through the present chapter, a series of developed studies among the last few years were presented with the clear objective to understand the mechanical behaviour of cold-formed steel columns specially when subjected to fire.

It was also presented a relevant analysis regarding the current standard for Europe (EN 1993-1-2, 2005) which in this case was showed to have a few limitations, proving the need to be reviewed in order to obtain better results that can accurately represent real life conditions. It is of extreme importance to accurately evaluate both mechanical and thermal properties of CFS, and from the researches showed previously it is clear the current guidelines (EN 1993-1-2, 2005) available for CFS members are not applicable. The predicted yield factors presented in EN 1993-1-2 (2005) were proven to be conservative for several high steel structural types in

several ranges of temperatures. A few experimental researches has showed that the predictions available in the EN 1993-1-2 (2005) are very different from the respectively results (Chen and Young, 2007b).

The current European standard, EN 1993-1-3 (2006), and both design methods available, namely the Direct Strength Method and the Effective Width Method, regarding behaviour of CFS columns at ambient temperature are able to determine the strength of a single CFS column. In the case of built-up columns there is still a lack of research, and as a consequence the available standardise guidelines only suggest small recommendations for built-up columns (Craveiro, 2015).

Regarding the behaviour of CFS columns when subjected to fire there are a few important studies both experimental and numerical, however there are no specific standardised methodologies for the design of CFS columns when subjected to fire. The main problem lies in the fact that the guidelines presented in EN 1993-1-2 (2005) for hot-rolled steels with class 4 cross-section are also applicable to cold-formed steels, using the same reduction factors and fixing the critical temperature in 350ºC, which was already proven to be conservative (Craveiro et al., 2014).

3   EXPERIMENTAL   ANALYSIS   ON   COLD-FORMED   STEEL COLUMNS

3.1   Introduction

In the present chapter, the experimental investigation on cold-formed steel columns with sigma-plus cross-section at fire conditions is thoroughly detailed. This research was developed on a test set-up capable to simulate both rotational and axial stiffness of the surrounding structure of a CFS column. The results obtained experimentally and presented here will endorse a better understanding about the behaviour of CFS columns subjected to fire, act as a strong basis supporting both calibration and validation of the numerical model developed further, which will allow to extend the research to greater number of different types of CFS columns, taking an important role in the definition of new design methodologies.

3.2   Test specimens

The CFS specimens experimentally tested in this research were supplied by the company voestalpine Sadef nv (http://www.sadef.com). Two different types of sigma-plus cross-sections were used in this investigation, namely single and built-up. The sigma-plus profiles were fabricated using high strength steel S320GD+Z275 (zinc coating of 0.04 mm ($275g/m^2$), yield strength of 280 MPa and an ultimate tensile strength of 360 MPa, according to EN 10346 (2015)) with 2950 mm long, 250 mm tall, 70 mm wide and with 2.5 mm thickness. The edge stiffeners were 25 mm tall with a 3 mm inside bend radius, while the intermediate stiffeners had an angle of 60º with the web of the profile with the same inside bend radius. The built-up columns were fastened using self-drilling screws Hilti S-6.3×19MD03Z along the length of the column spaced 625 mm.
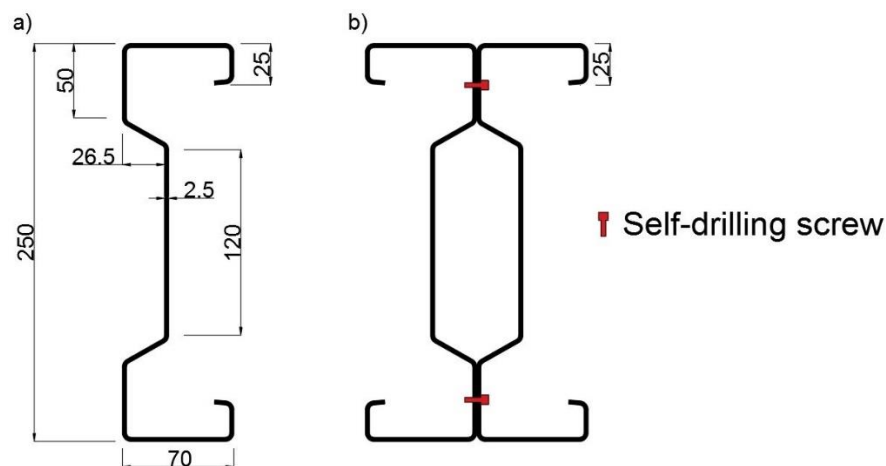
Figure 3.1 - Dimensions of the cross-section studied (unities in mm) a) single and b) built-up.

3.3   Test Set-Up

The experimental system adopted to test the CFS columns was developed in UC, which bears a variable system allowing to simulate different types of axial stiffness. The advantage of having a three-dimensional system allows not only the access to different levels of axial stiffness but also to rotational stiffness imposed by the surrounding structure to a CFS column subjected to fire. This experimental system was previously developed by many authors such as Craveiro (2015) and Laím (2013).

The test set-up used to test the CFS columns include a two-dimensional reaction steel frame (1 in Figure 3.2) and a three-dimensional restraining steel. The two-dimensional reaction frame is composed by two HEB 500 columns 6600 mm tall and one HEB 600 beam 4500 mm long with M27 grade 10.9 bolts in the connections. The three-dimensional restraining steel (2 in Figure 3.2) comprises two HEB 300 columns and four HEB 400 beams with S355 steel orthogonally disposed in the bottom and on the top of the structure with stiffeners within the flanges. To connect the different structural members of the three-dimensional restraining steel were used M24 grade 10.9 bolts, except the connections between the peripheral columns and the top beams that was used threaded rods M27 grade 10.9.

Figure 3.2 - Global view of the experimental set-up

The CFS columns tested are subjected to a constant compression loading in order to simulate the load that an ordinary column is normally subjected in a structure. This loading was applied in the column through a Enerpac RR-1006 hydraulic jack (3 in Figure 3.2) with a maximum loading capacity in compression of 933 kN supported by the two-dimensional reaction steel frame. The applied loading was controlled by a TML CLC-100A load cell (4 in Figure 3.2) with maximum compression capacity of 1000 kN, placed between the top beams of the three-dimensional restraining steel and the hydraulic jack. Additionally, the load cell is connected to servo hydraulic central unit W+B NSPA700/DIG2000 (5 in Figure 3.2), where the applied loading could be measured and kept constant during all the test.

The thermal action was applied by a vertical modular electric furnace of Termolab (6 in Figure 3.2) programmed to reproduce the standard fire curve ISO 834 (1999). This furnace was composed by two vertical modules of 1500x1500x1000 mm with 90 kVA of power and one last of 1500x1500x500 mm with 45 kVA of power. When the two parts of the furnace merge together, a closed chamber was conceived around the CFS column.

The end-support devices were specifically designed and built (Figure 3.3) to test both pinned and fixed-end support conditions. Built with a set of plates, a steel pin lubricated with Teflon lined with 1 mm thickness, a rectangular hollow section welded to the top of the steel plate and to the end-support device. The adjustment of the inner steel plates was made using bolts and nuts welded to the holes were the bolts came through. This way it was possible to test both single and built-up columns on the same end-support devices. This type of end-support device lead to different lengths for fixed and pinned-end columns, 3050 and 2850 mm respectively, that were taken into account on the calculations of the buckling loads for the tested columns.
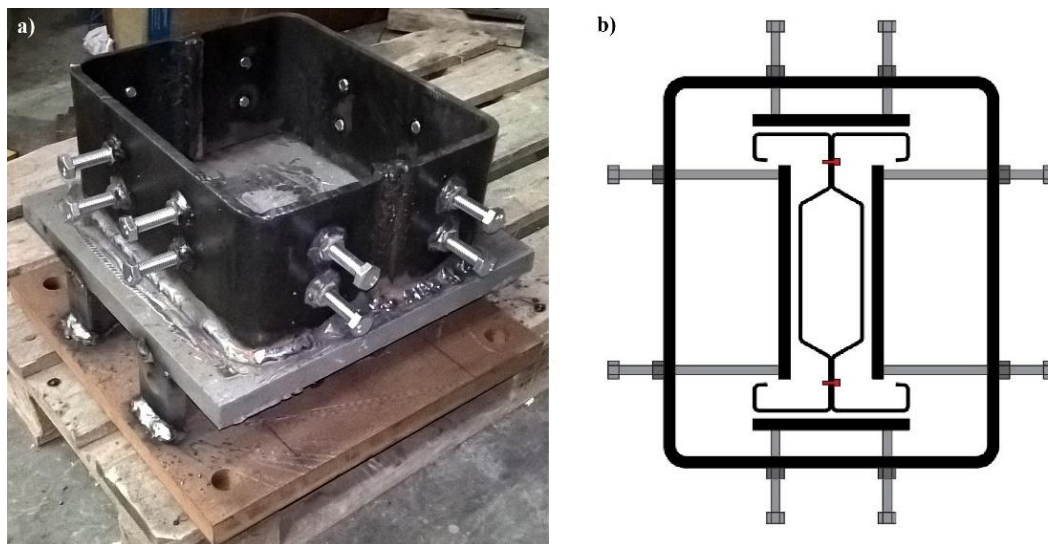
Figure 3.3 - a) End-support device and b) Schematic of the adjustable system adopted to fix the tested specimens

A special device was built in order to measure the restraining forces generated on the testing CFS column during the heating process (7 in Figure 3.2) as a result of the thermal expansion that the column is subjected. This device it consists a hollow steel cylinder, rigidly connected to the top of the three-dimensional restraining steel, which bears inside another steel cylinder rigidly connected to the CFS column tested. The surface between both cylinders is covered by Teflon (PTFE) in order to minimize the friction between the cylinders. Inside the cylinders a load cell TML CLC-50A with maximum capacity of 500 kN was placed in order to access the restraining forces. The load cell is compressed when the columns starts to expand during the heating process.

To evaluate the evolution of the temperature through all the CFS column, type K (*cromel-alumel*) thermocouples were welded in specific points of the cross-section, namely on the flanges on the web and on the web-to-flange connection (Figure 3.4 b)). Five different sections were measured with four thermocouples each, making a total of twenty thermocouples (Figure 3.4).
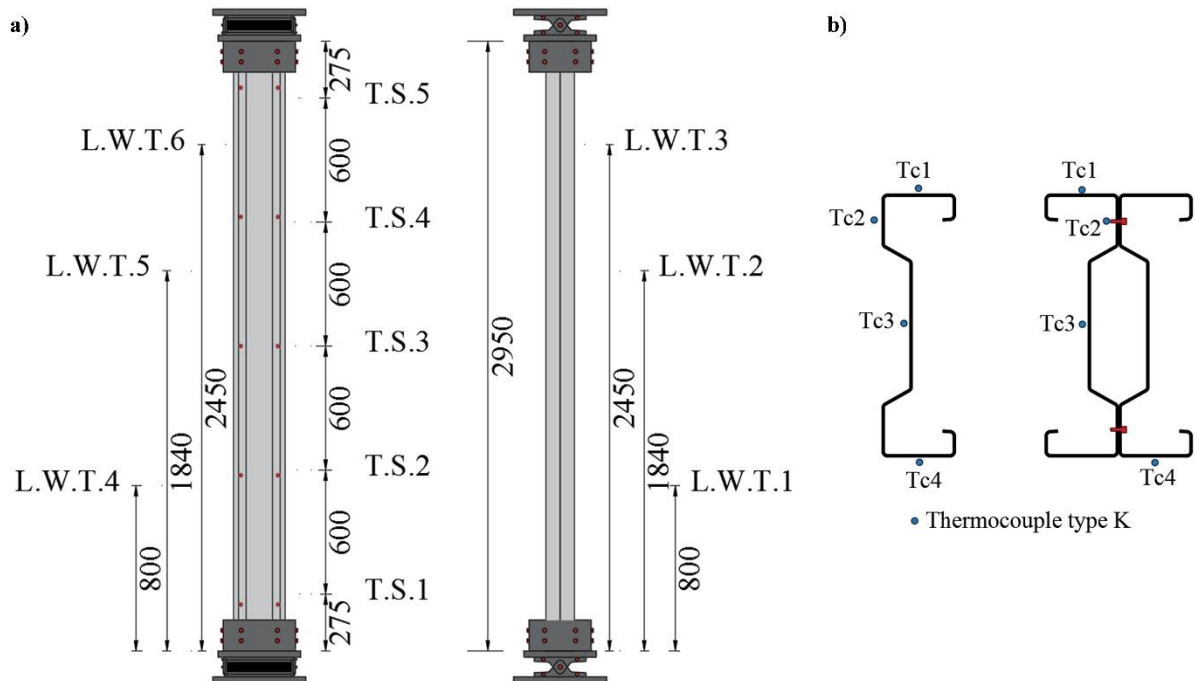
Figure 3.4 - a) Sectional positioning of thermocouples and LWT along the column and b) Positioning of the thermocouples in the cross-sections.

To access the axial displacements of the tested columns, eight linear variable displacement transducers (LVDT) TML SDP-200D and CDP-100 (Figure 3.5 b) and c)) were used, which four of them were to the bottom and the other four to the top of the column respectively. The lateral displacements were measured using 6 linear wire transducers (LWT) TML DP-1000D placed through all the column (Figure 3.4 a)), measuring the displacements in two directions (x_1 and x_2).
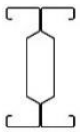
The axial stiffness ($K_{Ra} = 30$ kN/mm) of the three-dimensional restraining steel was determined based on obtained values in previous experimental studies, where the axial stiffness is determined as function of the restraining force and displacements registered (Azevedo, 2016; Ramos, 2016). This value of axial stiffness is known for a regular storage in a real-life situation. The rotational restraint was also adopted based on a previous study with the value of $K_{Rr} = 94615$ kN/mm (Frangi et al., 2012).

3.4   Test plan

The objective of the test plan is to evaluate the mechanical behaviour of CFS single and built-up sigma-plus columns when subjected to fire, and observe the influence of the end-support conditions.

From the twelve predicted experimental tests, only a total of eight were developed on CFS sigma-plus columns under fire situation with restraint to thermal elongation, in which were used two different cross-sections − single sigma-plus and built-up sigma-plus − and two different support conditions. In Table 3.1 the test plan is briefly summarized, the reference $\Sigma+\_PP\_01$, indicates the first test (01) of columns with single sigma-plus cross-section ($\Sigma+$) and with pinned-end support condition (PP), while for $2\Sigma+\_SR\_03$ refers to the third test (03) with built-up sigma-plus cross-section ($2\Sigma+$) and with semi-rigid end-support condition.

Table 3.1 - Test plan for the tested columns

No	Test Reference	Cross-section	End-support	$N_{b,Rd}$ (kN)	P_0 (kN)
1	$\Sigma+\_SR\_01$				
2	$\Sigma+\_SR\_02$		Semi-rigid	186.8	93.40 (50%)
3	$\Sigma+\_SR\_03$				
1	$\Sigma+\_PP\_01$				
2	$\Sigma+\_PP\_01$		Pinned	102.2	51.10 (50%)
3	$\Sigma+\_PP\_01$				
1	$2\Sigma+\_SR\_01$				
2	$2\Sigma+\_SR\_02$		Semi-rigid	524.24	262.12 (50%)
3	$2\Sigma+\_SR\_03$				
1	$2\Sigma+\_PP\_01$				
2	$2\Sigma+\_PP\_02$		Pinned	422.44	211.22 (50%)
3	$2\Sigma+\_PP\_03$				

3.5   Test procedure

The experimental test began with the application of an axial compression load to the column under analysis. To ensure that all the load applied is being transferred to the tested column, and not partially transferred to the surrounding structure, the threaded rods that connect the peripheral columns to the top beams have been slightly loosened. After the load applied to the tested column reaches the value correspondent to the 50% of the design buckling load, the threaded rods are tightened and the restraining frame (2 in Figure 3.2) started to impose axial and rotational restraint to the CFS column being tested. With the initial loading applied to the CFS column and the axial and rotational restraint imposed it as possible to start the test.

Bear in mind that despite the full length of all columns tested was 2950 mm, only 2650 mm of each specimen was exposed to high temperatures, this was due to the fact that the columns ends were placed inside the end-supports from which needed to be properly thermally insulated.

Due to the complexity of the experimental tests, in which are greatly affected by innumerous factors, it became necessary to establish and thoroughly follow a list of steps in order to ensure a correct functioning of the system and the integrity of the test as well.

The plugs from thermocouples were firstly connected to a compensation cable, then along with the wire line transducers and linear variable displacement transducers (Figure 3.5 b) and c)) were both connected to the data acquisition system TML TDS-530 in order to read and register all the data during the test.

As previously mentioned the end-supports have to be properly thermally insulated, in order to be used in the followed tests. The junction of both parts of the furnace was also insulated, and some parts inside the furnace were given renewed insulation from time to time due to the damage over the use. All parts referred above were insulated using ceramic wool (Figure 3.5 a)).

The last step before the starting the test was to assign each of the eight LVDT's, used to register the axial displacements, both on the top and on the bottom of the column.
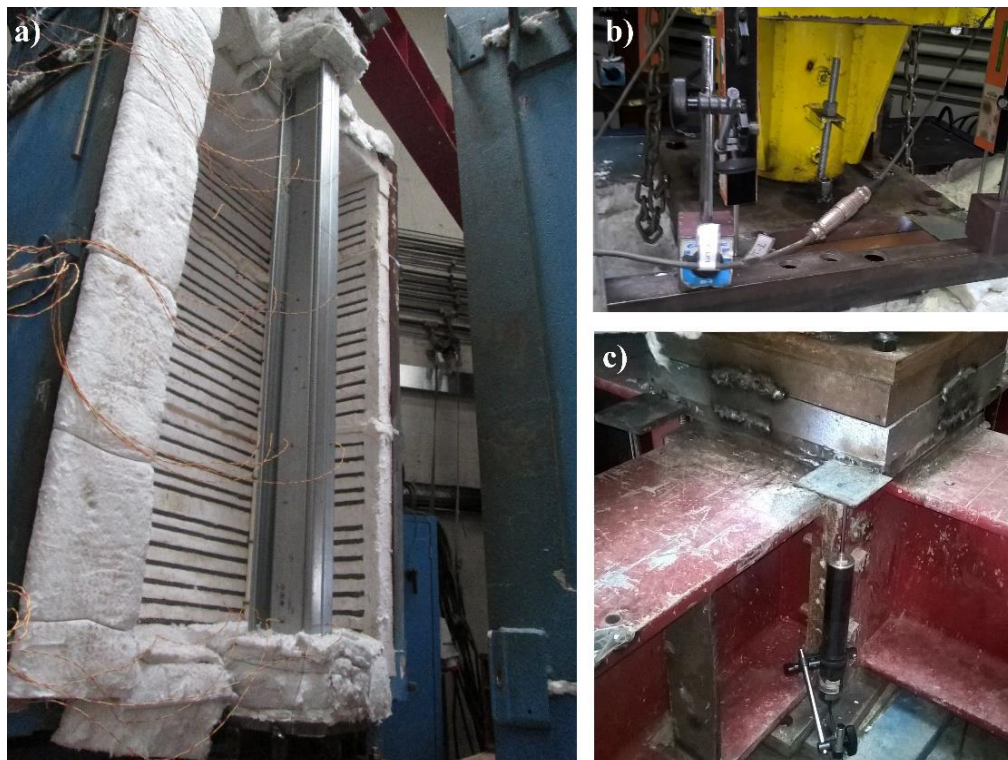
Figure 3.5 - a) Thermal insulation inside the furnace and in the end-supports and b) LVDT's positioning in the top and c) In the bottom.

3.5.1 Mechanical action

The first step of the test was to apply a compressive load to the column under analysis. As previously mentioned, this load was applied using a Enerpac RR-1006 hydraulic jack (Figure 3.6). To achieve the initial load in the tested column a procedure already described before was performed, loosening the threaded rods connecting the peripheral columns and the top beams and tightening it again after the compressive load in the column matches the initial load.

The compressive load applied has the objective to simulate the initial load that a column is normally subjected in a real-life situation, with a loading rate of 1 kN/s over the central junction of the top beams of the three-dimensional steel restraining frame.

Figure 3.6 - Hydraulic jack just before applying the compression load to the column.

3.5.2 Thermal action

After the initial compression load is applied in and the threaded rods tightened again, the restraining frame starts to impose axial and rotational restraint to the column under analysis. The next step was to subject the column to high temperatures.

As mentioned before, the thermal action was applied by a vertical modular electric furnace of *Termolab* programmed to reproduce the standard fire curve ISO 834 (1999).

3.6   Results and discussion

3.6.1 Temperature evolution

As previously mentioned, it was attempted to reproduce the standard curve ISO 834 (1999), however the furnace used has showed some difficult in reproducing the same thermal action, especially in the initial minutes (Figure 3.7). This was due to several factors, namely the type

of furnace used (electric furnace), the volume inside the furnace, and eventually some ineffective insulation mostly caused by damage over use.

Figure 3.7 presents the average furnace temperature evolution for single and built-up sigma-plus cross-section, for both pinned and semi-rigid end-support conditions, and it is compared with the fire curve ISO 834 (1999). The curves presented are representative of the remaining tests.
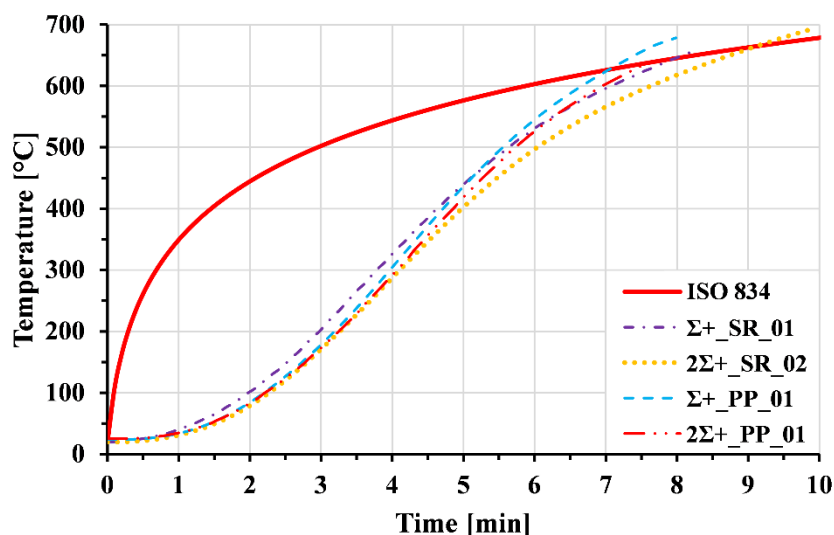
Figure 3.7 - Comparison between the temperature evolution inside the furnace during the experimental tests and the ISO 834 fire curve.

As previously mentioned, all sigma-plus columns were instrumented with 20 thermocouples divided in five different sections along the length of the column. With the registered temperature gathered form each thermocouple (T_i) on each section, the mean temperature ($\bar{\theta}_s$) for each one of those sections was determined considering the influence areas defined by the thermocouples welded to the cross-section. Using the average temperature registered in each measured section, the temperature distribution along the length of the column as a function of time was determined, and therefore it was possible to determine the mean temperature of the column ($\bar{\theta}_c$). This value is the integral of the mean temperatures calculated for cross-section *TS2*, *TS3* and *TS4*. This can be explained by the fact that the end-supports were thermally insulated which lead to temperatures significantly lower when compared with other sections. So, in order to have a mean temperature more trustworthy the sections near the edges of the columns (TS1 and TS5) were not included in the calculation of its mean temperature.

A comparison between the evolution of temperature in *TS3* section for both cross-sections tested, the ISO 834 (1999) fire curve, the average temperature inside the furnace, the mean temperature in the *TS3* cross-section ($\bar{\theta}_s$) and the mean temperature of the column ($\bar{\theta}_c$) are presented in Figure 3.8. Bear in mind that the curves chosen are representative of the remaining tests.
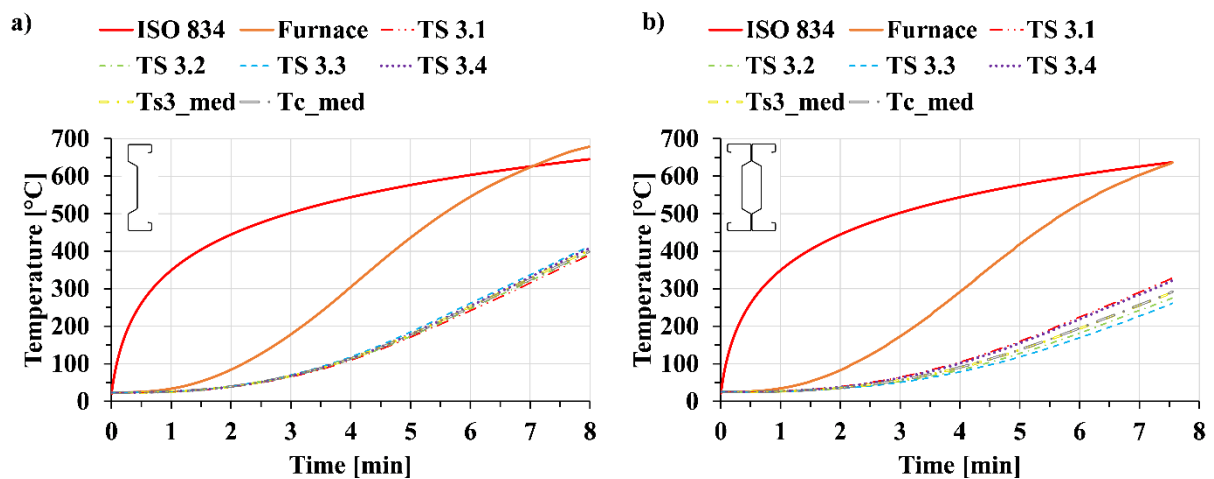
Figure 3.8 - Evolution of temperature in the cross-section TS3 for a) Single sigma-plus and b) Built-up sigma-plus columns.

In this results it is possible to observe that the evolution of the temperature in the thermocouples was almost uniform for single sigma-plus cross-sections (Figure 3.8 a)), as for built-up sigma-plus cross-sections the temperature registered was not uniformed in the cross-section (Figure 3.8 b)). For the built-up cross-sections, the thermocouples placed in the flanges (T1 and T4) registered higher temperatures over the thermocouples welded in the web and in the web-to-flange connections (T2 and T3). This was due to a greater thickness on the web-to-flange connections (5 mm) and the thermal conductance between two CFS profiles. The positioning of the web in relation to the electrical resistances may have resulted in zones that were not directly exposed to radiation in the web-to-flange connections, which can also explain the non-uniform temperature evolution in the built-up cross-section. Also, the existence of confined air in the interior of the web of the built-up cross-section, which has low thermal conductivity, may have contributed to lower temperatures registered in this part of the cross-section.

It was possible to state, based on Figure 3.9 that the evolution of temperature depended on the cross-section shape considering the different temperature rates in both cross-sections, namely 59 °C, and 69 °C per minute for single and built-up sigma-plus cross-section respectively. The temperature rates were determined considering 100 °C as the initial temperature in order to reduce the influence of the initial inertia of the furnace.

Experimental and numerical analysis of compressed cold-formed steel
elements with sigma plus cross-section subjected to fire

3 EXPERIMENTAL ANALYSIS
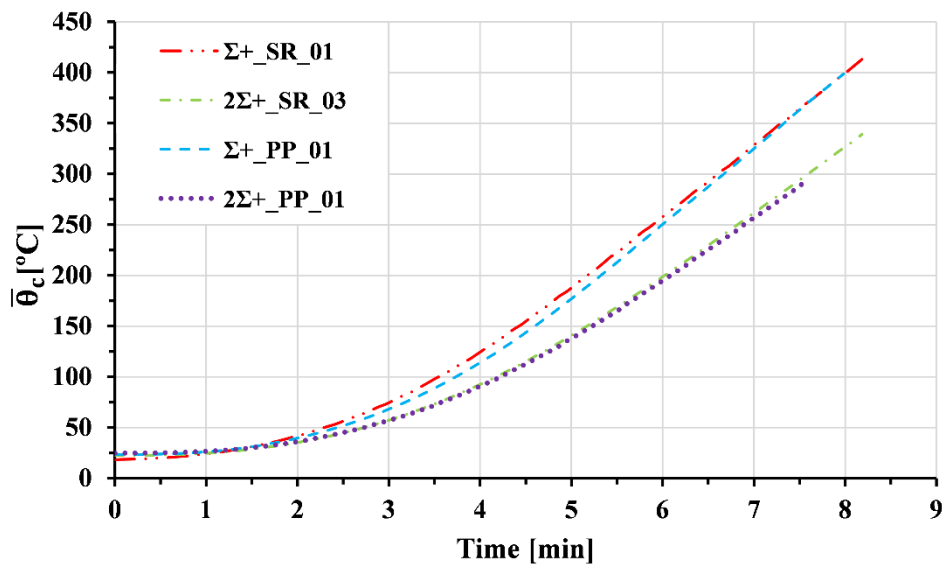
Figure 3.9 - Evolution of the mean temperature of the column on tested cross-sections for both end-support conditions.

In Figure 3.10 it is possible to observe the evolution of temperature along the length of the column as a function of time. The mean temperature is plotted for each one of the five instrumented sections ($\bar{\theta}_s$) for different time periods. As previously mentioned, the temperatures registered in the edges of the columns (TS1 and TS5) were significantly lower than the ones registered in the interior sections, due to the thermal insulation with ceramic wool of the end-supports and also to heat losses through thermal conduction, which is clear in Figure 3.10.
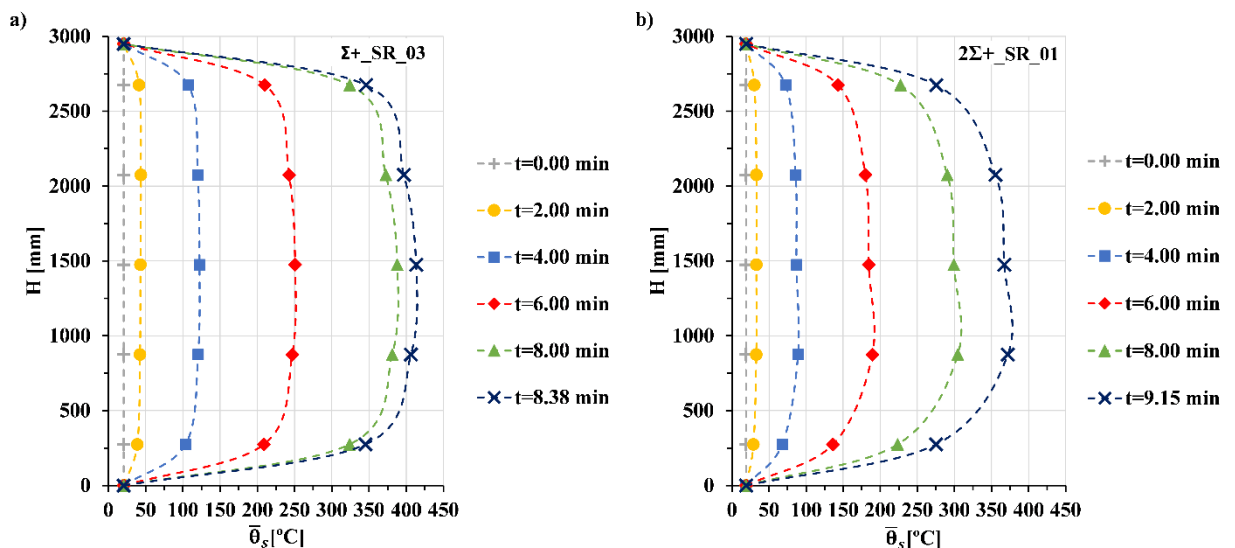
Figure 3.10 - Evolution of temperature along the full length of the column. a) +Σ_SR_03. b) 2Σ+_SR_01.

3.6.2 Restraining forces

The restraining forces generated during the tests are here presented for each type of test, being the curves selected representative of the remaining tests. Using the restraining forces, it is possible to compare the behaviour of different columns when subjected to fire. These forces are presented in a non-dimensional P/P_0 ratio (being P the absolute value of compressive load in each moment divided by P_0 the initial load applied and kept constant during all test which corresponded to 50% $N_{b,Rd}$) as a function of the mean temperature of the column ($\bar{\theta}_c$). As mentioned before, the axial restrain imposed by the three-dimensional frame was 30 kN/mm. Bear in mind that the analysis to the experimental results in Table 3.2 is made only in terms of the mean values for each test type.

The ratio of restraining forces increases along with the temperature rinsing in the column during the restraining period to thermal elongation, until it reaches its peak (P_{max}). After reaching the peak, the restraining forces (P) decrease matching again the initial load applied (P_0), mostly due to the degradation of the mechanical properties of the steel. When the restraining forces ratio reaches its maximum, the column can no longer bear more load than the currently supported, therefore the critical time (t_{cr}) and critical temperature (θ_{cr}) are defined as the failure criteria in these experimental tests (Table 3.2).

In Figure 3.11 the evolution of the restraining forces as a non-dimensional ratio is presented as a function of the mean temperature of the column.
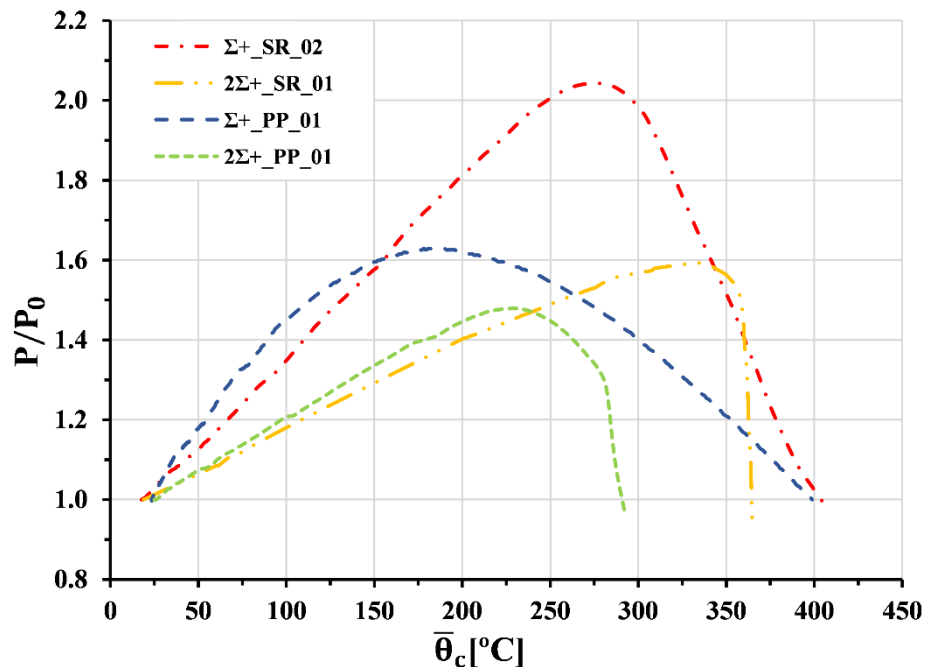
Figure 3.11 - Non-dimensional restraining forces ratio for single and built-up sigma-plus columns with both end-support conditions tested.

It is possible by observing Figure 3.11, a linearity in the evolution of the restraining forces, in all curves presented, until its peak is reached. Before the maximum load-bearing capacity is reached, the evolution of the relative restraining forces is quite similar for the same cross-section type. Also by observing Figure 3.11, the end-support type did not prove to be preponderant factor in this evolution, but in the instant where the maximum load-bearing capacity was achieved instead. Also, in Table 3.2, the moment when the column achieved the maximum load-bearing capacity (t_{peak}) is presented as well as its current temperature (θ_{peak}).

Table 3.2 - Results from the experimental tests

Test Reference	θ_{peak} [°C]	t_{peak} [min]	P_{max} [kN]	P_{max} / P_0	θ_{cr} [°C]	t_{cr} [min]
$\Sigma+\_SR\_01$	253.15	5.93	187.29	1.98	413.00	8.18
$\Sigma+\_SR\_02$	275.44	6.57	193.99	2.04	407.46	8.47
$\Sigma+\_SR\_03$	231.62	5.77	171.27	1.82	405.44	8.38
μ	253.40	6.09	184.18	1.95	408.63	8.34
σ	17.89	0.34	9.53	0.10	3.20	0.12
CV [%]	7%	6%	5.18%	4.90%	0.78%	1.42%
$2\Sigma+\_SR\_01$	331.54	8.58	417.40	1.59	364.80	9.15
$2\Sigma+\_SR\_02$	288.34	9.37	437.01	1.67	313.25	9.92
$2\Sigma+\_SR\_03$	288.66	7.42	399.25	1.48	339.09	8.18
μ	302.84	8.46	417.89	1.58	339.05	9.08
σ	20.29	0.80	15.42	0.08	21.05	0.71
CV [%]	7%	9%	3.69%	4.90%	6.21%	7.81%
$\Sigma+\_PP\_01$	186.46	5.13	81.71	1.63	398.77	7.98
$\Sigma+\_PP\_02$	-	-	-	-	-	-
$\Sigma+\_PP\_03$	-	-	-	-	-	-
μ	186.46	5.13	81.71	1.63	398.77	7.98
σ	0.00	0.00	0.00	0.00	0.00	0.00
CV [%]	0	0	0.00%	0.00%	0.00%	0.00%
$2\Sigma+\_PP\_01$	230.51	6.58	304.79	1.48	292.21	7.55
$2\Sigma+\_PP\_02$	-	-	-	-	-	-
$2\Sigma+\_PP\_03$	-	-	-	-	-	-
μ	230.51	6.58	304.79	1.48	292.21	7.55
σ	0.00	0.00	0.00	0.00	0.00	0.00
CV [%]	0	0	0.00%	0.00%	0.00%	0.00%

Due to the great number of experimental investigations being conducted in the laboratory and the lack of time, it was not possible to fulfil the test plan initially considered.

Regarding the post-critical behaviour (after the restraining forces reached its maximum and started to decrease), it was observed a notorious difference between tests with semi-rigid and pinned as end-support conditions. For columns with single sigma-plus cross-section a gradual decrease of restraining forces followed by a gradual increase of the lateral displacements was observed, whereas for columns with built-up sigma-plus cross-section the decrease of the

restraining forces occurred more suddenly with lower increase of the lateral displacements. From the results presented, the semi-rigid as support condition columns with single sigma-plus cross-section type registered a critical temperature 1.61 times greater than peak temperatures, reaching critical temperatures of 408.63 ºC. Using the same support condition but with built-up sigma-plus cross-section type, the relation between critical and peak temperatures was 1.12 reaching a maximum value of 339.05 ºC. For pin-ended columns with single sigma-plus cross-section the critical temperature reached was 398.77 ºC, whereas for built-up sigma-plus cross section the maximum temperature registered was 292.21 ºC. Comparing the maximum restraining forces presented in Table 3.1 with the ones registered in the experimental tests, it was found that in some cases the maximum load reached exceeded the design buckling load at ambient temperature ($N_{b,Rd}$). Craveiro (2015) conducted both experimental tests at both ambient and elevated temperatures on CFS columns and observed that the P_{max} values ranged approximately from 78% to 186% of the buckling load at ambient temperature explaining with this that the design buckling load may be too conservative.

As previously mentioned, in order to reduce the friction in the hinge of the end-support device, Teflon was used between the steel pin and the steel plates for the pin-ended supports. Despite the use of Teflon, the friction was not totally removed and the pinned-end support condition cannot be guaranteed, instead this end-support condition may be classified as semi-rigid with a low rotational restraint. Due to this fact, the obtained results may not correspond to the lowest limit of load-bearing capacity, critical temperatures and critical times of the sigma-plus columns.

3.6.3 Displacements

The axial displacements, as well as the restraining forces, bear a great importance in the analysis of the behaviour of CFS columns in fire situation. Additionally, to the axial displacements, the lateral displacements were also monitored in all tests conducted in this experimental analysis. Similar to the analysis of the evolution of temperatures, in the lateral displacements different time periods were plotted in order to have a better understanding of the evolution of the deformed shape until it reaches its final form.

The evolution of lateral deflections about the minor axis is presented in Figure 3.12 for all tested cross-sections and end-support conditions in order to have a better understanding of the deformed shape. Bear in mind that the curves presented for both axial and lateral displacements are representative of the remaining tests conducted.

Experimental and numerical analysis of compressed cold-formed steel
elements with sigma plus cross-section subjected to fire

3 EXPERIMENTAL ANALYSIS
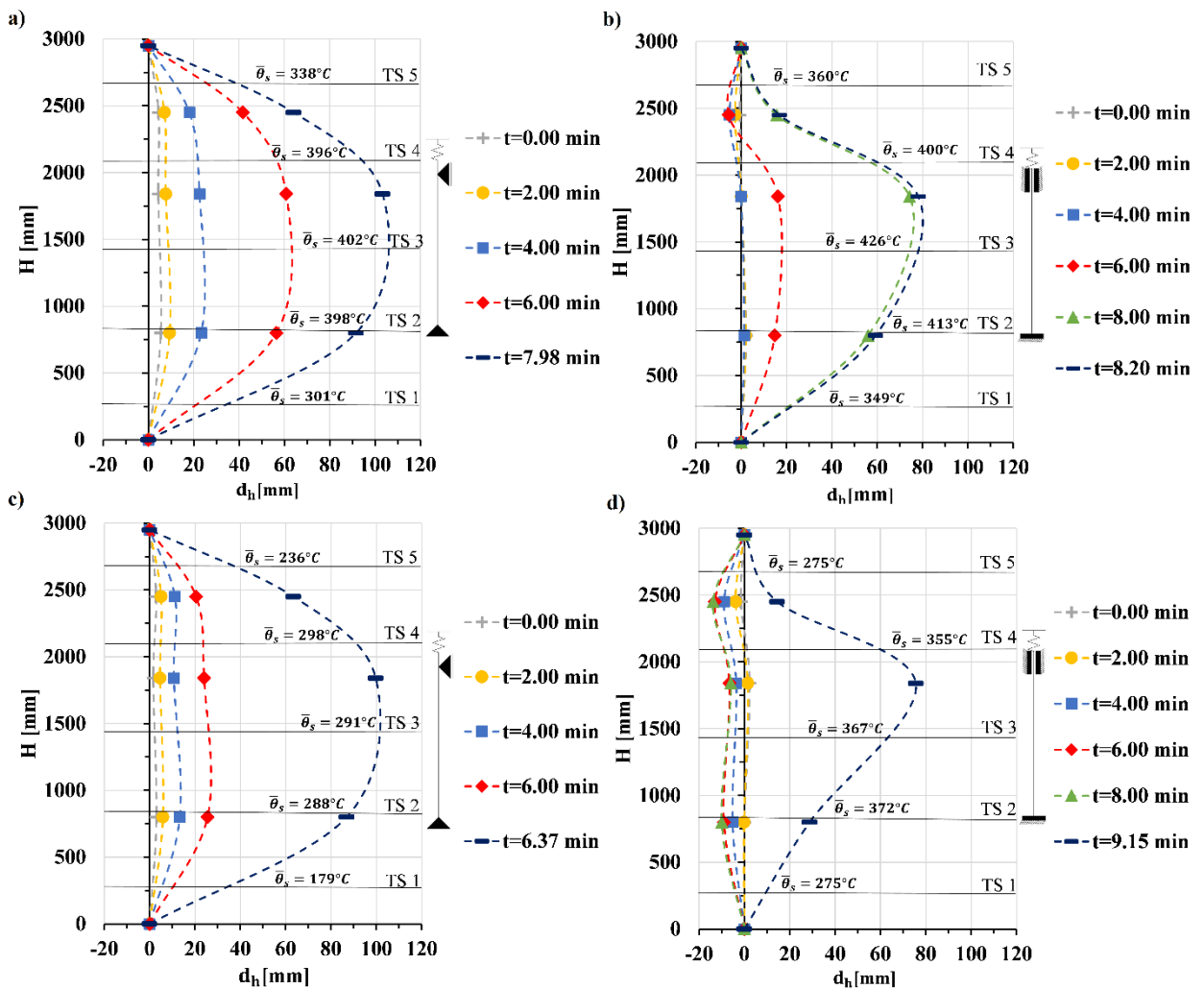
Figure 3.12 - Lateral deformations about the minor axis for the CFS columns tested. a) Σ+_PP_01 b) Σ+_SR_01 c) 2Σ+_PP_01 d) 2Σ+_SR_01.

By observing the obtained curves for the lateral displacements throughout the length of the column it was found that for columns with semi-rigid end-support conditions, the direction of the lateral displacement reversed during the fire test. It is clear by observing Figure 3.12 b) and d) that initially the column starts to buckle in one direction and then buckled in the opposite direction until it reached its final deformed shape. This can be explained by the geometrical imperfections present in the tested specimens or even in the restraining frame. Another possibility to explain this phenomenon could be due to the fact that possibly the load was not applied in the geometric center of cross-section, therefore the existence of some small eccentricities could lead to the changing of direction of lateral displacements.

The pin-ended columns are clearly recognizable in Figure 3.12 a) and c) by its deformed shape. As previously showed before, it was used steel plates inside the end-support devices in order to fix the column and prevent its rotation. Even though that in every test each specimen was carefully assigned, the results of the lateral deformations in the bottom end showed that columns

with semi-rigid end-support presented a small rotation inside the support device. This can be clearly seen in the single sigma-plus tests, and can be explained by the extreme difficulty to fix the specimens inside the end-support devices. Given its complex cross-section geometry, these columns might not have been properly fixed inside the end-supports, and after the buckle occurred it was observed that the web was crushed allowing the bottom edge of the column to rotate. In the upper end the inflection points are clearly recognizable in the final deformed shape (Figure 3.15 e) and Figure 3.17 e)). Finally, regarding the lateral displacements about the major axis, is worth mentioning that its results were not relevant for the presented experimental conditions.

Regarding the axial displacements, it is possible to observe a similarity between the curves of the restraining forces and the axial displacements (Figure 3.13). It is possible to observe that the axial displacements also increase reaching a maximum value and then decreasing. Also, it is perceptible by Figure 3.13 that columns with semi-rigid end-support conditions have greater thermal elongation with the built-up sigma-plus column reaching the maximum value. For pin-ended columns the axial displacements are not as notorious as for semi-rigid conditions, since the lateral displacements are more affected by thermal expansion leading to lower axial displacements in these columns.

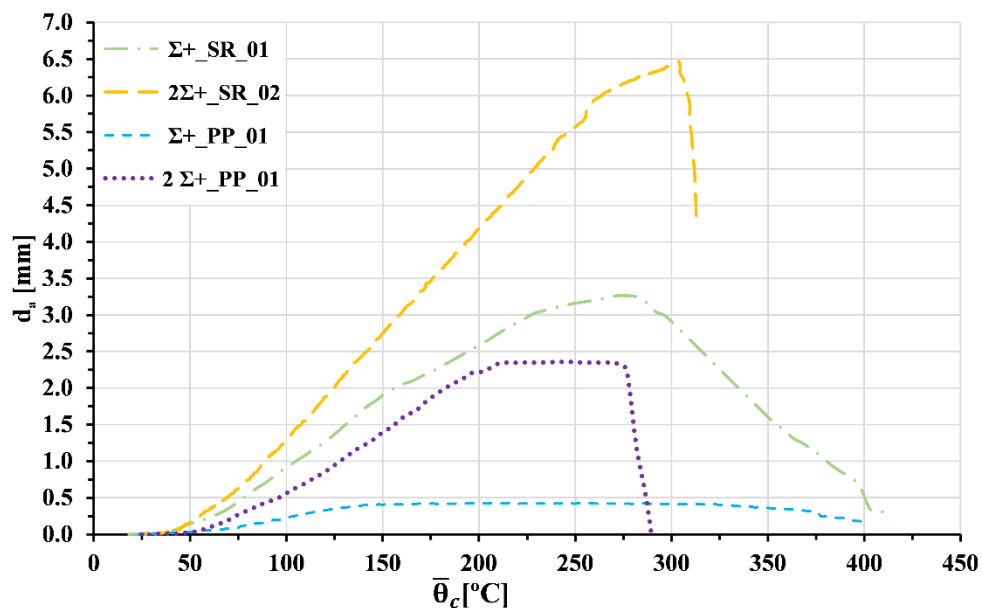

Figure 3.13 - Axial displacements for all tested CFS sigma-plus columns.

3.6.4 Failure modes

Given the fact that all tests were conducted inside vertical modular electrical furnace only the final deformed shape was observed. In all the CFS columns tested the predominant failure mode observed was the flexural buckling, however in some specimens it was also observed distortional buckling.

For the pin-ended columns with single sigma-plus cross-section, as previously mentioned; the predominant failure mode was global flexural buckling about the minor axis in interaction with a minor distortional buckling (Figure 3.14). It was observed a slightly opening of the lips at approximately mid-height of the column (Figure 3.14 d)). The double edge stiffeners may explain the small opening of the lips.

Still in single sigma-plus cross-section, but with semi-rigid end-support conditions it was observed that the predominant failure mode was the interaction between global flexural buckling about the minor axis and distortional buckling (Figure 3.15). The distortional buckling is clearly more perceptively than for pin-ended columns, and it was observed at approximately mid-height with an opening of the lips (Figure 3.15 d)). Despite being a column with semi-rigid end-support condition local buckling was not observed. The inflection point cannot be observed in the bottom end of the column due to a small rotation of the column inside the end-support device is evident (Figure 3.15 e)).

Regarding the pin-ended built-up columns the predominant failure mode observed was the interaction between global flexural buckling about the minor axis and distortional buckling at approximately mid-height of the column (Figure 3.16). The distortional buckling was only observed in one of the lipped channel profiles namely in the profile moving towards the other (Figure 3.16 d)). Once again, the distortional buckling was characterized by lips and flanges moving outwards of the profile.

For columns with built-up sigma-plus cross-section with semi-rigid support conditions the dominant failure mode observed was again the interaction between flexural buckling and distortional buckling, again at approximately mid-height of the column (Figure 3.17). The distortional buckling was far more severe for semi-rigid end-support conditions than for pin-ended conditions, playing a more important part not only in the failure of the column but in its final deformed shape (Figure 3.17 d)). For semi-rigid end-support conditions the distortional buckling was observed in the two lipped channel profile with lips and flanges moving outwards and inwards of the respective profile namely, the one buckling in the direction of the web of the lipped channel and the other moving in the direction of the lips of the cross-section. Once again, the local buckling was not observed in these experimental tests.

Figure 3.14 - Failure modes for specimen Σ+_PP_01. a), b), c) and e) Flexural buckling. d)
Minor distortional buckling.

Figure 3.15 - Failure modes for specimen Σ +_SR _01. a), b), c) and e) Flexural buckling. d)
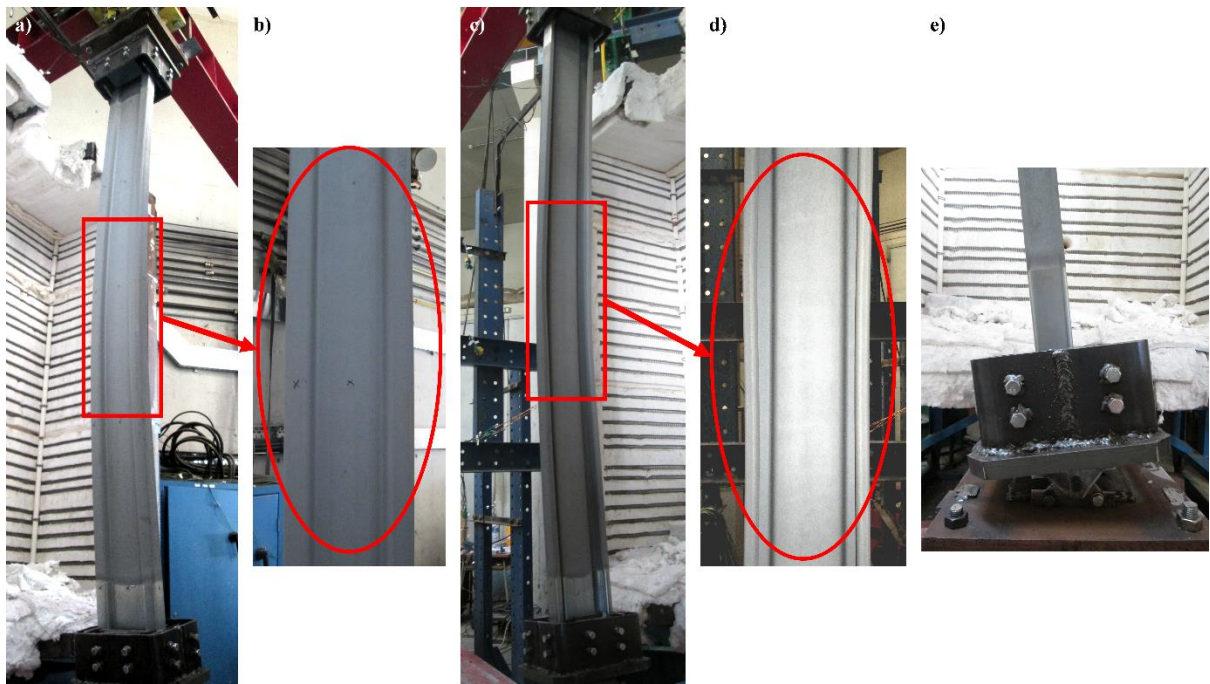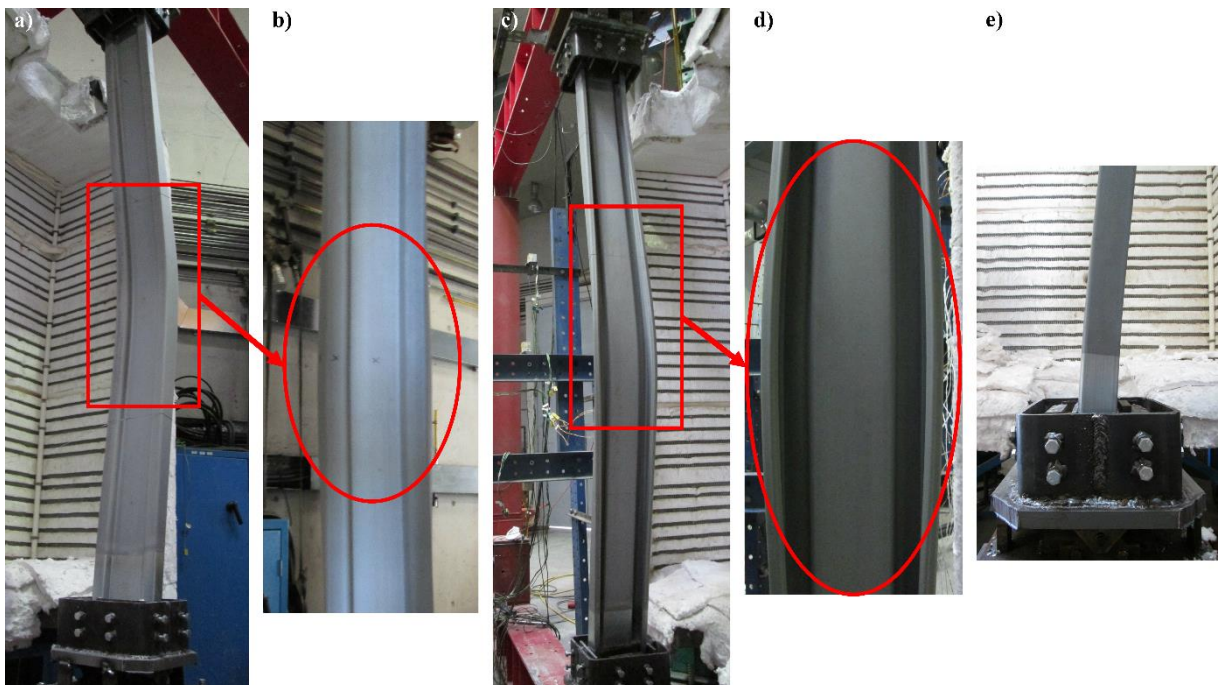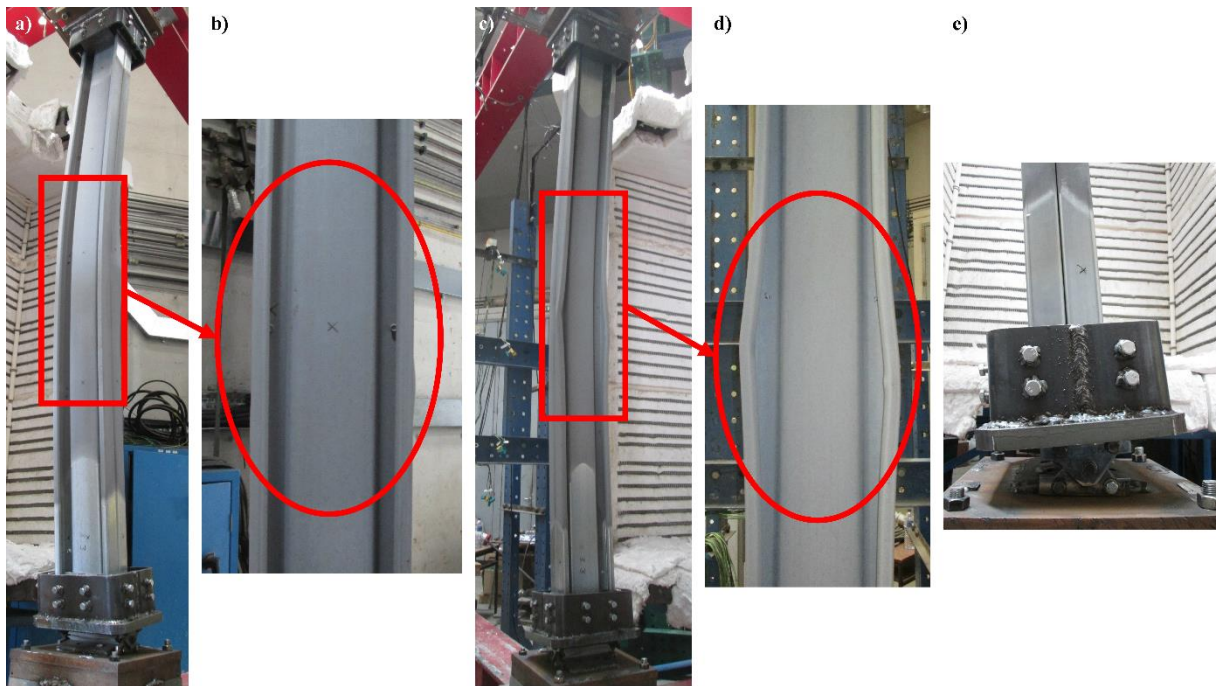Distortional buckling.

Figure 3.16 - Failure modes for specimen $2\Sigma + \_PP\_01$. a), b), c) and e) Flexural buckling. d)
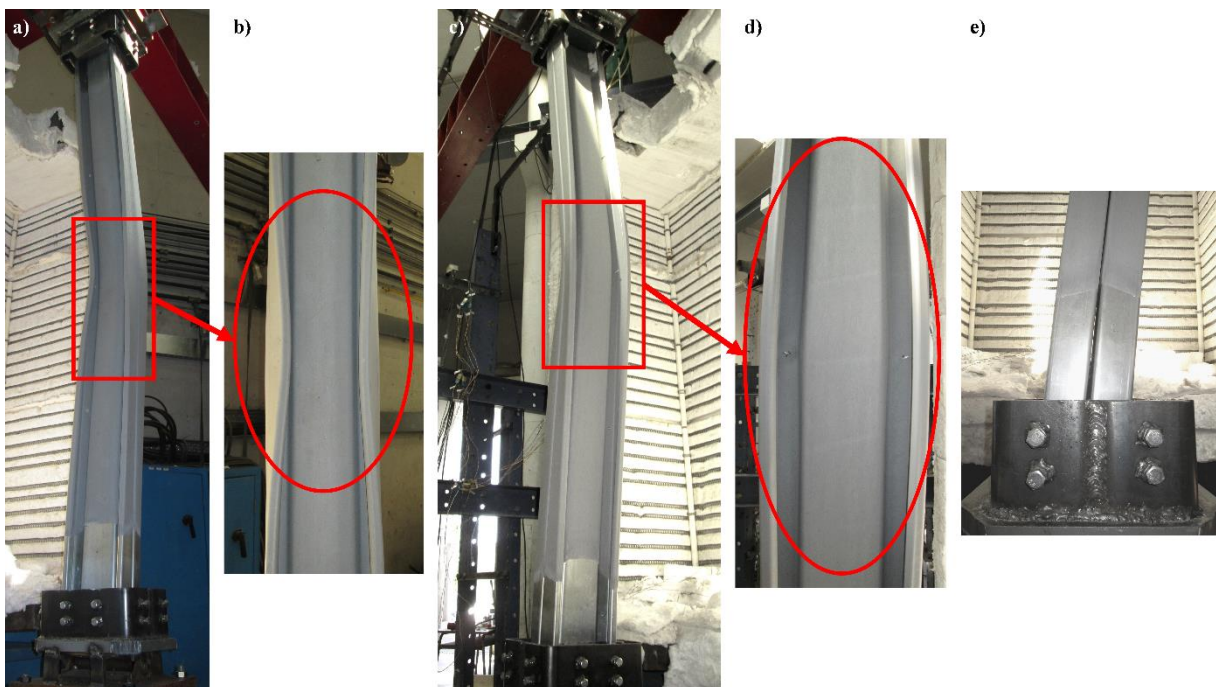Distortional buckling.

Figure 3.17 - Failure modes for specimen $2\Sigma + \_SR\_03$. a), c) and e) Flexural buckling. b) and
d) Distortional buckling.

3.7 Final remarks

The experimental campaign conducted had as main objective to study the behaviour in fire situation of CFS sigma-plus columns, under axial compression and with the restraint to thermal elongation.

Considering the eight experimental tests conducted and presented along the present dissertation with specimens 2950 mm tall, two different cross-section types – single and built-up sigma-plus – and with two different end-support conditions namely, semi-rigid and pinned-end support the main conclusions of this research study are mentioned bellow.

Regarding the temperature evolution, it was observed that the cross-section shape has a direct impact in its distribution. For instance, in single sigma-plus columns higher temperatures were registered in the thermocouples placed in the web an on the web-to-flange connection, whereas for built-up sigma-plus columns the higher temperatures registered were in the flanges with the web reaching lower values. This was due to the double thickness in web-to-flange connections and to the thermal conductance between the two CFS profiles. Also, the existence of confined air in the interior of the web of the built-up cross-section, which has low thermal conductivity, may have contributed to lower temperatures registered in this part of the cross-section of built-up columns.

As mentioned before, the buckling load of each CFS column was determined for both end-support conditions. Regarding the semi-rigid end-support, it is worth mentioning the difficulty to guarantee that all rotations are supressed in the experimental tests. Therefore, the actual boundary conditions could be described as semi-rigid with very high values of rotational stiffness. As for pin-ended support conditions, as mentioned previously, despite the use of Teflon in order to reduce the friction between the steel pin and the steel plate functioning as a hinge, the columns tested did not exactly represent perfect pinned-ends due to the existence some of friction in the end-support devices. Consequently, the actual boundary conditions could be described as semi-rigid as well but it a low value of rotational stiffness. These observations converge with the final deformed shapes. By observing the final deformed shapes of the tests for semi-rigid support condition it can be stated that the actual buckling length could be slightly higher than 0.5L.

Concerning the influence of restraint to thermal elongation in the behaviour of CFS columns two restraining frames were used. I was observed that the cross-section type played a relevant role in the evolution of the P/P_0 non-dimensional ratio of restraining force. For instance, the single sigma-plus showed considerably higher values for the P/P_0 ratio than the built-up columns. As for the post-critical behaviour, the columns with single sigma-plus cross-section showed a gradual decrease of restraining forces followed by a gradual increase of the lateral displacements, whereas for columns with built-up sigma-plus cross-section the decrease of the restraining forces occurred more suddenly with lower increase of the lateral displacements. It can be stated that for built-up columns the restraint to thermal elongation seemed to control the

failure, whereas for single columns the failure was due to the temperature increase leading to the degradation of the mechanical properties. The end-support conditions influenced directly the maximum value of restraining forces reached.

Regarding the failure modes, it was observed that the predominant failure mode was the interaction between global flexural buckling and distortional buckling. Also by comparing each test it was found that depending on the type of cross-section tested and the type of end-support used the distortional buckling could be more expressive. For instance, it was registered that for pin-ended columns the distortional buckling was not as expressive as for columns with semi-rigid support conditions. For columns with semi-rigid as end-support conditions the distortional buckling played a more important role and the existence of the double edge stiffeners may have prevented a more expressive distortional buckling with a wider opening between the lips and flanges of the channel profile. It is possible that the existence of imperfections may have influenced the failure modes obtained.

The critical temperature registered in the CFS columns studied showed a considerable increase when compared to similar studies developed previously. Craveiro (2015), conducted a series of experimental tests on CFS columns with different cross-section types for different values of axial stiffness and two initial values of buckling load. The level of axial restraint imposed to a CFS column is defined as the ratio between the axial stiffness of the surrounding structure to the CFS column and the axial stiffness of the column (Craveiro, 2015). The author imposed levels of axial restraint of 0.290 for columns with C profiles and 0.140 for built-up C columns, from which the author concluded that for higher levels of axial restraining the critical temperature did not suffer a significantly change. The levels for axial restraint used in the present dissertation were 0.357 and 0.193 for single and built-up columns respectively. Considering only higher values of axial stiffness and 50% of the design buckling load, the critical temperatures registered for C profiles was 338.53 ℃ for pin-ended support, and 415.48 ℃ for fix-ended conditions respectively. As for the values registered in the present dissertation were 398.77 ℃ for pin-ended support, and 408.63 ℃ for semi-rigid-ended conditions respectively. For columns with built-up double C profile the author presented a critical temperature of 251.99 ℃ for pin-ended support, and 266.01 ℃ for fix-ended support conditions. In the present dissertation, the critical temperatures for the built-up sigma-plus columns were 339.05 ℃ and 292.21 ℃ for semi-rigid and pin-ended support conditions respectively. This shows a significant improvement registered in the structural behaviour of these elements and can be explained by the existence of the double edge stiffeners and the intermediate stiffener along the column.

4   NUMERICAL ANAYSIS

4.1   Introduction

The present chapter has the objective to explain the methodologies adopted in the developing process of the numerical models using the finite element software *Abaqus* (2014). The results obtained will be analyzed and discussed in order to understand the behavior of CFS sigma-plus columns with restraint to thermal elongation when subjected to fire.

The fire safety is a key feature of the structural design, and it is mandatory to develop specific methodologies to be used as design guidelines in order to achieve a better understanding of the mechanical behavior of CFS columns when subjected to fire.

Numerical models have been assuming an important role in scientific investigations and it is considered a valid alternative to experimental tests. Due to the complexity of experimental tests and since these are lot more time consuming with a large number specimens required, and usually with high costs associated, the computer simulations have become more popular among the academic community. Still, the computer simulations do not replace experimental tests but are able to reduce the number of tests needed to develop a research.

The finite element analysis software used was the *Abaqus CAE* (2014), and it is one of the solving applications most used among researchers. It can simulate a wide number of engineering problems, from heat transfer to structural analysis which were used in the scope of this investigation.

4.2   Structural Analysis

Two different finite element models were developed to simulate the structural behavior of CFS sigma-plus columns in fire situation previously tested in the Laboratory of Testing Materials and Structures of Coimbra University. First it was developed a two-dimensional finite element model with the objective to simulate the evolution of the temperature along the cross-section followed by a three-dimensional finite element model built to simulate the mechanical behaviour of CFS sigma-plus columns in fire situation.

The retrieved data from the experimental analysis previously presented in this dissertation, were considered and used in the developing and calibration process of the numerical models, with the objective to increase the simulations to a greater number of cases not tested experimentally.

4.2.1 Finite element type

All CFS columns were modelled by using shell elements which are commonly used to model thin-walled structural elements. There are several types of shell elements present in the finite element software *Abaqus* (2014) with S4R being the chosen one (Figure 4.1 a)). The abbreviation S4R stands for shell element (S) with four nodes with reduced integration (R) with hourglass control.

The self-drilling screws used in built-up sigma-plus columns were modelled with the finite element C3D8R (Figure 4.2 b)) and it is defined as a three-dimensional (3D) continuum (C) hexahedral and an eight-node brick element with reduced integration (R) hourglass control and first-order interpolation.
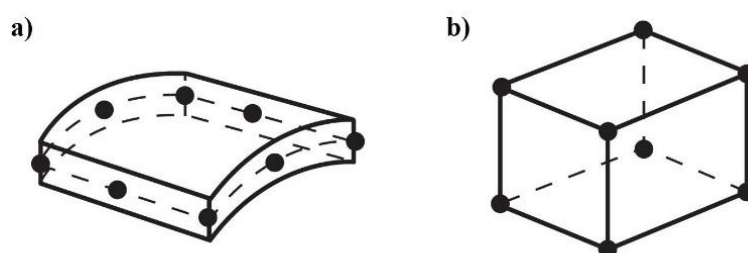
Figure 4.1 - Schematic representation of the finite element chosen, a) S4R and b) C3D8R (ABAQUS, 2014).

4.2.2 Material modelling

To fully represent both thermal and the mechanical behavior, it was considered in the numerical models the respective material properties. In the finite element software, using the module property, it was introduced the thermal and mechanical properties of CFS as a function of the temperature evolution.

4.2.2.1 Thermal properties

In order to perform an accurate thermal analysis, it was mandatory to introduce in the numerical models CFS properties such as specific heat, thermal conductivity, thermal elongation and specific weight.

Thermal conductivity is the ability of a material to conduct heat, whereas for specific heat is defined as the amount of energy required to change the unit mass of a substance by one degree in temperature. The thermal elongation is the tendency of matter to change in shape, area, and volume as result of a change in temperature due to heat transfer.

The properties were chosen following a study conducted on the mechanical and thermal properties of the structural steel S320GD+Z by Craveiro et al (2016) were the author concluded that the experimental results and the one presented in the normative were very similar with the exception to thermal elongation. The predictions available in the EN 1993-1-2:2005 were

considered to be over-conservative, for the thermal elongation, by Craveiro et al (2016), Chen and Young (2007), therefore the authors presented and compared with many design standard predictions for thermal elongation (Figure 4.2 c)). In the numerical models, it was adopted the predictions proposed by Chen and Young (2007) for thermal elongation and the ones presented in EN 1993-1-2:2005 (2005) for specific heat and thermal conductivity (Figure 4.2 a) and b)).
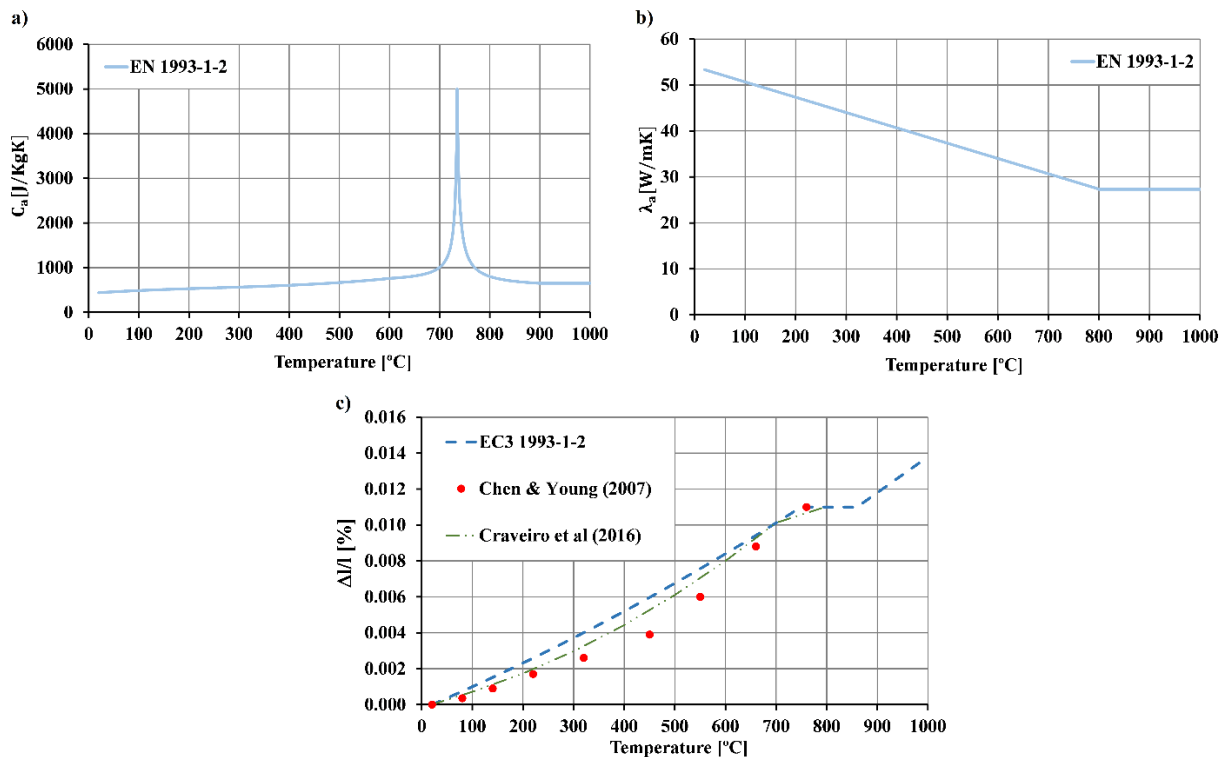
Figure 4.2 - Properties used in thermal analysis. a) Specific heat. b) Thermal conductivity. c) Thermal elongation comparison between EN 1993-1-2:2005 and new predictions (Chen and Young, 2007b; Craveiro et al., 2016).

4.2.2.2 Mechanical properties

The degradation of the mechanical properties of CFS is a phenomenon that is directly associated with its mechanical behavior, causing a significantly decreasing in its load-bearing capacity specially when the steel is subjected to elevated temperatures.

The mechanical properties were chosen according to the predictions available in the EN 1993-1-2:2005 (2005). For the steel used experimentally – S320GD+Z – the relation between stress and strain was defined (Figure 4.3) with using three different parameters, namely the elastic modulus, the proportional limit strength, and the effective yield strength obtained using a reduction factor also predicted by the normative as a function of time.
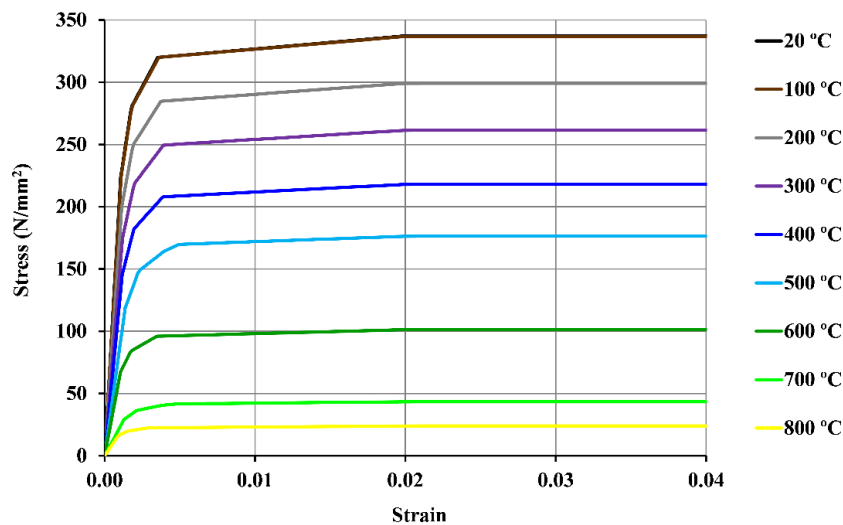
Figure 4.3 - Stress and strain curves used as input in the numerical models for the steel S320GD+Z (EN 1993-1-2, 2005).

4.2.3 Finite element mesh

The size of the mesh determines the accuracy of the finite element model and it is important to establish an equilibrium between the accuracy of the mesh and computational time since computational resources are limited. Craveiro (2015) studied different mesh sizes, namely 5 mm × 5 mm, 10 mm × 10 mm and 20 mm × 20 mm for CFS columns and the obtained results were presented for the estimation of the buckling load of the column at ambient temperature. After analyzing the obtained results, the author concluded that the more accurate mesh could be used.

Following the same study, in the numerical models exposed in the present dissertation, the same mesh – 5 mm × 5 mm – was used for all tested cross-sections (Figure 4.4).
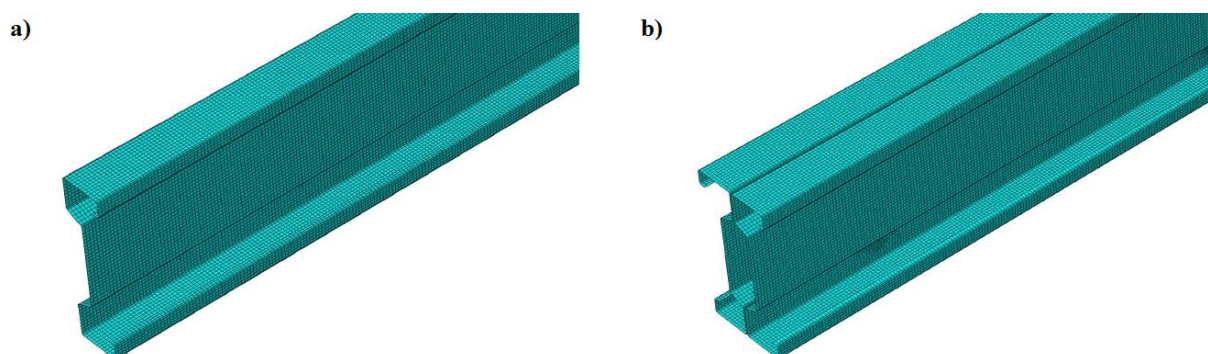
Figure 4.4 - Detail of the finite element size used in both sigma-plus columns, a) single and b) built-up.

4.2.4 Loading, boundary and contact conditions

To accurately reproduce the behavior of CFS sigma-plus columns registered in the experimental campaign, it was necessary to define appropriate loading, boundary and contact conditions, for both single and built-up sigma-plus columns in the numerical models (Figure 4.5).
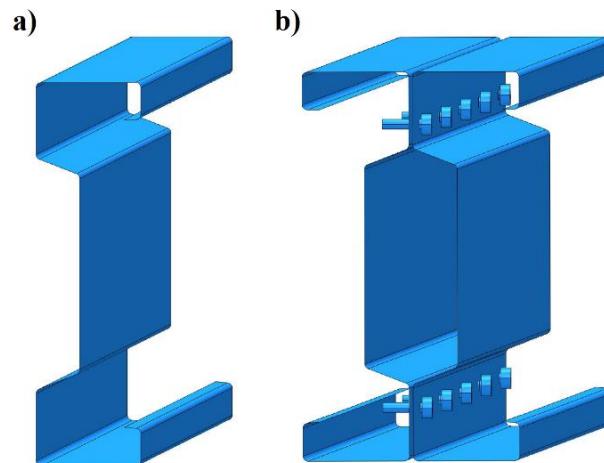
Figure 4.5 - Detail of the columns modelled, a) single and b) built-up.

Regarding the end-support conditions, as previously mentioned in Chapter 3, the friction between the steel plates and the steel pin of the end-support devices may have influenced the global behavior of CFS columns. The friction observed possibly prevented the tested columns from developing a complete free rotation inside the end-support devices, which could lead to overestimated values of generated restraining forces and buckling loads (Craveiro, 2015). In order to simulate this issue in the finite element model, and using the potential of the software *Abaqus* (2014), it was considered hinges in the boundary conditions of the finite element model. These hinges, acting as rotational springs, were placed in Z direction (preventing a complete free rotation about the minor axis of the column) simulating a rotational stiffness (Craveiro, 2015) (Figure 4.6). As previously mentioned, this end-support condition could be described as semi-rigid end-support with a low value of rotational restraint, consequently a low value of rotational stiffness should be used to simulate the friction in the pin-ended columns. Craveiro (2015) used in the finite element models, low values of rotational restraint to simulate this type of boundary condition ranging from 2% of *3EI/L* to 20% of *EI/L* [N.m/rad].

As for fixed-end columns, as previously mentioned in Chapter 3, it was observed that the columns did not present a fully fixed condition being described as semi-rigid end-support conditions with a high value of rotational stiffness, therefore the hinges acting as rotational springs can be used to simulate its behavior. In this case a high value of rotational stiffness should be used, and following Craveiro (2015), the value of 4*EI/L* [N.m/rad] was used to simulate the observed semi-rigid support condition for both tested cross-sections.

To fully simulate the thermal expansion of CFS sigma-plus columns when subjected to high temperatures with restraint to thermal elongation, a linear spring connected to the centroid of

the column was used to replace the surrounding structure used in experimental campaign (Figure 4.6). The value of this axial spring was the same considered for the experimental tests (K_{Ra} = 30 kN/mm).

A representation of the finite element models developed used to reproduce the results obtained in the experimental campaign is presented in Figure 4.6.
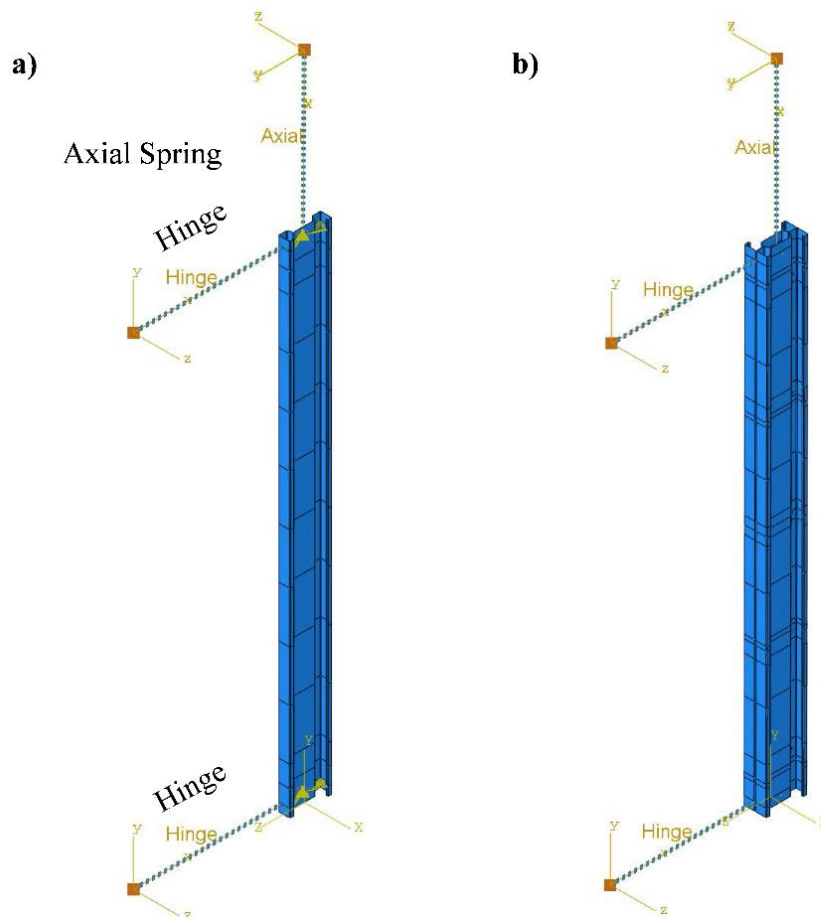
Figure 4.6 - Finite element model developed for both sigma-plus columns under simulated fire conditions with restraint to thermal elongation, a) single and) built-up.

Regarding the loading applied in the simulated columns, the axial compression load was applied as a concentrated nodal force at the top end of the column with the respective initial load for each column. This node (centroid) was then connected to the perimeter of the cross-section equally distributing the applied load along the perimeter of the cross-section (Figure 4.7 a)).

Concerning the built-up sigma-plus cross-sections tested in the experimental campaign, it was necessary to properly model this type of cross-section due to the fact that these columns were composed by two sigma-plus profiles bolted with self-drilling screws in different points in the cross-section and along the length of the column. Consequently, the contact between the CFS sigma-plus profiles and the self-drilling screws, and between the two sigma-plus profiles must be carefully modelled. Therefore, in modelling it was assumed, following a similar study on

CFS bolted profiles (Laím, 2013), a tangential friction coefficient of 0.2 for the contact behavior in tangential direction and a hard contact (full transmission of compressive forces and no transmission of tensile forces) for the contact behavior in normal direction between the profile surfaces (Figure 4.7 b)). Considering the *finite-sliding* tracking method to model the interaction between the surface of the individual profiles the contact *node-to-surface* was used. Additionally, for the contact between the two CFS profiles and the self-drilling screws (Figure 4.7 c)) a *rough and hard contact* was also used (Craveiro, 2015).
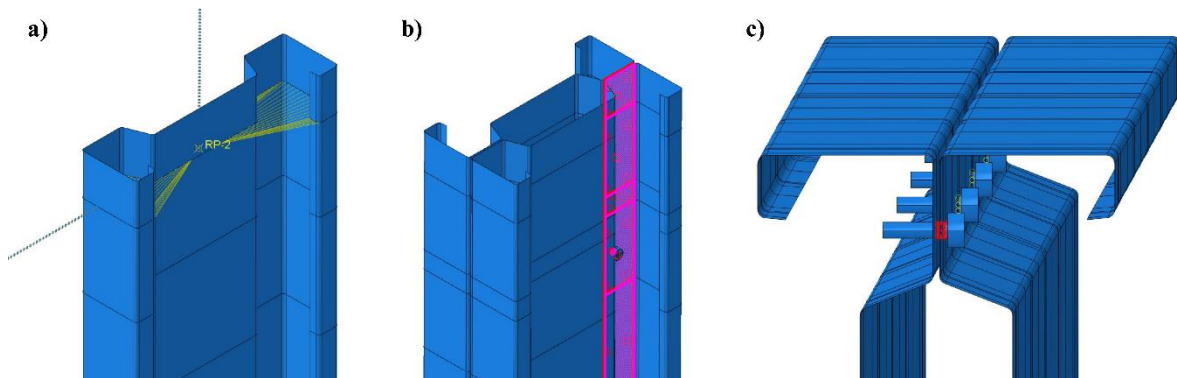
Figure 4.7 - Detail of the loading applied distributed for all perimeter of the cross-section, and the detail of the contact between b) profiles and c) self-drilling screws and the CFS profile.

Regarding the high temperatures exposure, the calibrated results for the thermal analysis were inputted in the validation process of the finite element model. For each one of the thermocouples monitored, influence areas were defined depending on the position of specific thermocouple and its temperature as a function of time was inputted along that area in order to reproduce the non-uniform temperature distribution observed in the experimental campaign. The thermal analysis, and posteriorly the respective calibration was made using the potential and capabilities of the software *Abaqus* (2014) and the experimental results gathered, and is thoroughly described in the Section 4.4 and Subsection 4.5.1 respectively.

4.3   Analysis method

Finite elements three-dimensional models were created for all tested cross-sections with both end-support conditions for fire tests with restraint to thermal elongation. It was conducted two different type of analyses, namely buckling analysis and nonlinear static analysis. The buckling analysis is made to determine the associated buckling modes that will be used later to input the geometric imperfections in the nonlinear analysis. Even though the first buckling mode could be the critical mode, it was observed during the experimental tests an interaction between different buckling modes, consequently two buckling modes were considered, the first for the global flexural buckling and the second the distortional buckling. For all tested columns, the initial adopted values for global flexural imperfections was *L/1000*, whereas for distortional imperfections the initial value adopted was *t*. It is worth pointing out that in some simulations

the initial geometric imperfections were applied in the opposite direction, in order to fully reproduce the final deformed shape observed in the experimental tests.

4.4   Thermal analysis

A two-dimensional numerical model was developed in order to reproduce the temperature distribution in each cross-section monitored, adopting a 4-node linear heat transfer or mass diffusion quadrilateral element, DC2D4. As previously mentioned, the temperatures registered inside the furnace during the tests were very different from the ISO 834 (1999) curve due to the thermal inertia of both column and the electrical furnace, therefore in order to obtain similar temperatures evolution and distribution to the ones achieved in the experimental campaign it was developed a non-linear model analysis using the curves registered inside the furnace, and given the fact that the experimental tests were short in time this method will not compromise the numerical validation of the models. The vertical modular furnace used in the experimental test is composed by three modules in which it was registered the temperature evolution for each one. In the columns tested it was monitored five different sections along its length, and using the software *Abaqus* (2014) it was introduced for each section the respective module temperature curve being the section one and two affected by the temperature curve of the bottom module, the third and fourth section affected by the intermediate module and the fifth section affected by the top module.

In thermal analysis, the fire action was defined in the finite element model using two types of surfaces namely, *film condition* and *radiant to ambient*, which correspond to heat transfer by convection and heat transfer by radiation, respectively. For the fire tests curves, the adopted convective heat transfer coefficient (α_c) was 16 W/m^2K (Craveiro, 2015) (lower than 25 W/m^2K used for ISO 834 fire curve) for all models, whereas for the radiative heat flux the values used were differing by section and section elements in both single and built-up considering a maximum value ($\varepsilon_{th} = 0.210$) calculated using a steel (cold-formed steel with zinc coating) emissivity of 0.3 and 0.7 for the furnace electrical resistances (Craveiro, 2015). The temperature distribution obtained from these two-dimensional numerical models will be used to input in the mechanical three-dimensional model.

For the built-up sigma-plus cross-section it was necessary an additional consideration due to the existence of confined air inside the column, which as a low thermal conductivity. In order to simulate the air inside the cross-section it was assumed as a solid material, neglecting the heat transfer by convection in the open space created. The contact between the air and the steel cross-section was modelled considering thermal contact conductance coefficient of 10 W/m^2K, whereas for the contact between the two sigma-plus cross-sections a coefficient of 200 W/m^2K was adopted (Craveiro, 2015). The thermal properties of air, specific heat and the thermal conductivity, with temperature increase were also inputted in finite element model (Figure 4.8). The specific weight was assumed to be constant with the value 1.16 kg/m³. Finally,

the type of element chosen was the same as for the CFS cross-section, namely a 4-node linear heat transfer or mass diffusion quadrilateral element, DC2D4.

a)   b)
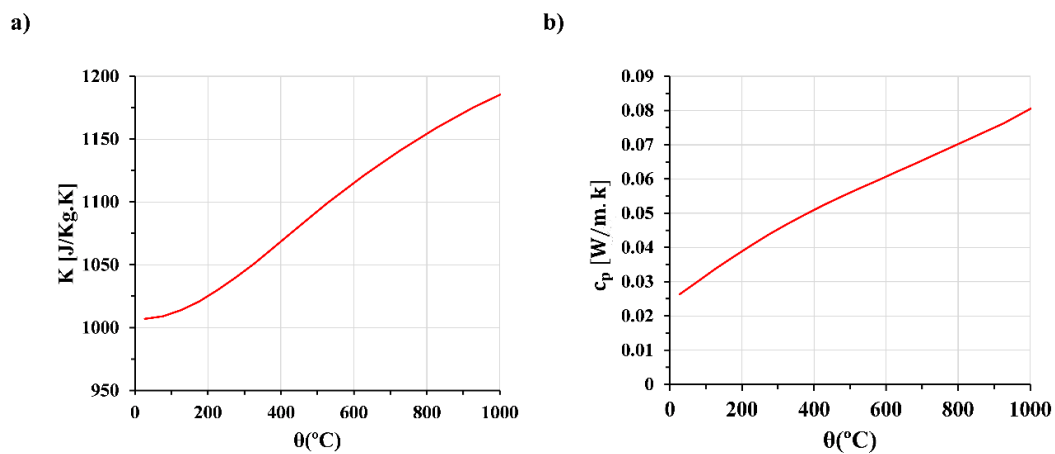
Figure 4.8 - Thermal properties of air at one atmospheric pressure as a function of temperature. a) Thermal conductivity. b) Specific heat.

4.5   Validation of the finite element model

After comparing the results obtained through the numerical analysis with the gathered experimental data, the discussion and validation of the finite element models developed is now possible, in order to enable the study on CFS sigma-plus columns subjected to fire with restraint to thermal elongation.

4.5.1 Thermal calibration

The thermal calibration of the structural elements studied consisted in a comparison between the evolution of the temperatures as a function of time registered in each one of the specimens, during the experimental tests and in the numerical analysis. To establish this comparison, temperatures were monitored in same points were the thermocouples were placed in the experimental campaign.

As previously mentioned, the thermal action that these elements were subjected was the temperature evolution registered inside the electrical furnace instead the standard fire curve ISO 834 (1999) in order to properly validate the numerical model.

Initially, in the thermal analysis, it was considered that all the exterior surfaces and the interior surface of the web were exposed to radiative heat flux (Figure 4.9 a)), considering that all the remaining interior surfaces were affected by shadow effect. The temperatures evolution obtained from this approach did not match the temperatures gathered in the experimental campaign, and it was necessary to add more fire surfaces, namely in the interior surfaces of the flanges. A significant increase of the temperatures was observed but the gathered data from the numerical analysis still did not matched the experimental results. A final iteration was performed, dividing the fire surface in two groups, namely the surfaces where the section

registered lower temperatures and the surfaces where the section registered higher temperatures (Figure 4.9 b)). With this approach, it was possible to apply two different radiative heat flux coefficients in order to achieve the desire temperature evolution obtained in the experimental tests. Finally, to perform the thermal calibration multiple radiative heat flux coefficients were used ranging from 0.168 to 0.210 depending on the section analyzed, corresponding to 70 and 100% of the coefficient respectively.
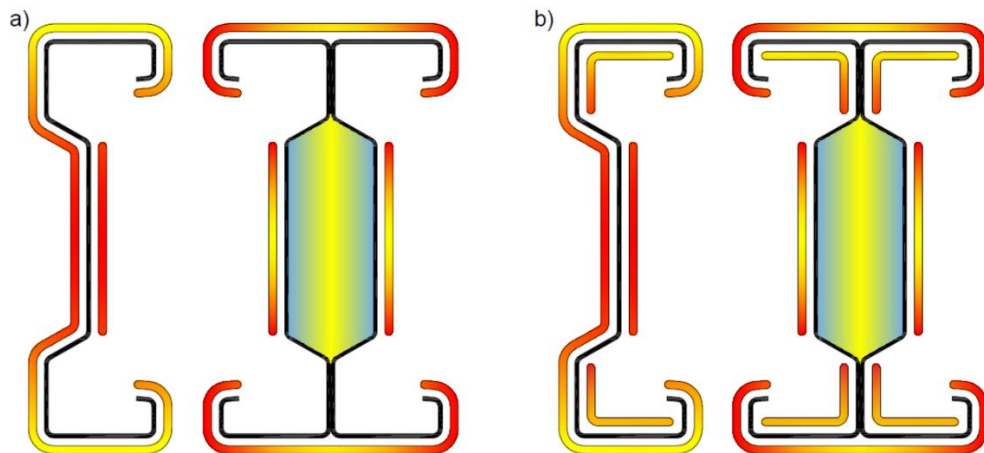
Figure 4.9 - Fire surfaces considered along the thermal calibration. a) Initial surfaces. b) Final calibrated surfaces.

In Figure 4.10 and Figure 4.11 it is possible to observe the comparison between the temperature evolution registered in the experimental tests and the one obtained in the numerical simulations for both cross-sections. It is easily observed a very good agreement between both experimental and numerical results in general. Bear in mind that the temperatures evolution displayed bellow are representative of the remaining simulations.
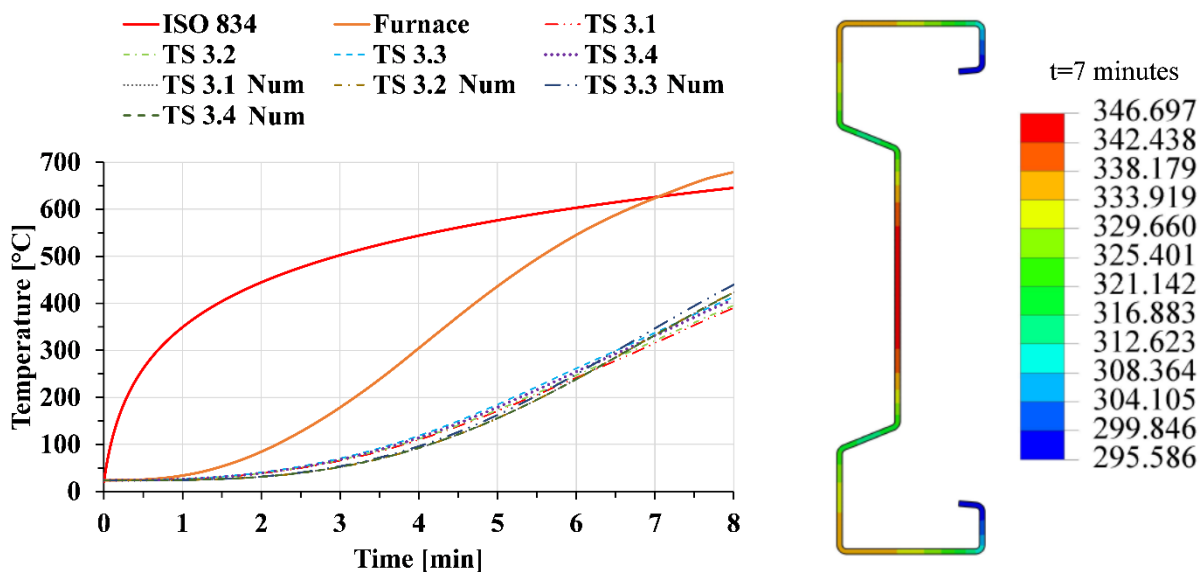
Figure 4.10 - Comparison between the test Σ +_PP_01 and Num temperature evolution.
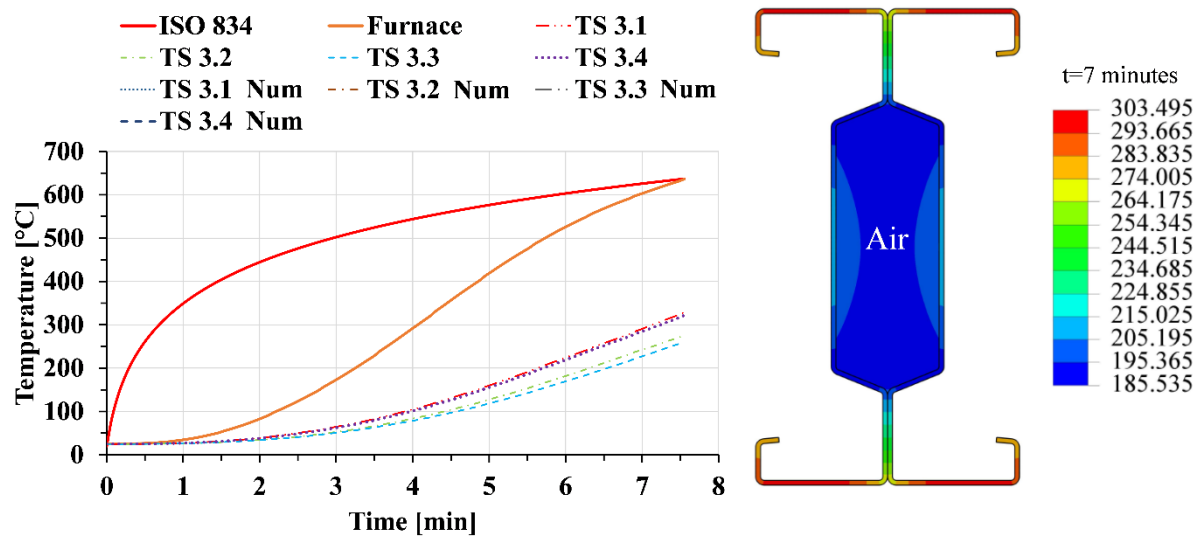
Figure 4.11 - Comparison between the test 2Σ +_PP_01 and Num temperature evolution.

4.5.2 Structural calibration

As mentioned before, the behavior of CFS sigma-plus when subjected to fire and with restraint to thermal elongation can be analyzed by comparing the evolution of the non-dimensional ratio between the generated restraining forces during the fire tests with the initial applied load (P/P_0) as a function of the mean temperature of the CFS column ($\bar{\theta}_c$).

As previously mentioned, it was created two rotational springs in order to simulate the friction observed inside the end-support devices in the experimental campaign. For columns with fix-ended support conditions it was defined high values of rotational stiffness, namely 4EI/L [N.m/rad] whereas for pin-ended columns the values adopted were ranging from 2% of $3EI/L$ to 20% of EI/L [N.m/rad] following a study on CFS compression members conducted by Craveiro (2015) where friction was also observed in the end-support devices. During the structural calibration, multiple values of rotational stiffness were tested on pin-ended columns, and it was observed that values below 11% of EI/L [N.m/rad] were insufficient to simulate the friction registered, and for values superior to 11% of EI/L [N.m/rad] the influence noticed in the results was not considerable. Therefore, in all tested cross-sections at mean value of 11% of $3EI/L$ [N.m/rad] was used.

Initially before the calibration of the three-dimensional structural model, the initial load was applied in the cross-section centroid of the top-end of the column, but the results obtained showed a maximum axial load superior to the ones registered in the experimental tests. Therefore, initial eccentricities were assumed in the applied load with 5 mm first, after observing that the maximum axial load still did not matched the one observed in the experimental campaign, a third iteration was made with an eccentricity of 10 mm. The experimental results may have been affected by some eccentricities in loading which could

explain the lower ultimate buckling loads observed. For all tested cross-sections with both type of end-support an eccentricity of 10 mm was used.

Regarding the imperfections, which as previously mentioned were added to the finite element model as input results from the buckle analysis, the initial values assumed were *L/1000* for global flexural imperfections and *t* for distortional imperfections. To fully reproduce the results achieved in the experimental campaign it was necessary to perform more iterations additionally to the already mentioned eccentricities. Consequently, the global flexural imperfection was increased from *L/1000* to *L/500*, whereas for the distortional imperfections the final value was 2*t* depending on the column simulated. Hence, that this series of approaches taken prove to be vital in the accurately simulation of the behavior of CFS sigma-plus columns subjected to fire with restraint to thermal elongation.

In order to show the accuracy of the finite element model a comparison between experimental and the numerical analysis (Num) results is presented in Figure 4.12. In Table 4.1 the Num results are thoroughly detailed and compared with the gathered experimental data, namely the maximum axial load and the critical temperature. It is possible to state that the finite element developed along this dissertation can accurately reproduce the behavior of CFS sigma-plus under fire conditions with restraint to thermal elongation.
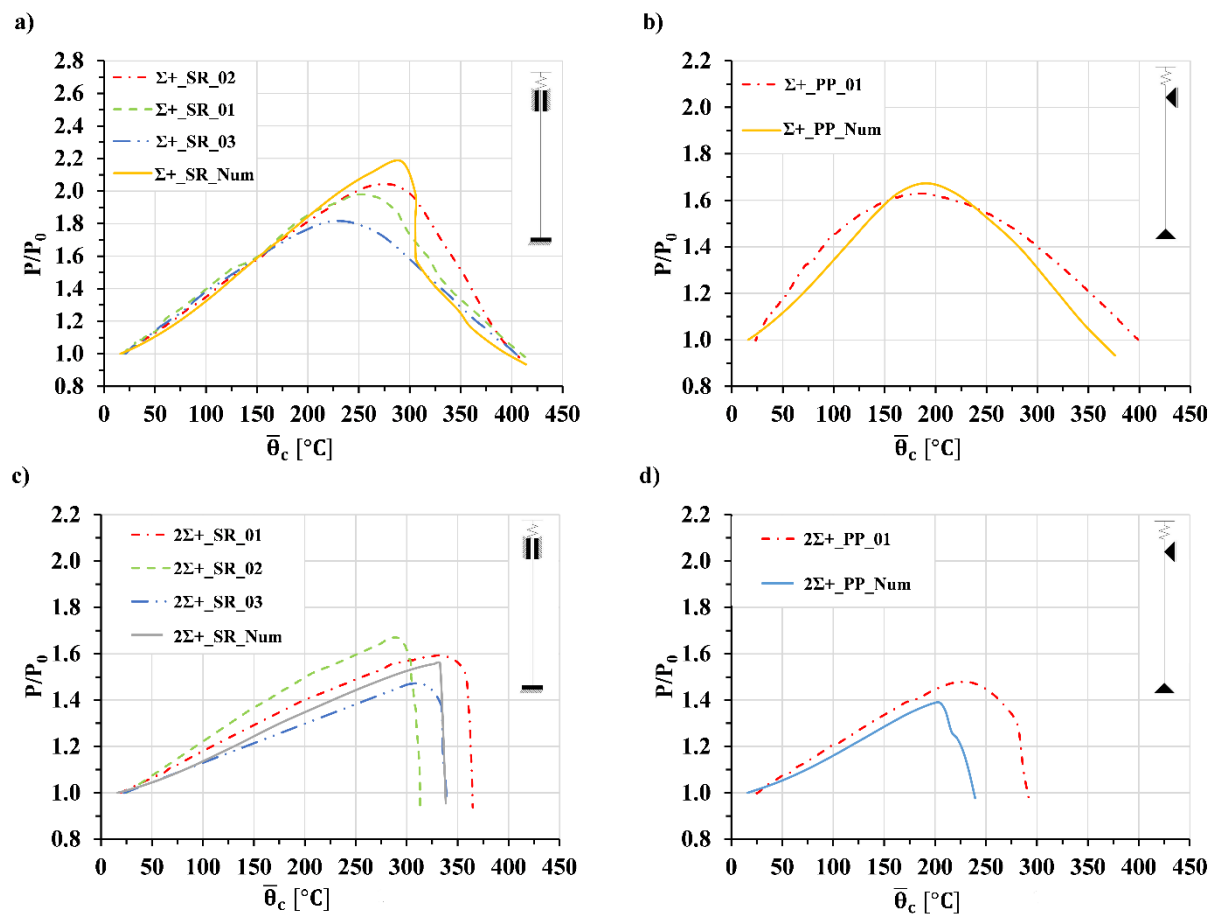

Figure 4.12 - Comparison between experimental and Num results for all columns tested.

Table 4.1 - Experimental and Num critical temperature and maximum axial load for all columns tested.

Test Reference	θ_{cr} [°C]	P_{max} [kN]	$\theta_{cr,Num}$ [°C]	$P_{max,Num}$ [kN]	$\theta_{cr}/\theta_{cr,Num}$	$P_{max}/P_{max,Num}$
Σ+_SR_01	413.00	187.29			1.00	0.92
Σ+_SR_02	407.46	193.99	414.06	204.03	0.98	0.95
Σ+_SR_03	405.44	171.27			0.98	0.84
μ	408.63	184.18	414.06	204.03	0.99	0.90
2Σ+_SR_01	364.80	417.40			1.08	1.02
2Σ+_SR_02	313.25	437.01	338.38	408.35	0.93	1.07
2Σ+_SR_03	339.09	399.25			1.00	0.98
μ	339.05	417.89	338.38	408.35	1.00	1.02
Σ+_PP_01	398.77	81.71			1.06	0.96
Σ+_PP_02	-	-	376.19	85.50	-	-
Σ+_PP_03	-	-			-	-
μ	398.77	81.71	376.19	85.50	1.06	0.96
2Σ+_PP_01	292.21	304.79			1.22	1.04
2Σ+_PP_02	-	-	239.32	293.29	-	-
2Σ+_PP_03	-	-			-	-
μ	292.21	304.79	239.32	293.29	1.22	1.04

4.5.3 Numerically calculated deformed shapes

In this chapter, the obtained failure modes observed in the experimental tests are compared with the ones obtained in the numerical simulations. The comparison between the experimental and numerical failure modes is made to enhance the validation of the developed finite element model to fully reproduce the behavior of CFS sigma-plus under fire conditions with restraint to thermal elongation. The numerical failure modes observed presented flexural buckling about the minor axis along with distortional buckling, showing a very good agreement with the failure modes observed in the experimental tests. From Figure 4.13 to Figure 4.16 the comparison between the obtained failure modes is presented for single and built-up sigma-plus cross-section, with both end-support conditions.

Experimental and numerical analysis of compressed cold-formed steel
elements with sigma plus cross-section subjected to fire

4 NUMERICAL ANALYSIS

Figure 4.13 - Failure modes for pin-ended columns with single sigma-plus cross-section from
a) experimental and b) numerical analyses.

Figure 4.14 - Failure modes for semi-rigid columns with single sigma-plus cross-section from
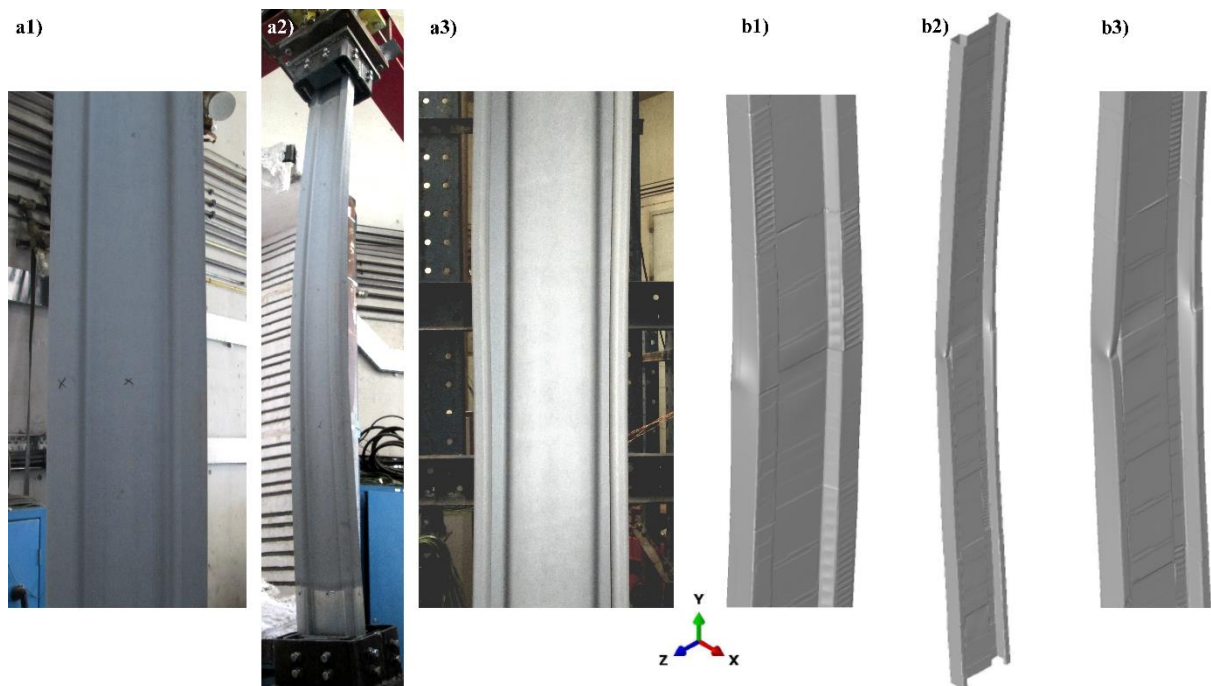a) experimental and b) numerical analyses.
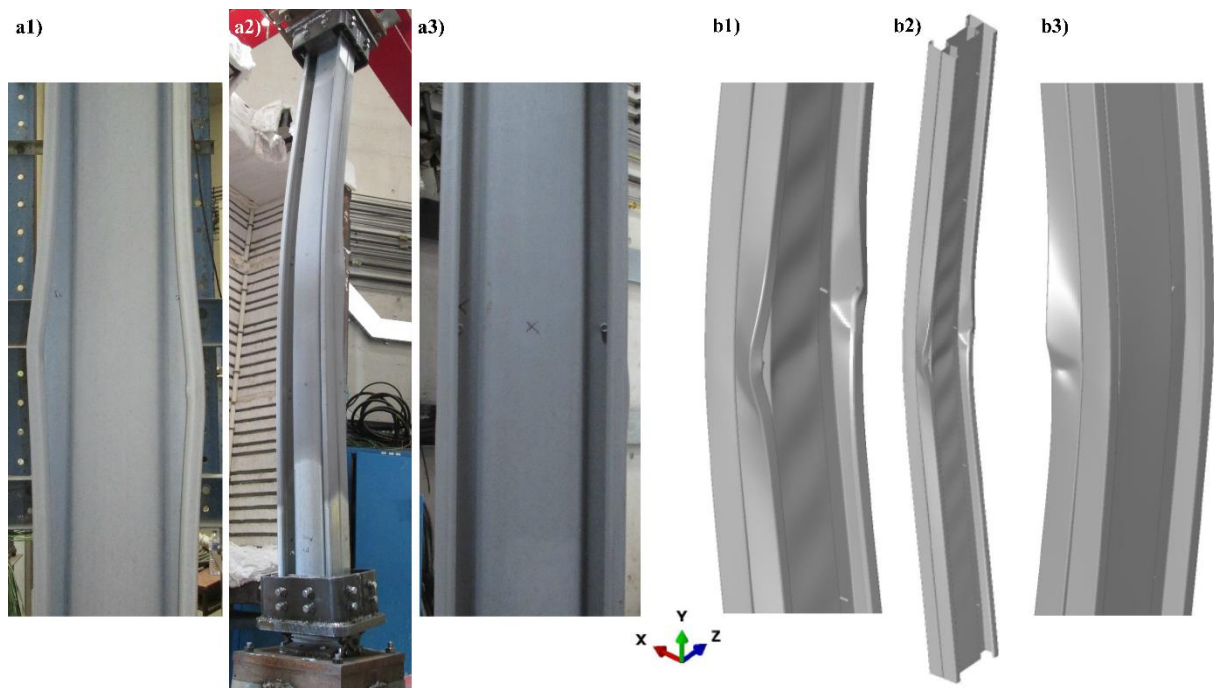
Figure 4.15 - Failure modes for pin-ended columns with built-up sigma-plus cross-section
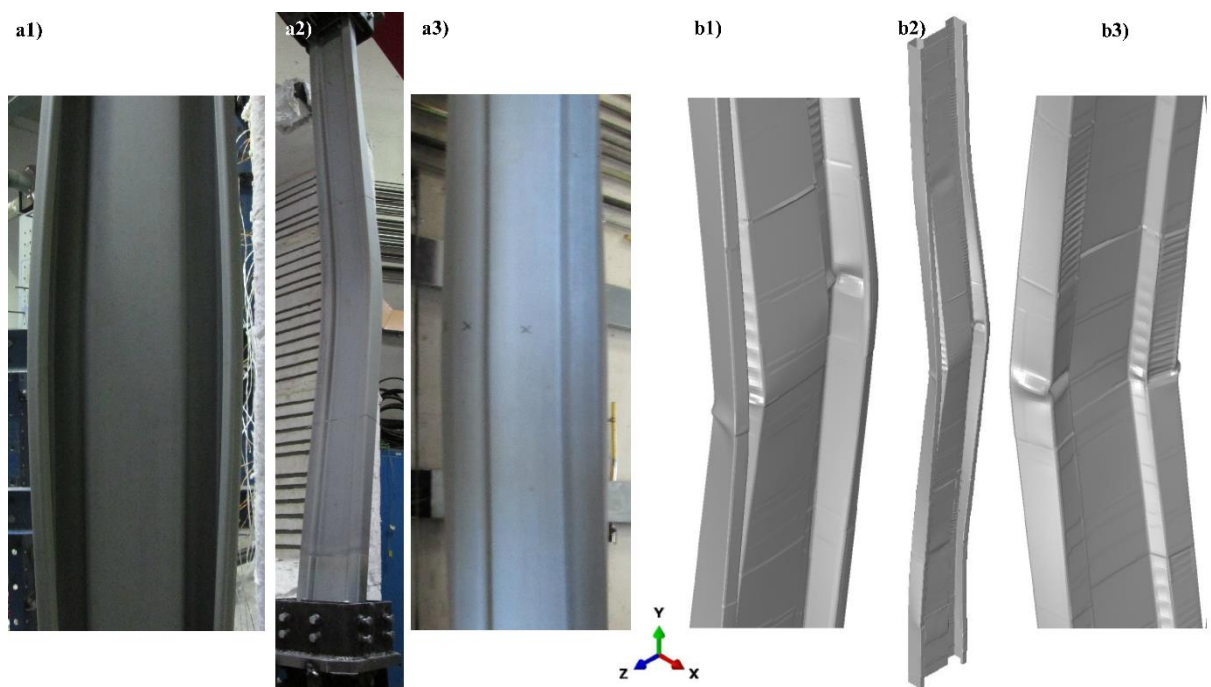from a) experimental and b) numerical analyses.
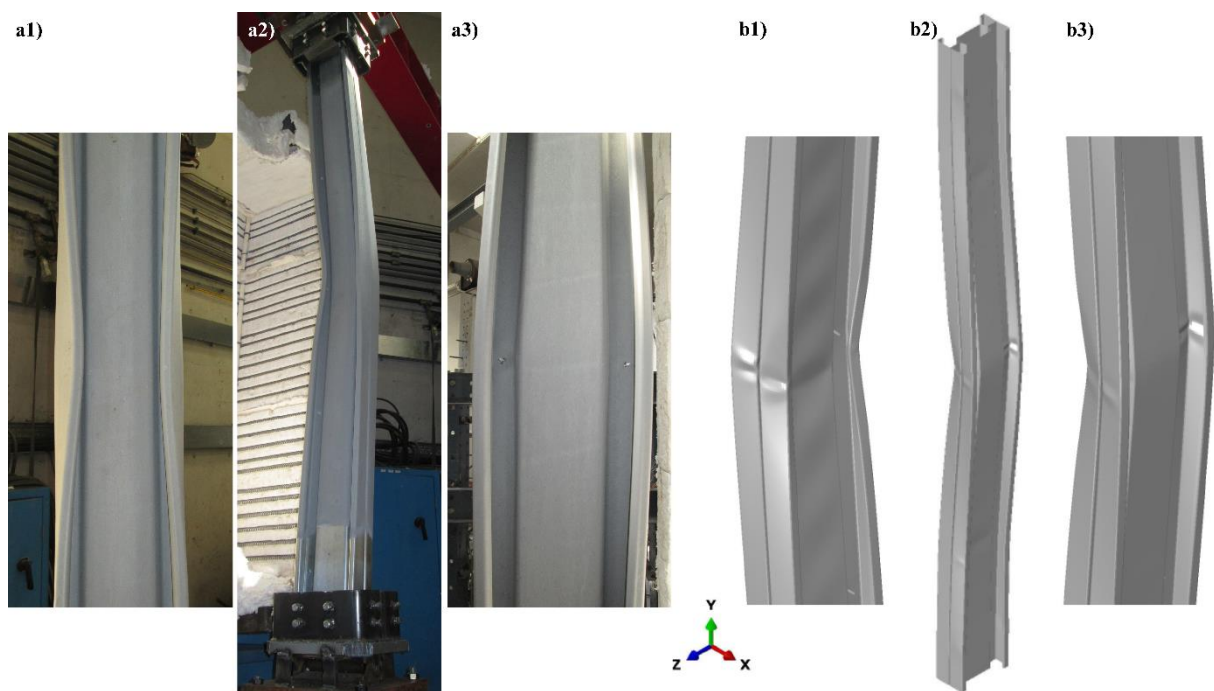
Figure 4.16 - Failure modes for semi-rigid columns with built-up sigma-plus cross-section
from a) experimental and b) numerical analyses.

4.6   Final remarks

The present chapter, using the finite element analysis software *Abaqus* (2014), presented the numerical analysis of the behavior of CFS sigma-plus columns when subjected to simulated fire conditions.

It is clear that the non-linear two-dimensional model developed to simulate the heat transfer along the cross-section of the column lead to an accurate temperature distribution and evolution in each one of the monitored sections during the experimental campaign. The temperature registered inside the furnace was the thermal action used instead of the standard fire curve ISO 834 (1999).

The finite element model developed along this chapter was presented and validated in terms of the maximum generated force, critical temperature and failure modes. Comparing the obtained failure modes and the ones observed in the experimental tests it was found a good agreement between the Num and the experimental tests.

Based on the results presented for the numerical analysis it can be stated that the developed finite element model should be used to develop future parametric studies, in order to study other parameters that was not considered within this dissertation. Different levels of both axial and rotational restraint should be addressed, as well as columns with no restraint to thermal elongation – where columns can expand with no restraining – and columns fully restrained using the developed finite element model.

5   CONCLUSIONS AND FUTURE WORK

The use of CFS members have been increasing in the past few years assuming an important role in building construction industry, allowing a great number of different types of cross-section ensuring with a very good mechanical performance behaviour and an economic use of this steel.

The lack of researches conducted on CFS members especially regarding its behaviour when subjected to fire is still an important issue to be addressed, namely in columns with restraint to thermal elongation. This issue is an important aspect to have in mind in the study of the fire behaviour of these structural elements, considering both axial and rotational stiffness of the surrounding structure, simulating therefore a real life situation when a column is fully part of a structure.

This dissertation consisted in an extensive study on the behaviour of CFS compressed members with sigma-plus cross-section when subjected to fire with restraint to thermal elongation. This research comprehended an experimental research conducted in the Laboratory of Testing Materials and Structures (LEME) of Coimbra University, with the objective to access the thermomechanical behaviour of the specimens tested. Additionally, a three-dimensional finite element model, using the capabilities of the finite element analysis software *Abaqus* (2014), was developed within this dissertation, in order to accurately reproduce the behaviour of CFS columns at fire conditions with restraint to thermal elongation and to be of assist in future parametric studies and consequently, playing an important role in the development of specific guidelines for CFS, similar to the existing for hot-rolled steels.

5.1   Fire tests with restraint to thermal elongation

To understand the behaviour of CFS sigma-plus columns subjected to fire with restraint to thermal elongation it was necessary to access key factors which influence its resistance such as, the critical temperatures, the failure modes and the restraining forces.

During the experimental tests, it was observed that the cross-section shape has a direct impact in the temperature evolution. For instance, the observed temperature increase rate was different on each cross-section tested, namely 59 ºC, and 69 ºC per minute for single and built-up sigma-plus cross-section respectively. The built-up sigma-plus cross-sections presented lower temperature rate, mostly due to the double thickness in web-to-flange connections, to the thermal conductance between the two CFS profiles, and to the existence of confined air in the interior of the web of the built-up cross-section, which has low thermal conductivity. The

predictions established in EN1993-1-2:2005 (2005) are over-conservative when comparing the critical temperatures gathered in the experimental campaign for single columns imposing a limit of 350 ºC. As for built-up columns, the critical temperature stayed within the bounds of the predicted values established.

Regarding the failure modes, it was observed that the predominant failure mode was the global flexural buckling for all columns tested. Additionally, distortional buckling was also identified at mid-height of the column taking a minor expression depending on the type of cross-section tested and the type of end-support used, namely for single sigma-plus pinned-end. The distortion buckling was clearly more visible for columns with semi-rigid as end-support conditions directly contributing for the final deformed shape of the column.

Concerning the influence of restraint to thermal elongation in the behaviour of CFS columns, it was observed that columns single sigma-plus cross-section type presented considerably higher values for the P/P_0 when compared to the built-up columns. Also, the post-critical behaviour was different for both cross-section types, with single sigma-plus columns presenting a gradual decrease of restraining forces followed by a gradual increase of the lateral displacements, whereas for built-up columns the restraining forces decreased more suddenly with lower increase of the lateral displacements. It is possible that failure of built-up columns may be controlled by the generated axial restraining forces, whereas for single columns the temperature increase seems to be the decisive factor controlling failure.

Both pinned and fixed-end support conditions presented additional complications. Friction may have influenced the overall mechanical behaviour for pinned-ended columns, whereas for fix-ended columns the lack of points of inflection was noticeable and its final deformed shape was clearly influenced by it.

5.2   Finite element analysis

The complex finite element model was developed and fully calibrated along the presented dissertation in order to accurately reproduce the behaviour observed within the experimental campaign. The accurately characterization of the mechanical properties of the material modelled was decisive in order to present valid and realistic model.

The two-dimensional thermal model developed, presented an accurately heat transfer when compared to the temperature evolution registered during the experimental tests, for both single and built-up columns, posteriorly used as input temperatures in order perform a non-linear analysis.

Regarding the calibration and validation of the three-dimensional thermomechanical model, the comparison between the results achieved in the Num and the experimental results was established between the maximum axial restraining forces generated and the critical temperatures. The rotational springs used to behave as hinges in order to simulate the friction observed previously in the experimental tests proved to reproduce successfully the friction

pretended. Hence, this hinges can simulate different end-support conditions with different levels of rotational restraint. For the pined-end built-up model, the calibration was not fully achieved registering an error of 22%. This can be explained due to the fact that only one test was conducted for this column type and it is recommended to perform more in order to improve and validate the developed model. It can be stated that the remaining models can be used for future parametric studies reaching average error values within 10%, heavily contributing to the development of specified design methodologies for CFS columns under fire situation.

5.3   Future research work

The numerical model developed and validated within the present dissertation could be addressed as an important tool in future parametric studies in thermomechanical analysis of CFS sigma-plus columns, accessing different cross-section types in order to develop new or improved design guidelines for this type of steel in fire situation.

CFS columns with slenderness different from the ones studied along this dissertation should be addressed changing multiple parameters, namely the variation of the cross-section geometry, the thickness of the cross-section and the length of the column. The influence of the positioning of the self-drilling screw is an issue to be studied with different spacing to access its structural behaviour. Different levels of axial and rotational restraint imposed by the surrounding structure in fire situation should be addressed with both experimental and numerical analyses, in order to access its influence as well as initial levels of applied load, and therefore, extend the existing studies to a larger range of CFS columns establishing the comparison with the already available predictions for CFS members.

Other fundamental parameters could be under consideration within the next few years in order to expand the knowledge already obtained such as, other cross-section types composed columns built with two single profiles.

Experimental and numerical analysis of compressed cold-formed steel
elements with sigma plus cross-section subjected to fire

REFERENCES

REFERENCES

ABAQUS (2014). "Abaqus User's Manual - Version 6.14", Dassault Sysèmes Simulia Corp, Providence, RI, USA.

Ádány, S. and Schafer, B.W. (2006a). Buckling mode decomposition of single-branched open cross-section members via finite strip method: Application and examples, Thin-Walled Structures, Vol. 44, pp. 585–600.

Ádány, S. and Schafer, B.W. (2006b). Buckling mode decomposition of single-branched open cross-section members via finite strip method: Derivation, Thin-Walled Structures, Vol. 44, pp. 563–584.

Advantage Fabricated Metals@ (2009). http://www.advantagefabricatedmetals.com, Metal components manufacturer, (Accessed: 20th April 2016).

AISI (2001). AISI specification for the design of cold-formed steel structural members. American Iron and Steel Institute, Washington (DC), USA; 2001.

AS/NZS 4600 (1996). Cold-Formed steel structures. New Zealand standard, Australia.

Azevedo, J. (2016). Análise termomecânica de colunas tubulares mistas de secção quadrada e retangular em situação de incêndio, Dissertation for the degree of Master of Civil Engineering, Department of Civil Engineering, Faculty of Science and Technology of the University of Coimbra.

BS 5950 (1987). Structural Use of Steelwork in Buiding – Part 8: Code of Practice for Fire Resistance Design. British Standards Institution (BSI), London, UK.

Camotim, D. and Dinis, P.B. (2011). Coupled instabilities with distortional buckling in cold-formed steel lipped channel columns, Thin-Walled Structures, Vol. 49, pp. 562–575.

Chen, J. and Young, B. (2007a). Cold-formed steel lipped channel columns at elevated temperatures, Engineering Structures, Vol. 29, pp. 2445–2456

Chen, J. and Young, B. (2007b). Experimental investigation of cold-formed steel material at elevated temperatures, Thin-walled Structures, Vol. 45, pp. 96–110

Craveiro, H.D., Rodrigues, J.P.C. and Laím, L. (2014). Cold-formed steel columns made with open cross-sections subjected to fire, Thin-Walled Structures, Vol. 85, pp. 1–14.

Craveiro, H.D., Rodrigues, J.P.C., Santiago, A., et al. (2016). Review of the high temperature

Experimental and numerical analysis of compressed cold-formed steel
elements with sigma plus cross-section subjected to fire

REFERENCES

mechanical and thermal properties of the steels used in cold formed steel structures - The case of the S280 Gd+Z steel, Thin-Walled Structures Vol. 98, pp. 154–168.

Craveiro, S. (2015). Fire resistance of cold-Formed steel columns, Dissertation for the degree of Doctor of Philosophy in Fire Safety Engineering, Department of Civil Engineering, Faculty of Science and Technology of the University of Coimbra.

Rondal, J., Dubina, D. (2005). Light gauge metal strucutres: recent advances, International centre for mechanical sciences (CISM), Udine, Italy, 259 p.

Dubina, D., Ungureanu, V. and Landolfo, R. (2012). Design of Cold-formed Steel Structures. Eurocode 3: Design of Steel structures. Part 1-3: Design of cold-formed steel structures, ECCS - European Convention for Constructional Steelwork, Wiley-Blackwell, 676 p.

EN 1993-1-1 (2005). Eurocode 3: Design of steel structures - Part 1-1: General rules and rules for buildings. Brussels: European Convention for Standardisation, Brussels, 91 p.

EN 1993-1-2 (2005). Eurocode 3: Design of steel structures - Part 1-2: General rules - Structural fire design, European Convention for Standardisation, Brussels, 78 p.

EN 1993-1-3 (2006). Eurocode 3 - Design of steel structures - Part 1-3: General rules - Supplementary rules for cold-formed members and sheeting Eurocode, European Convention for Standardisation, Brussels, 125 p.

EN 1993-1-5 (2006). Eurocode 3: Design of steel structures - Part 1-5: General rules - Plated structural elements. European Convention for Standardisation, Brussels, 55 p.

Feng, M., Wang, Y.C. and Davies, J.M. (2003a) Axial strength of cold-formed thin-walled steel channels under non-uniform temperatures in fire, Fire Safety Journal, Vol. 38, pp. 679–707.

Feng, M., Wang, Y.C. and Davies, J.M. (2003b) Thermal performance of cold-formed thin-walled steel panel systems in fire, Fire Safety Journal, Vol. 38, pp. 365–394.

Fontana, M., Frangi, A., and Knobloch, M. (2012). Structures in fire - SIF'2012, Proceedings of the 7th international conference on Structures in Fire, Zurich, Switzerland, pp. 563-565.

GEM Nexus@ (2013). http://www.nexus.globalquakemodel.org, Scientifc community platform, (Accessed: 20th April 2016).

Kaitila, O. (2002). Finite element modelling of cold-formed steel members at high temperatures, Helssinki (Finland), 2002, 90 p. Thesis, Science and Technology, Helsinki University of Technology.

Kankanamge, N.D. and Mahendran, M. (2011). Mechanical properties of cold-formed steels at elevated temperatures, Thin Walled Structures, Vol. 49, pp. 26–44

Kàrmàn, T. Von, Sechler, E.. and Donnell, L.. (1932). The strength of Thin Plates in Compression, Transactions of thee American Society of Mechanical Engineers, Vol. 54, pp.

Experimental and numerical analysis of compressed cold-formed steel
elements with sigma plus cross-section subjected to fire

REFERENCES

53-57.

Laím, L. (2013). Experimental and numerical analysis on the structural behaviour of cold-formed steel beams subjected to fire, Dissertation for the degree of Doctor of Philosophy in Fire Safety Engineering, Department of Civil Engineering, Faculty of Science and Technology of the University of Coimbra.

Li, Y., Li, Y., Wang, S., et al. (2014). Ultimate load-carrying capacity of cold-formed thin-walled columns with built-up box and I section under axial compression, Thin-Walled Structures, Vol. 79, pp. 202-217.

Li, Z. and Schafer, B.W. (2010). Application of the finite strip method in cold-formed steel member design, Journal of Constructional Steel Research, Vol. 66 pp. 971–980.

Outinen, J., Kaitila, O. and Mäkeläinen, P. (2000). A Study for the Development of the Design of Steel Structures in Fire Conditions, Proceedings of the 1st International Workshop of Structures in Fire, Copenhagen, Denmark, pp. 267–281.

Outinen, J. and Mäkeläinen, P. (2002). Mechanical properties of structural steel at elevated temperatures and after cooling down, Proceedings of the 1st International Workshop of Structures in Fire, Christchurch, New Zealand, pp. 273–290

Ramos, M. (2016). Resistência ao Fogo de Colunas Tubulares de Secção Circular e Elíptica com Restrição à Dilatação Térmica, Dissertation for the degree of Master of Civil Engineering, Department of Civil Engineering, Faculty of Science and Technology of the University of Coimbra.

Ranawaka, T. and Mahendran, M. (2009). Experimental study of the mechanical properties of light gauge cold-formed steels at elevated temperatures, Fire Safety Journal, Vol. 44, pp. 219–229

Schafer, B.. and Peköz, T. (1998a). Computational modeling of cold-formed steel: characterizing geometric imperfections and residual stresses, Journal of Constructional Steel Research, Vol. 47 pp. 193–210.

Schafer, B.W. and Peköz, T. (1998b). Direct strength prediction of cold-formed steel members using numerical elastic buckling solutions, In: Proceedings of the 14th international specialty conference on cold-formed steel strucutres, St. Louis, Missouri, USA, pp. 69–76.

Silvestre, N. and Camotim, D. (2002a). First-order generalised beam theory for arbitrary orthotropic materials, Thin-Walled Structures, Vol. 40 Issue 9, pp. 755–789.

Silvestre, N. and Camotim, D. (2002b). Second-order generalised beam theory for arbitrary orthotropic materials. Thin-Walled Structures, Vol. 40, Issue 9, pp. 791–820

Simões, R.A.D. (2007). Manual de Dimensionamento de Estruturas Metálicas: Eurocódigo 3: Projecto de Estruturas de Aço: Parte 1-1: regras gerais e regras para edifícios, 2ª ed. Coimbra: CMM - Associação Portuguesa de Construção Metálica e Mista, 2007. Xxiv, 221p.

Experimental and numerical analysis of compressed cold-formed steel
elements with sigma plus cross-section subjected to fire

REFERENCES

Structure Magazine@ (2014). http://www.structuremag.org, Structural engineer magazine, (Accessed: 20th April 2016).

Yan, J. and Young, B. (2002). Column tests of cold-formed steel channels with complex stiffeners, Journal of Structural Engineering, Vol. 128, Issue 6, pp. 737-745.

Yan, J. and Young, B. (2004). Numerical investigation of channel columns with complex stiffeners - Part I: Test verification, Thin-Walled Structures, Vol. 42, pp. 883–893.

Yang, D. and Hancock, G.J. (2004). Compression tests of high strength steel channel columns with interaction between local and distortional buckling, Journal of Structural Engineering, Vol. 130, no. 12, pp. 1954–1963.

Young, B. and Chen, J. (2008). Design of cold-formed steel built-up closed sections with intermediate stiffeners, Journal of Structural Engineering, Vol. 134, No. 5, pp. 727–737.

Young, B. and Rasmussen, K.J.R. (1998). Tests of fixed-ended plain channel columns, Journal of Structural Engineering, Vol. 124, Issue 2, pp. 131–139.

Yu, W. and LaBoube, R.A. (2010). Cold-Formed Steel Design – Fourth Edition, John Wiley & Sons, Inc., USA, 767 p.

Zhang, J.H. and Young, B. (2012). Compression tests of cold-formed steel I-shaped open sections with edge and web stiffeners, Thin-Walled Structures, Vol. 52, pp. 1–11.